Quantitative Flow Measurement and Visualization of Cavitation Initiation and Cavitating Flows in a Converging-Diverging Nozzle

by

ZAYED AHMED

B.E., Osmania University, 2015

A THESIS

submitted in partial fulfillment of the requirements for the degree

MASTER OF SCIENCE

Department of Mechanical and Nuclear Engineering
College of Engineering

KANSAS STATE UNIVERSITY
Manhattan, Kansas

2017

Approved by:

Co-Major Professor
Dr. M. H. Hosni

Approved by:

Co-Major Professor
Dr. B. Terry Beck

Copyright

Abstract

Cavitation is the formation of vapor phase from the liquid phase by reduction in its absolute pressure below the saturation pressure. Unlike boiling, where the temperature of the liquid is increased to cause vaporization, the reduction in the pressure alone can cause the liquid to turn into vapor. Cavitation is undesirable in many engineering applications as it is associated with reduction in efficiency and is known to cause damage to pump and propeller components. However, the endothermic nature of cavitation could be utilized to create a region of low temperature that could be utilized to develop a new refrigeration cycle.

The work presented in this thesis is part of ongoing research into the potential cooling capacity of cavitation phenomena, where the cavitation in a converging-diverging nozzle is being investigated. Due to the constricting nature of the throat of the converging-diverging nozzle, the liquid velocity at the throat is increased, obeying the continuity law. With an increase in velocity, a reduction in absolute pressure is accompanied at the throat of the nozzle according to the Bernoulli's principle. The local absolute pressure at the throat can go lower than the saturation vapor pressure, thereby causing the fluid to cavitate. The effect of water temperature on the flowrates, the onset of cavitation within the nozzle, and the resulting length of the cavitation region within the nozzle are the subject of this thesis. Experimental results and analysis are presented which also show that near the onset of cavitation, the flowrate can go beyond the choked flowrate, causing the local pressure in the throat to go well below zero for an extended amount of time in the metastable state, before nucleating (cavitating) into a stable state. Flow visualization using a high speed digital camera under different operating conditions was aimed at investigating the region of cavitation onset, which appears to be associated with boundary layer separation just downstream of the nozzle throat. In order to delay the boundary layer separation point in the

downstream section of the nozzle, the diffuser region of the nozzle was modified to enable two flow paths, where one path would suck the flow near the inner walls of the nozzle and the other would allow the bulk of the flow to pass through. This was achieved with the use of inserts. Various inserts were tested in an attempt to capture the effect of inserts on the cavitation phenomena. Their effect on the flowrates, length of two phase region, and cavitation onset are presented in this thesis.

Table of Contents

List of Figures

List of Tables

Acknowledgements

I would first like to thank my family for understanding and supporting my decision to travel halfway around the world for higher education. I am grateful to Dr. Beck, who guided me in the technical aspects of this research work and helped me grow as an engineer. My sincere thanks goes to Dr. Hosni for giving me the motivation and support when I needed it the most. Thanks to Dr. Eckels and Dr. Sorensen for providing thoughtful insights into the research while serving on my committee. I would like to acknowledge the KSU scientific glassblower, Jim Hodgson, for making the glass nozzle and inserts with high precision and accuracy. In addition, I would like to thank Eric Wagner from MNE Shop and Brendan Gundy from IER for their help in machining various parts and components. Special thanks to Abhinav Gairola for providing his help and motivation in writing this thesis. Finally, I must express my profound gratitude to the following individuals for providing me with unfailing support and continuous encouragement through the process of researching and writing this thesis: Monsur Abbas, Syed Asrar Ahmed, Ayyappan Elangovan, Megan Menth, Shashank Pathak and Sai Pradeep.

Chapter 1 - Introduction

Cavitation is a phenomenon where liquid vaporizes due to reduction in its absolute pressure below the saturated vapor pressure at that temperature. For the phase change to occur, the absolute vapor pressure of the fluid has to go below the saturated vapor pressure, which is a function of the fluid temperature. Unlike boiling, which commonly takes place when the temperature is increased keeping the absolute pressure roughly constant, the reduction is absolute pressure alone can cause the fluid to vaporize. The two basic ways of vaporizing water are depicted in Figure 1 for water. In simple words, cavitation is the boiling of a fluid by reducing its pressure rather than by increasing its temperature.

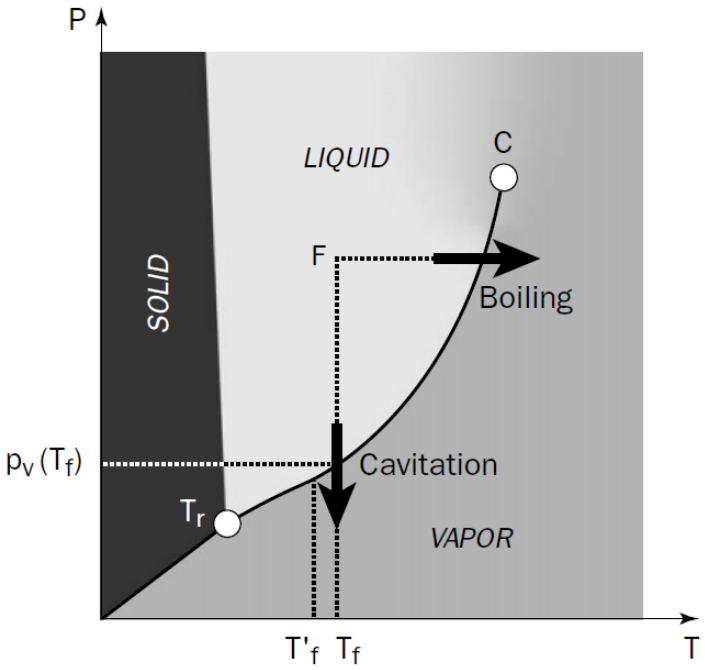

Figure 1: Phase Diagram of water indicating cavitation and boiling [1]

Cavitation is generally undesirable in many engineering applications as it is known to cause damage to pump and propeller components. It is also responsible for creating noise, vibrations and a loss of efficiency. Vapor bubbles are formed where the local pressure in these components gets very low. There is an accompanied collapse of the vapor bubbles when the local pressure gets

higher than the saturation pressure. When these vapor bubbles collapse, they release large amounts of energy which causing “pitting” on the component surface. The pitting caused by collapse of the bubbles dramatically shortens a propeller or pump’s lifetime. Cavitation also introduces “choking” in control valves, which limits the flowrates that can be achieved in a flow system.

Although cavitation has many negative effects, it can be exploited to be advantageous towards achieving various engineering goals. A cavitating Venturi, which results in a choked flow, has been used as a passive flow control technique in rocket engines to control the flow rates of the fuel and the oxidizer [2]. Research conducted by Brinkhorst [3] presents the possibility of using cavitating Herschel Venturi tubes for flow metering applications.

Cavitation can also be used for potential performance gains in a refrigeration system. Research conducted my Alkotami [4] and Asher [5] showed the possibility of utilizing the cavitation phenomena in developing a refrigeration cycle that modifies the traditional vapor compression refrigeration cycle. A vapor compression refrigeration cycle typically uses standard refrigerants as the working fluid. Traditional refrigerants, however, have been associated with Ozone level Depletion Potential (ODP) and significant Global Warming Potential (GWP). An innovative cooling technology has been investigated using sonic multi-phase flow in a critical-flow nozzle to create a low-pressure and low-temperature region for heat absorption. The strength of the new technology was its potential to produce cooling using water as the working fluid with low ODP and GWP. While the full potential for using water as the working fluid may not be fully realized from a refrigeration viewpoint because of its material properties, water may still provide useful insights for investigating the underlying cavitation phenomena for the development of the new technology.

The work presented in this thesis is part of ongoing research where the cooling potential of cavitation in a converging diverging nozzle is under investigation. The objective of this effort is to develop a practical cooling system that uses the low pressure and low temperature in the sonic multi-phase flow region within a cavitating nozzle for heat absorption while using water as the working fluid.

In a traditional vapor compression refrigeration cycle, the compressor increases the temperature and pressure of the refrigerant. Heat is subsequently transferred out of the condenser to the surroundings, which has a lower temperature than the refrigerant. The fluid then goes to an expansion valve where the pressure is lowered and the temperature is reduced below the ambient temperature of the compartment, or the refrigeration space. Heat is then taken up by the refrigerant from the refrigeration space through the evaporator. The fluid then goes to the compressor and the cycle repeats. A sonic cavitating nozzle could also be utilized for heat absorption. In a converging-diverging nozzle, the flow area is gradually reduced in the converging section where the lowest area is achieved at the throat, followed by a gradual increase in the flow area in the diverging section. In a steady state system, the mass flow rate entering the system is equal to the mass flow rate leaving the system. Thus the mass flow rate at any given cross section is constant along the nozzle. At a reduced flow area, the velocity of the fluid has to be high to maintain a constant mass flow rate. These highest velocities are achieved at the area of lowest cross section, i.e. at the throat of the converging-diverging nozzle. By Bernoulli's principle, as the velocity of a fluid increases, the pressure decreases. Therefore, the lowest pressure is expected to occur at the throat of the nozzle, if friction and flow separation effects are not considered. For a given geometry, the absolute pressure at the throat could go below the saturated vapor pressure at that temperature, causing the fluid to cavitate near the throat of the nozzle. The two phase mixture is extended into the diverging

section, where a region of low temperature and pressure is achieved. This region could be utilized in developing a new refrigeration system.

1.1 Literature Review

Brennen published a book titled "Cavitation and Bubble Dynamics", which is a general reference book for researchers working on cavitation. Brennen distinguished between four kinds of cavitating flows: travelling bubble cavitation, attached cavitation, vortex cavitation and shear cavitation. Other references have also identified and discussed these kinds of cavitating flows [6][7]. The different types of cavitating flows are represented in Figure 2.

In travelling bubble cavitation, represented by A in Figure 2, the bubbles develop from the weak points in the liquid. These weak points are called as cavitation nuclei. Typically, microbubbles present in the flow act as cavitation nuclei. These microscopic cavitating bubbles become macroscopic cavitating bubbles as they go through regions where the local pressure is lower than the vapor pressure. Attached cavitation, represented by B in Figure 2, occurs when flow is separated along a surface. This kind of cavitation is attached to the wall in a quasi-permanent manner. The surface of the cavity is often smooth since the separating boundary layer is usually laminar. Many high Reynold's number flows contain a region of concentrated vorticity. The pressure in the core of the vortex is significantly smaller than the rest of the flow, even going below the saturation pressure. Cavitation develops in the core of the vortex as shown by C in Figure 2. This kind of cavitation is observed at the tips of Marine propellers where a vortex is generated at the tip of the propeller blade. Shear cavitation, represented by D in Figure 2, is observed in the wake region of bluff bodies or in submerged liquid jets [7].

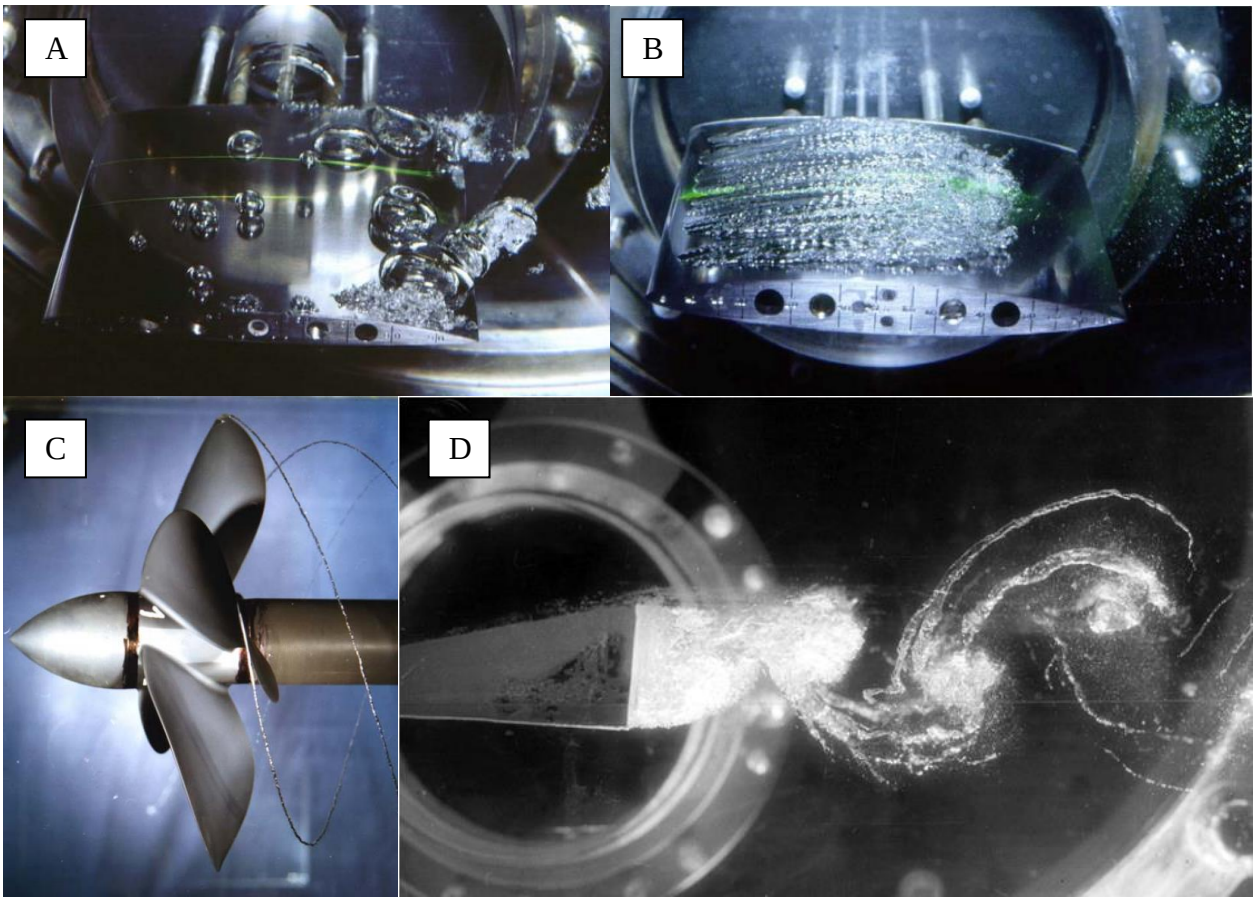

Figure 2: Examples of different cavitating flows: (A) Travelling Bubble Cavitation, (B) Attached Cavitation, (C) Vortex Cavitation, (D) Shear Cavitation [7] (© NATO STO)

Wilms [8] identified different cavitating flow structures in nozzles through flow visualization technique. The attached wall cavitation was found in venturi nozzles and featured a sheet of vapor attached to the inner walls of the nozzle. Shear cavitation was found in nozzles with a rapid expansion, typically through an orifice. The flow exiting the orifice was in the form of a liquid jet at the center of the flow with vapor around it. The vapor was formed due to the shear forces from the liquid jet coming out of the orifice. Swirl cavitation was found in nozzles with rapid expansion, where the flow was rotated prior to the inlet of the nozzle. The flow after exiting from the orifice formed a large vapor region around the central jet. Travelling bubble cavitation was found when there were dissolved gases in the liquid. When the absolute pressure near the throat of the nozzle

got lower than the vapor pressure, these gases separated from the liquid in the form of bubbles and acted as nucleation sites for the liquid to cavitate.

As mentioned earlier, cavitation occurs when the minimum pressure in the flow is lower than or equal to the vapor pressure at that temperature. A non-dimensional component is often used to characterize the cavitation phenomena, and this non dimensional cavitation parameter is called cavitation number. This cavitation number was introduced by Brennen [6] and it is defined by:

$$\sigma = \frac{p_\infty - p_v}{\frac{1}{2}\rho_L {V_\infty}^2} \tag{1}$$

This cavitation parameter can be considered as an index that measures the degree of development of cavitation for two phase flow. Any flow, cavitating or not, has some value of σ. If σ is sufficiently large, single phase liquid flow will occur. As σ is reduced, cavitation will occur at some particular value of σ called the incipient cavitation number, denoted by σ_i. Developed cavitation occurs at values of σ lower than the incipient cavitation number, σ_i.

The cavitation number is also a measure of the potential to cavitate in a single phase flow. σ can be lower than the incipient cavitation, σ_i while still being in a single phase liquid state. Under this condition, any disturbance in the flow will cause the liquid to cavitate. Any impurities in the liquid will act as nucleation sites and will cause travelling bubble cavitation to occur. The instability caused when flow separates will cause other kinds of cavitation explained earlier. When the liquid is free of any impurities, and no disturbances or nucleation sites are present, the liquid will not cavitate even though the local pressure of the liquid is much lower than the saturation pressure. The pressure in the liquid can go so low, that it becomes negative, without cavitating. As mentioned by Caupin [9], when the liquid is in a negative pressure, the molecules in the liquid are further away from each other, but their mutual attraction allows the system to remain in a

metastable state. The lowest pressure the system can reach while being in a metastable state, is referred to as the spinodal pressure, and at this limit, the stretched liquid ceases to be in a metastable state and becomes macroscopically unstable. When the liquid is in a metastable state, any impurity will cause the liquid to reach a more stable state by causing the fluid to vaporize, or cavitate. Caupin [9] compiled various experimental results in which very low pressures were achieved before cavitating. The lowest pressures recorded were -140 MPa by a Quartz Inclusion method, -27.7 MPa by centrifugation method and -24 MPa by an acoustic method. Low pressures can be achieved in the throat of a converging-diverging nozzle before cavitation would occur. No hydrodynamic experiments have been reported where large negative values of cavitation have been achieved. Large negative pressures can be achieved in the nozzle if the liquid being used is pure, and no surface irregularities that induce nucleation are present.

The surface irregularities, or sudden expansions in the flow area cause the flow to separate from the surface. The presence of flow separation has been linked to the cavitation originating along the surfaces of separation, as suggested by Appel [10]. The boundary layer separation causes formation of turbulent vortices in the flow and these turbulent vortices result in significant local transient pressure depressions. These local pressure depressions can be lower than the mean pressure of the flow, even going lower than the saturation vapor pressure, hence inducing nucleation or cavitation. Therefore, cavitation can occur even without the mean pressure in the fluid approaching the saturation vapor pressure.

While the cavitation begins in the leading edge when a sharp leading edge is encountered, experimental work done by Arakeri [11] found that the position of cavitation lies considerably downstream from the point of flow separation in case of a smooth curved leading edge. Arakeri

[11] also proposed a criteria to predict the position of cavitation based on the position of flow detachment.

Flow separation in converging-diverging nozzles was studied using Particle Image Velocimetry (PIV) technique by Schmidt [14] to conduct measurements of the fluid velocity field in a converging-diverging nozzle. Areas near the wall in the diverging section of the nozzle exhibited reversed flow, or the formation of vortices and eddies due to flow separation. The flow in the diverging section detached from the wall, forming a central wavering jet with transient low velocity or recirculating flows around the central jet. PIV results showed that the areas of recirculation also nearly coincided with the cavitation front, a few millimeters downstream of the throat in the diverging section.

Cavitating flow in a converging-diverging nozzle is typically associated with the onset of a so called "choked flow" condition. Under this condition, the flow rate through the nozzle remains unaltered regardless of any increase in the driving force across the nozzle. In other words, the flowrate through the nozzle would stay constant even if the pressure in the downstream region of the nozzle (generally referred to as the back pressure) is reduced beyond a certain limit. This was demonstrated by Davis [12] in his experimental study of cavitation in aviation fuel in a converging-diverging nozzle. Choked flow condition in a cavitating Venturi is utilized in engineering applications as a flow control device in rocket engines [2]. Brinkhorst [3] explored the possibility of using a cavitating Herschel Venturi as a flow metering device for household application. Sudden changes in flow area that are accompanied with sharp edges promote cavitation. The geometry of the Herschel Venturi tube used by Brinkhorst [3] promoted cavitation at the beginning of the straight section, just downstream of the converging area. The schematic of the Herschel Venturi tube used by Brinkhorst [3] is shown in Figure 3.

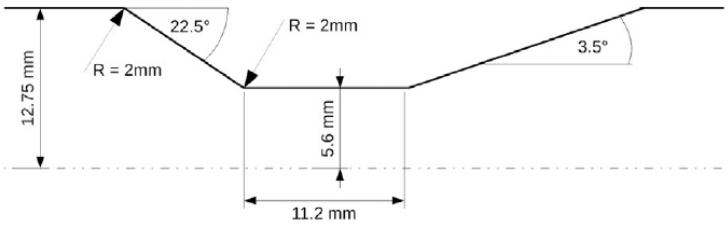

Figure 3: Schematic of the Herschel Venturi tube used by Brinkhorst [3]

Very stable flow behavior under choked conditions was demonstrated in this setup. The flow stayed at a constant flowrate when the pressure ratio (ratio of outlet to inlet pressure across the test section) across the Herschel-Venturi tube was lower than about 0.85. It was shown that the cavitation inception, did not correlate with the choked flow conditions. The flow cavitated when the flowrate through the nozzle was lower than the choked flowrate. Before reaching choked conditions, a sudden increase in the cavitating length was observed. This sudden increase in cavitation length was attributed to complex pressure field stabilizing itself. The stable behavior of the flowrate and the variation of the cavitation length is represented in Figure 4. A method to predict the choked flowrate in a cavitating nozzle flow was also presented by Brinkhorst [3].

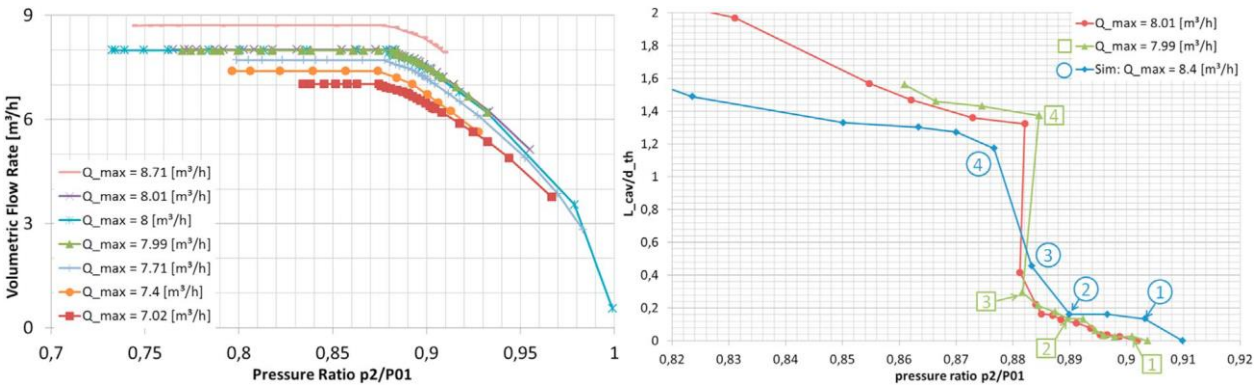

Figure 4: Flowrate and cavitation length variation with pressure ratio across the tube [3]

The cavitation length was measured as the distance in the nozzle up to which the flow stayed in a two phase liquid-vapor mixture zone. Under choked conditions, the condensation of the two-phase liquid-vapor mixture into a single phase liquid was accompanied by a condensation shock

as demonstrated by Davis [12]. After certain distance within the diverging section of the nozzle, the two phase flow condensed into the liquid phase accompanied by an abrupt rise in static pressure. The condensation of the two phase mixture in the converging diverging nozzle used by Davis is shown in Figure 5.

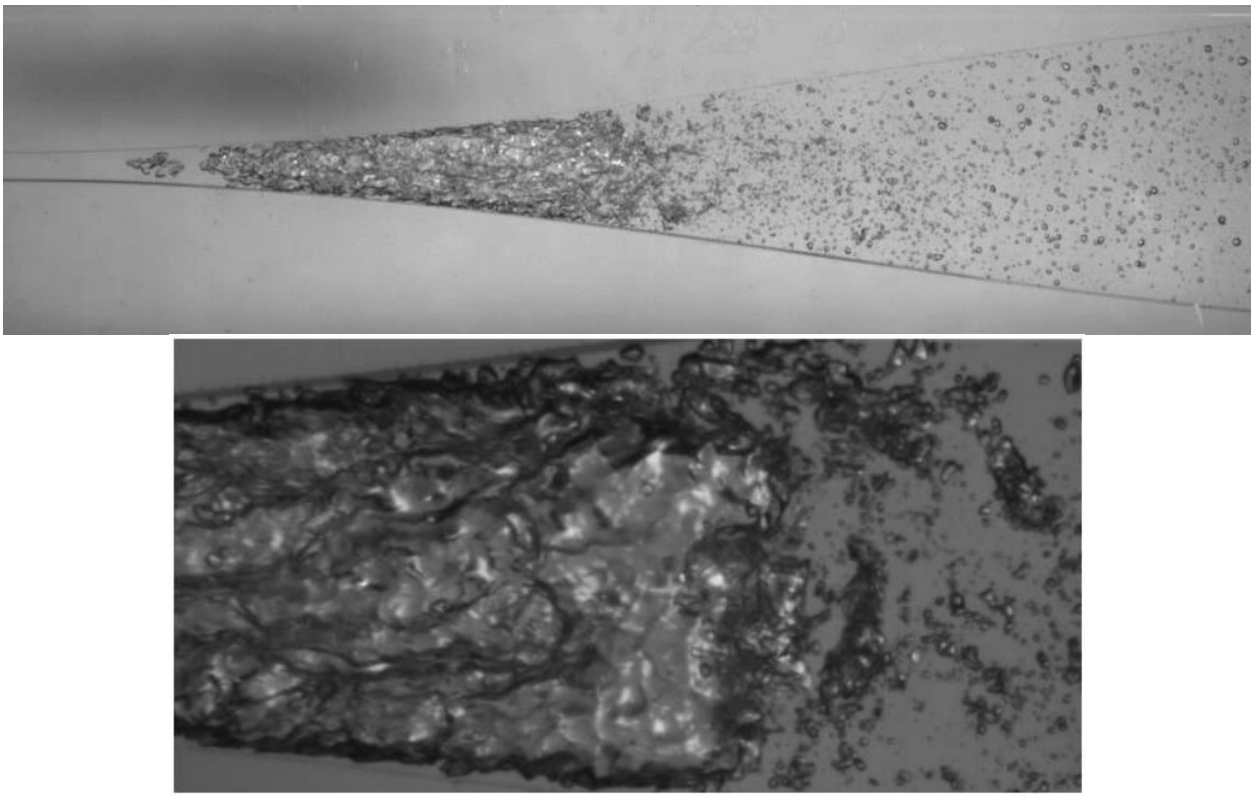

Figure 5: Cavitation of water in the converging-diverging nozzle (top); Close up of bubble collapse through a shock in the diverging section [12]

Pressure measurements were taken at various locations along the test section and these are shown in Figure 6. For the non-choked flow condition, represented by Case 1 and Case 2 in Figure 6, the pressure recovery was gradual in the diverging portion of the nozzle. Whereas for the choked flow condition, represented by Case 3 and Case 4 in Figure 6, a sudden pressure rise occurred at different locations in the diverging section depending on the back pressure to the nozzle. This sudden rise in pressure, coincided with the condensation of the liquid-vapor mixture into a single phase liquid in the form of a condensation shock.

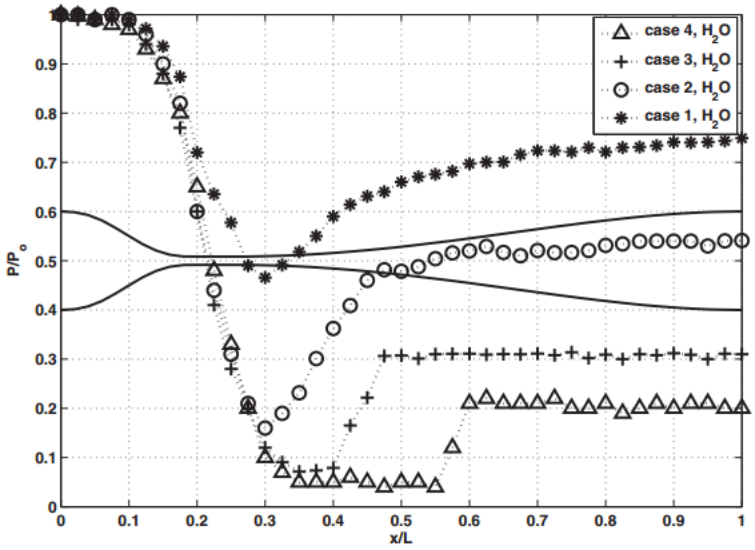

Figure 6: Axial pressure distribution across the nozzle for water flow [12]

In the experimental study by Sou [13], cavitation in a two dimensional nozzle and liquid jet in the vicinity of the nozzle exit, were visualized using high speed cameras to investigate the effects of cavitation on liquid jet under various conditions of Reynolds number and cavitation number. The cavitation was classified into the following regimes: 1- no cavitation, wavy jet; 2- developing cavitation, wavy jet; 3- super cavitation, spray; and 4-hydraulic flip, flipping jet. These are represented in Figure 7.

The normalized cavitation length, L_{cav}^{*}, which is a ratio of the cavitation length to the nozzle length, was measured and plotted against the Reynolds number and the cavitation number, as shown in Figure 8. It was found that the cavitation length and the cavitation regime were not strongly affected by the Reynold's number, but showed significant dependence on the cavitation number σ.

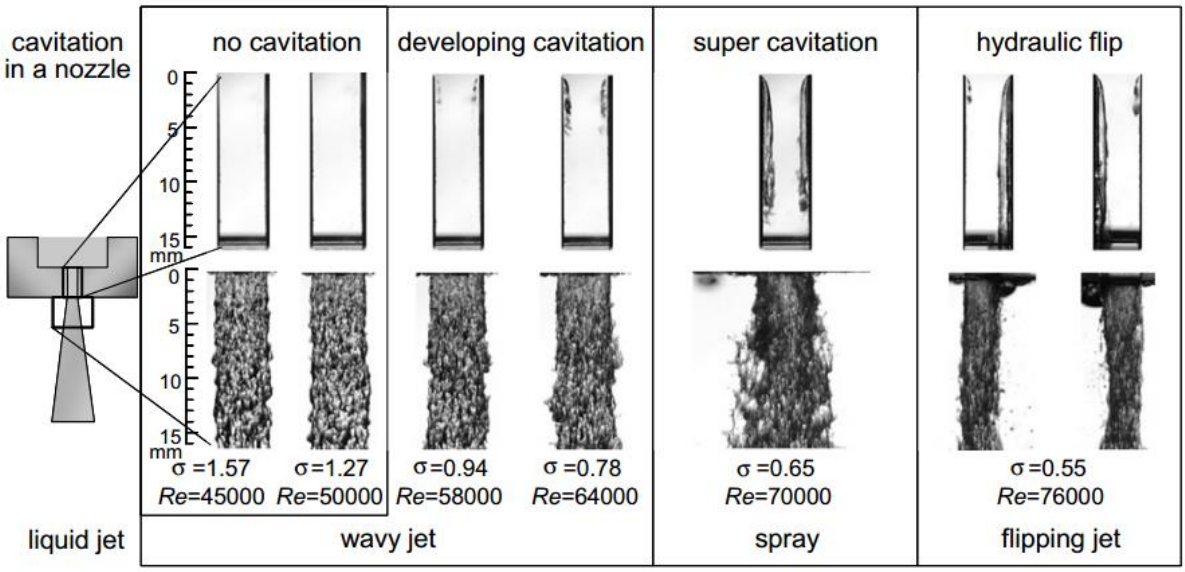

Figure 7: Visuals of the different cavitation regimes in a 2D nozzle and liquid jet [13]

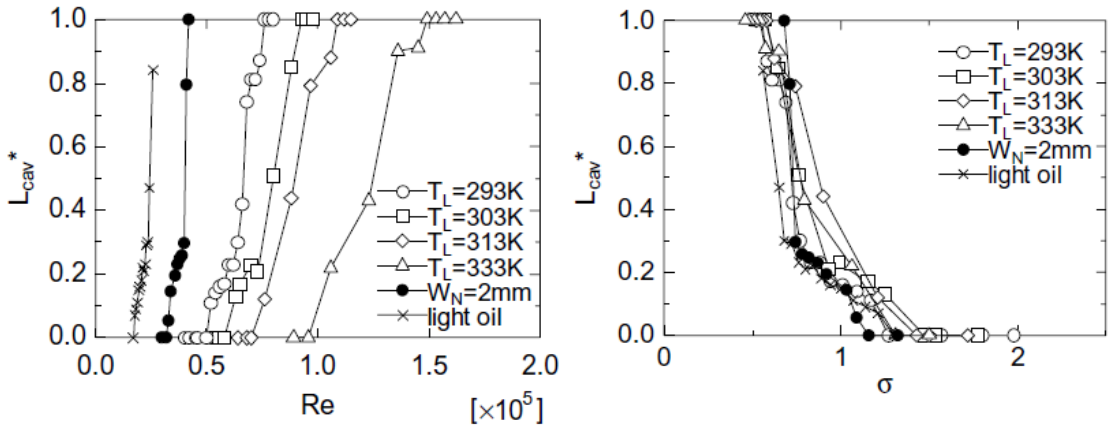

Figure 8: Effect of Reynolds number, *Re* and cavitation number σ, on the cavitation length [13]

1.2 Research Objectives

The work presented in this thesis was aimed to experimentally characterize the cavitation phenomena in a converging diverging nozzle. From the literature review, it was found that the point of cavitation inception was dependent on the flow separation point in the nozzle. Also, the cavitation length was found to be dependent on the cavitation number or the pressure ratio across the nozzle. For further investigation, a glass nozzle was used for the work presented in this thesis. All the quantitative and qualitative analysis presented in this thesis is in reference to the same nozzle. Two kinds of experiments were performed. The first one involves studying cavitation by varying the fluid temperature. The second one involved the use of inserts to study the dependence of cavitation on the boundary layer separation.

1.2.1 Investigation of cavitation inception

The inception of cavitation was investigated as a function of the fluid temperature, inlet and outlet pressure to the nozzle. As the inception of cavitation was linked with the flow separation in the diverging section of the nozzle, various kinds of inserts were used in an attempt to delay the flow separation and to study its effects on the cavitation inception location. An indication of successful flow separation delay would be accompanied by a shift in the cavitation front location in the nozzle. The flow at the cavitation onset was investigated with the help of quantitative measurements of the flowrate as well as by a qualitative analysis (flow visualization) using high speed videography. Quantitative measurements of the flowrates were taken for different fluid temperatures and were verified with the predictions given by Brinkhorst [3].

1.2.2 Investigation of pressures in the throat

Negative pressures developed in the nozzle throat, especially in the metastable state right before cavitation onset were investigated by utilizing simplified Bernoulli's approximations through quantitative flowrate and pressure measurements in the flow system.

1.2.3 Quantification of the cavitation length

As the length of the two phase region directly corresponds to the heat transfer area in the proposed innovative refrigeration system, a technique was developed in an attempt to quantify the cavitation length in the nozzle as a function of the fluid temperature. Cavitation length measurements were taken as a function of back pressure for different fluid temperatures and were also taken for few positions of the inserts.

1.2.4 High Speed Visualization of the Cavitation Phenomena

A high speed digital camera was used to study the transient behavior of cavitation at different test section conditions using flow visualization. The dependence of the cavitation onset on fluid temperature was also analyzed under both quasi-steady state and steady state conditions. The cavitation onset location was studied for the different kinds of inserts and the various kinds of cavitation regimes were explored when these inserts were in place.

Chapter 2 - Experimental Facility

In order to obtain quantitative flow measurements and high speed visualization of cavitation in a converging-diverging nozzle, a blow down facility was designed. In this chapter, the nozzle test section, the experimental apparatus and instruments used to obtain measurements are described.

2.1 Flow System

A schematic of the experimental setup is shown in Figure 9. The upstream reservoir was open to the atmosphere and was kept at an elevation. The downstream reservoir was connected to a vacuum pump that created a region of low pressure in the downstream reservoir tank.

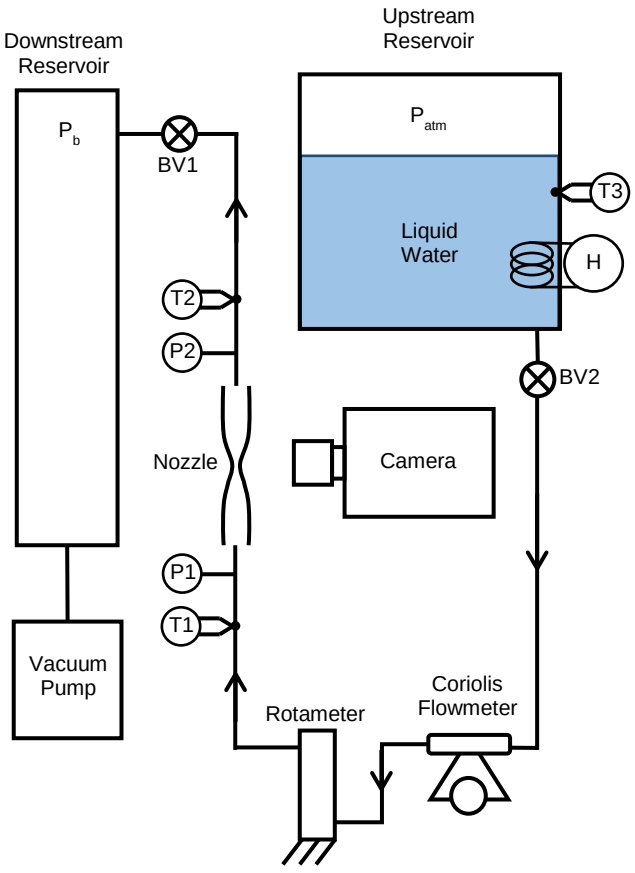

Figure 9: Experimental Setup

Because of the elevation of the upstream reservoir, a positive gauge pressure was developed at the nozzle inlet due to the gravitational head. Hence, the upstream reservoir acted as a high pressure chamber and the downstream reservoir as a low pressure chamber. This difference in pressures between the two reservoirs caused the water to flow from the upstream to the downstream reservoir. The nozzle test section was placed between the two reservoirs. The flow was controlled by creating appropriate vacuum or negative gauge pressure in the downstream reservoir. Further control was obtained through various valves located in the system.

2.1 Nozzle Test Section

The basic nozzle test section that was used for experiments is represented in Figure 10[1]. The nozzle was a converging-diverging type with was made of Pyrex glass. The nozzle was formed from a straight glass tube with an inside diameter of 9.3 mm. The nozzle measured to be approximately 400 mm in length with approximately 200 mm in length before the beginning of the converging section to provide a region for flow development. For flow development to occur in a turbulent flow regime, the development length should be nominally at least 10 times the hydraulic diameter of the flow section. The inlet and outlet diameters of the nozzle were 9.3 mm each. Since the nozzle was formed by hand, the exact internal profile of the nozzle was not accurately known at the time of fabrication. Therefore, a Refractive Index (RI) matching technique was used to measure the internal dimensions of the curved surface of the converging-diverging nozzle.

[1] Glass nozzles were made by hand from Pyrex glass tubes by Jim Hodgson, Senior Scientific Glassblower in the Department of Chemistry at Kansas State University.

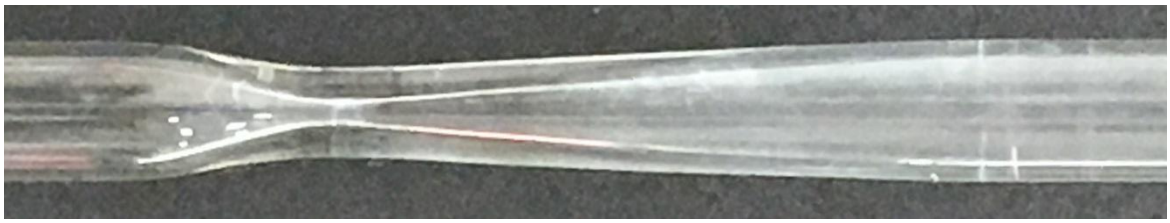

Figure 10: Nozzle test section

2.1.1 Refractive Index (RI) Matching Method

The idea behind using the refractive index (RI) matching method was to eliminate the refraction off the surface of the circular glass nozzle by immersing it in a liquid that had a similar RI as that of glass. This would cause only the internal profile of the nozzle, which had a different RI from glass, to be clearly visible; hence, it could be digitally photographed to make optical measurements of the internal dimensions.

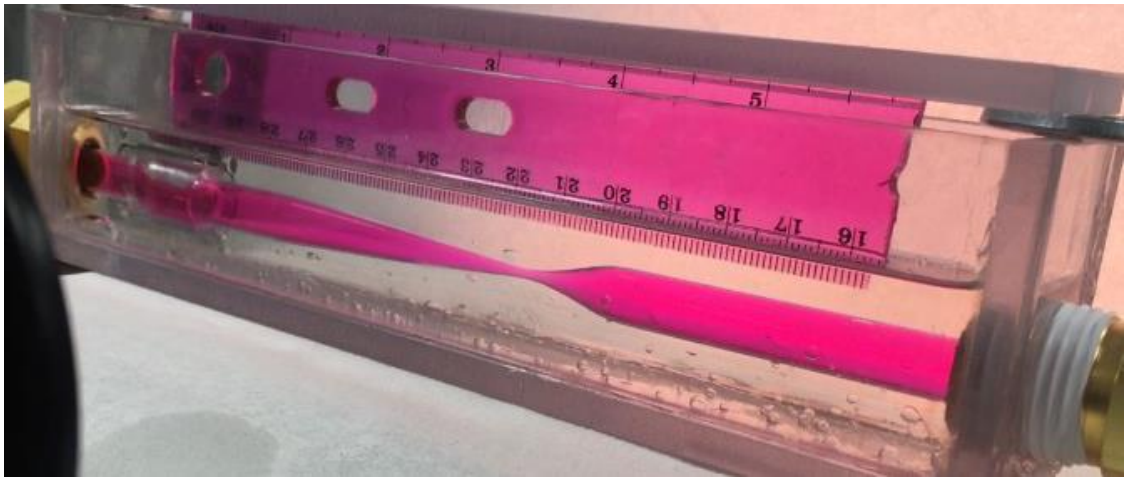

Figure 11: RI matching setup

A tank made of plexi glass was built that had provisions for the nozzle to be inserted horizontally in it. The tank was then filled with a mixture of Vegetable Oil and Baby Oil, which had refractive indices of approximately 1.48 and 1.46. These oils were mixed in the right proportions (approximately 3:1 ratio by volume) so that the RI of the mixture was close to the RI of the Pyrex glass, which was about 1.474. The nozzle was then inserted into the tank and the

nozzle interior was filled up with a Red liquid dye (Rhodamine B) dissolved in water that aided in making the internal geometry of the nozzle more visible. The setup is shown in Figure 11.

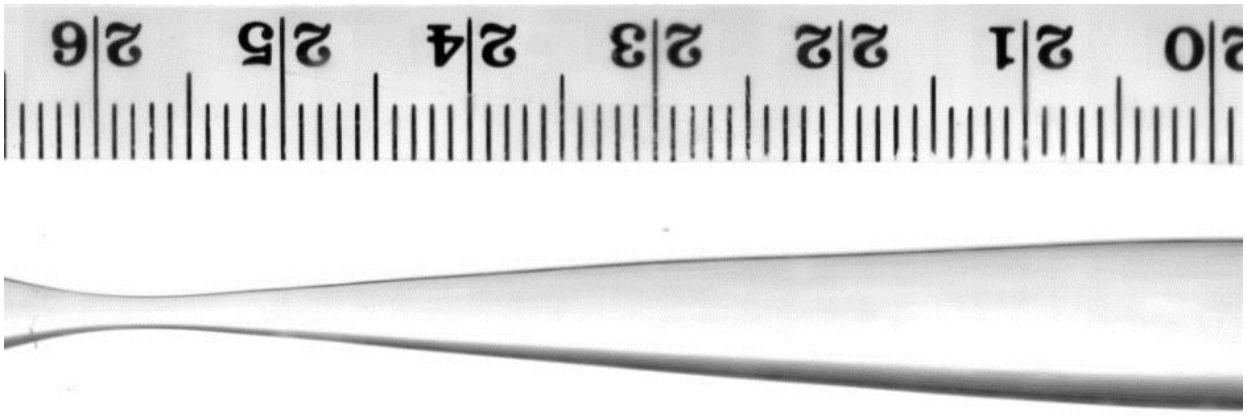

Figure 12: Internal Profile of the nozzle after RI matching

This setup was then digitally photographed alongside the scale shown, which had mm divisions. The digital photography yielded the picture shown in Figure 12. A digitizing software was used to generate a curve fit to the various digitized points, separately defining the internal profile dimensions for the converging and the diverging section dimensions of the nozzle with an uncertainty on the order of ±1 pixel or ±0.05mm. A 5^{th} order polynomial curve was fitted through these data points each for the converging and the diverging sections. The nozzle profile resulting from these equations is shown in Figure 13. The lengths of the converging and diverging sections were 22 mm and 72 mm, respectively. The throat diameter was 1.7 mm.

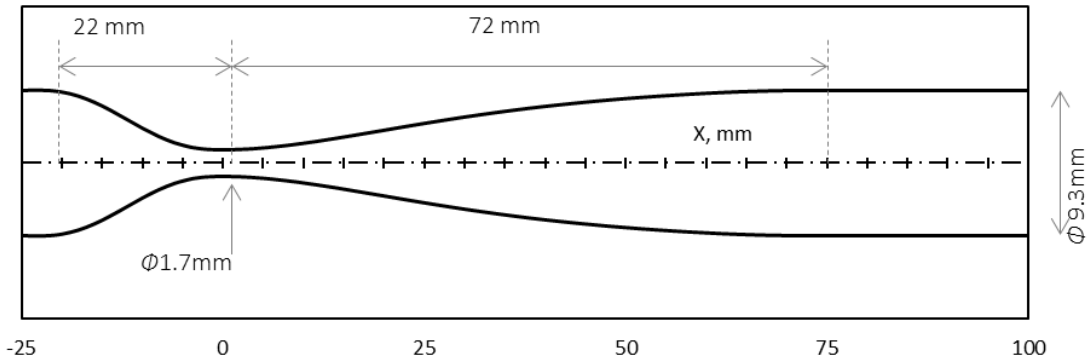

Figure 13: Profile of the nozzle used in experiments (not to scale)

2.2 Flow Visualization

Capturing the cavitation phenomena and performing a visual analysis required the phenomena to be recorded by a High-Speed Camera. Standard video cameras record at thirty frames per second. Since, the velocity of the fluid at the throat of the nozzle was in the order of 10-15 meters per second, it would only 0.33 ms to cover a distance of about 5 mm near the throat of the nozzle. Hence, the standard video cameras were concluded to be incapable of recording such high speed phenomenon. For High Speed imaging, a suitable High Speed Camera, proper lenses, and sufficient lighting were needed to get quality results at sufficient temporal and special resolution.

2.2.1 High Speed Camera

In order to have flexibility of different recording conditions needed for the project, a Photron SA5 High Speed Camera was used to capture visualization of cavitating flow. The camera had a maximum resolution of 1,024 by 1,024 pixels and the maximum frame rate at this resolution was 7,000 frames per second. To record at higher frame rates requires one to compromise on the resolution. The camera had the maximum capability to record at 775,000 frames per second, but at a much reduced resolution of 128 by 24 pixels. The camera was connected to a computer through

an Ethernet cable. The software accompanying the High Speed Camera was called Photron Fastcam Viewer (PFV) which allowed the user flexibility in controlling the camera. It also had various tools that aided in the timely analysis of the recorded videos. An AF Nikkor 60 mm f/2.8D lens was used for the recording.

2.2.2 Test Section Support Framework for Flow Visualization

Stable supports and mounts for the glass nozzle were needed to get good quality flow visualization through the High Speed Camera. Because of the material properties of Nylon, all the mounts that held the delicate glass nozzle were made of Nylon. These Nylon mounts were supported by a U-Channel that held the nozzle in a stable vertical position. The camera was mounted on a movable rail that allowed manual adjustment of the distance between the nozzle and the camera. The vertical height of the camera was controlled by a manual scissor jack. The entire setup was assembled on an optical table.

2.2.3 Lighting

The High Speed Camera requires more lighting than a regular video camera. Furthermore, as the frame rate is increased, more and more light is needed to achieve sufficient illumination intensity. Hence proper lighting gets very important to record at high frame rates. Proper lighting was achieved by using a fiber optic halogen light source provided by Thor Labs. The light being sent to the nozzle was sent through a frosted glass plate to provide a high intensity diffuse light illumination. Figure 14 shows the halogen light source with the fiber optic cable illuminating the back side of the nozzle.

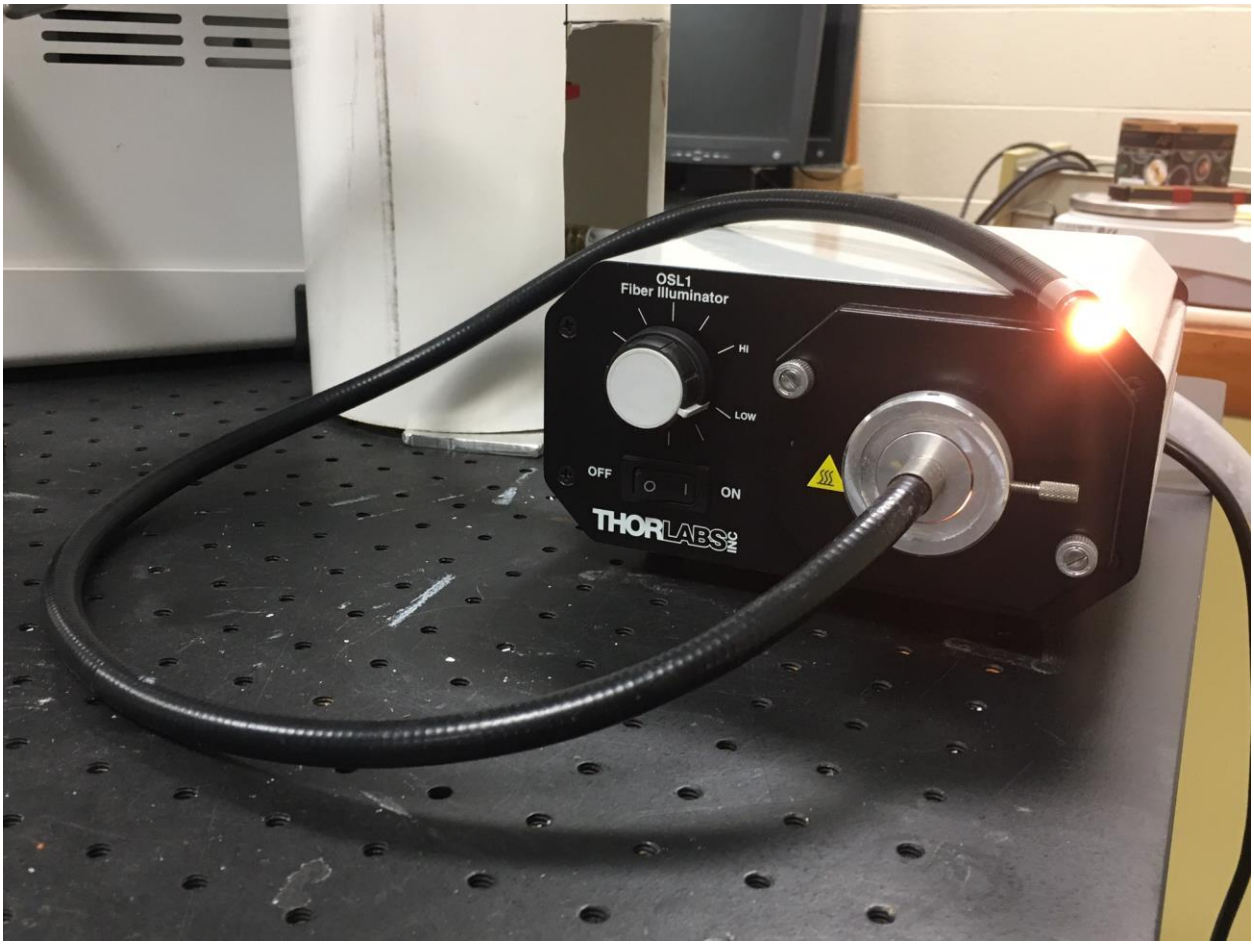

Figure 14: Lighting Source

2.3 Inserts

Analysis by Aaron Schmidt [14] showed that the flow separation point coincided with the cavitation initiation point in the diverging section of the nozzle. Through the analysis, it was found that the flow separated approximately 2 mm downstream of the throat in the diverging section and the cavitation initiation point also stayed at around 2 mm downstream of the throat. In order to prevent, or delay the flow separation, an arrangement had to be used where the flow detachment from the wall in the diverging section could be delayed by using vanes in the diffuser. This was created by installing Inserts.

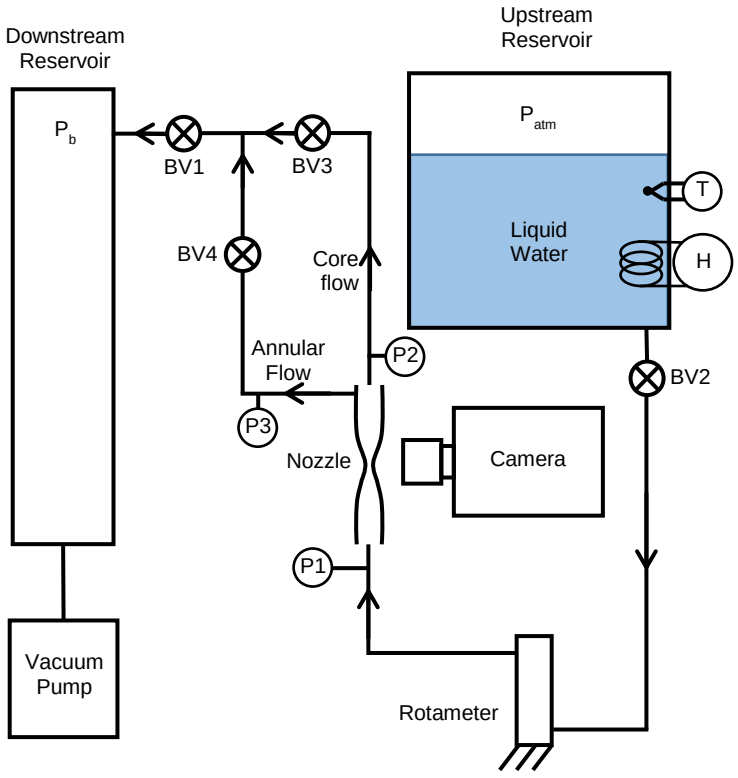

Figure 15: Experimental Setup with additional flow line to accommodate Inserts

These inserts were inserted in the diverging section of the nozzle with their tips near the vicinity of the throat as shown in Figure 16.

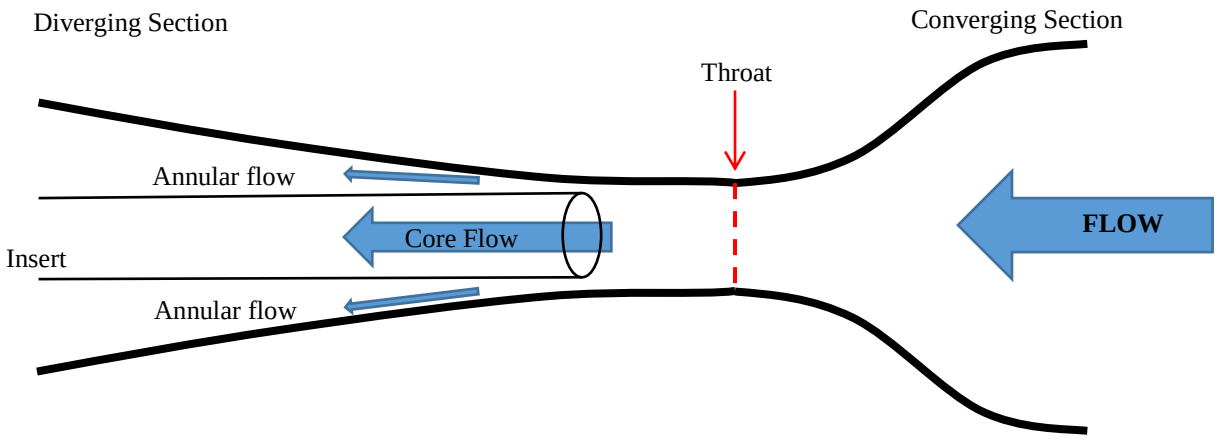

Figure 16: Schematic of insert placed in the nozzle

The inserts divided the flow into two flow paths: core flow and annular flow. The annular flow went around the insert and the core flow went through the insert. The annular flow path sucked off the fluid near the walls and caused the remaining fluid to flow through the core. These two flow paths were then combined into a single flow path before heading to the downstream reservoir. The inserts could be 3D printed so as to give more control over the shape of the annular diffuser. The schematic of the experimental setup with the additional flow path is shown in Figure 15.

2.3.1 3D Printed Solid Insert

A schematic of this insert is represented in Figure 17. This insert was designed with a gradually expanding flow area in the diverging section. It had a nose radius of 0.8 mm and had a straight section outer diameter of 3/8 inches (9.5 mm). Threads were added on one side in order to provide movement of the insert within the nozzle so that the distance between the insert tip and the nozzle throat could be adjusted with ease. Since the tolerance in the profile of the insert needed to be low, the insert was made by an Objet 30 Prime 3D Printer which is a poly jet machine. The material chosen was called *Veroclear*, provided by *Stratasys*. Veroclear is a transparent, rigid and nearly colorless material with good dimensional stability.

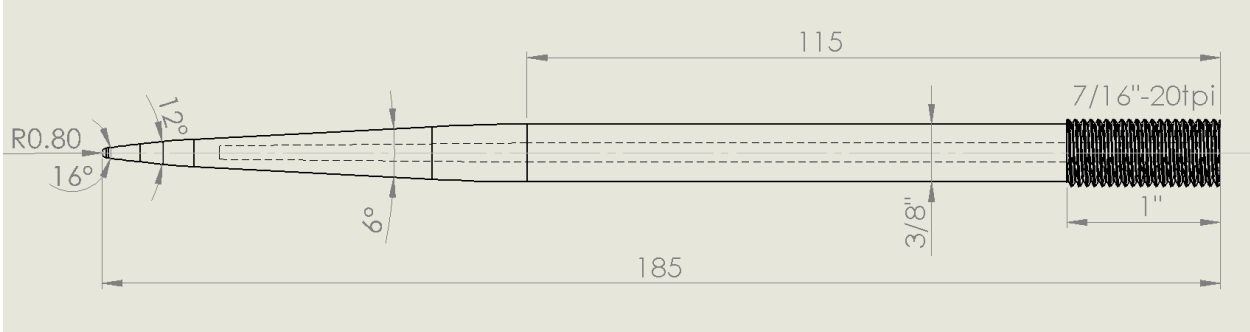

Figure 17: Schematic of the solid insert

After the part was printed and the support structures were removed by a water jet, post processing was performed to enhance the transparency of the part. The post processing comprised of three steps and they were: Dry-Sanding, Wet-Sanding and Polishing/Buffing. For the first step, i.e. Dry Sanding, the part was dried completely and a 200 grit sandpaper followed by a 320 grit sandpaper were used to remove any surface imperfections and unwanted layering. This process left some scratches on the surface and to remove them, the second step, i.e. Wet Sanding was done. The part was sanded by a finer sand paper with a 400 grit followed by an 800 grit and 1500 grit sand paper while keeping the surface to be sanded wet. The model was rinsed from time to time to remove any dust or debris. The part was then polished with a 3M Plastic Polish to give it a smooth surface finish. The final finished part had much better transparency after going through the processing and is represented in Figure 18.

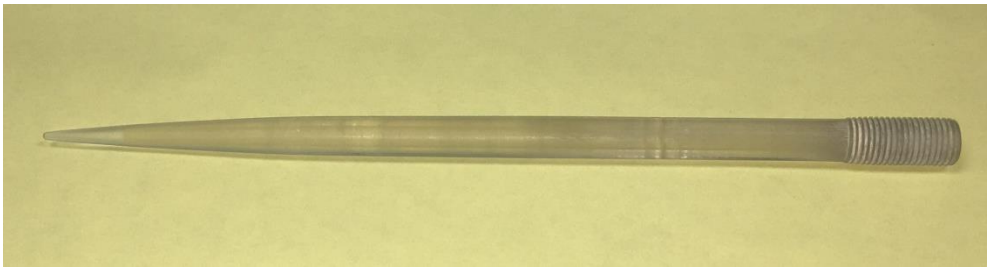

Figure 18: 3D Printed Solid Insert

The assembly of the insert in the nozzle is represented in the CAD drawing shown in Figure 19. The flow after going over the insert in the annulus region in the diverging section goes into the

branch of the Tee and proceeds towards the downstream reservoir. The other end of the tee provided lateral movement of the insert within the nozzle, making the adjustment of the position of the insert feasible.

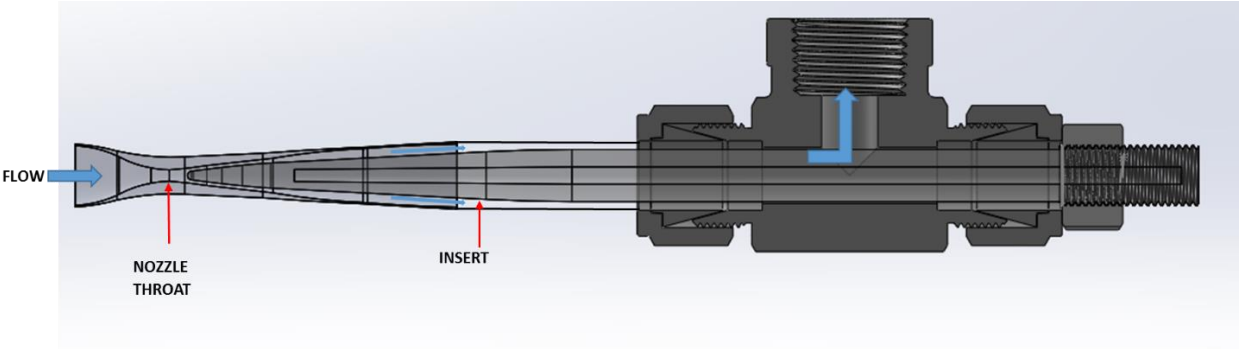

Figure 19: CAD Drawing of Nozzle Insert Assembly

2.3.2 Straight Tube Tubular Glass Insert

As an alternative to the insert above, straight sections of glass tubing were installed to get the flow into two separate flow paths, called the "Core" and "Annular" flow regions. As with the insert, this was considered a next step to testing out the theory that removing boundary layer would affect the initiation of cavitation. The experimental setup was modified by adding another flow passage in the downstream region. A schematic of the modified setup is represented Figure 15. The tube was placed in the downstream region to make two separate flow paths as explained earlier. The annular region would suck the boundary layer near the inner walls of the nozzle and hence cause the point of flow separation to go further downstream into the diverging section.

The Straight Tube glass insert was made of a thin NMR Tube that was attached to a 6 mm Outer Diameter (OD) glass tube with wall thickness of 1.1 mm. The insert had a step increment from the thin NMR tube to the regular thicker glass tube. NMR tubes were chosen for the tip of the insert as they have a very small wall thickness, thereby not allowing the wall thickness of the

tube to be an obstacle in the already small dimensions of the diverging section near the throat. The outer diameter of the NMR tube was 5 mm and it had a wall thickness of 0.015 in.

2.3.3 Straight Tube Brass Inserts

An issue with the straight NMR glass tube insert was that it was too fragile. Since the NMR tube had a very small wall thickness, the collapse of cavitation bubbles shattered the NMR tube after a few runs. The collapse of the cavitation bubbles also introduced vibrations in the system that may have contributed to the cracking of the thin walled NMR tubes.

In order to deal with this issue, a brass tube was used in place of the previous glass insert to eliminate shattering. Two brass tubes were used, each with a standard constant outer diameter of $1/8^{th}$ inch and $3/16^{th}$ inch. Both the brass tubes had a constant wall thickness that was measured to be 0.41 mm. Unlike the glass tube, the brass tubes were not transparent and hence did not allow visualization of cavitation in the core flow region. However, it was possible to observe cavitation around the outside of the brass tubes.

2.3.4 Tapered Tube Glass Insert

The diverging section of the nozzle had a conical characteristic downstream of the throat. Because of this, neither the straight tube glass insert nor the brass tube insert could be made parallel to the inner wall just downstream of the throat of the nozzle. The inlet of the insert produces sharp and abrupt interference with the flow entering the annular space between the insert and the inner wall of the nozzle. The solution to this issue, and a way to get even closer and more parallel to the inner wall downstream of the throat of the nozzle was to use a Pyrex glass tube with a tapered end that roughly had the same conical divergence angle as that of the diverging section. This tube is

illustrated in Figure 20. This tube had a tip diameter of about 3 mm and a wall thickness of 0.5 mm approximately near the tip.

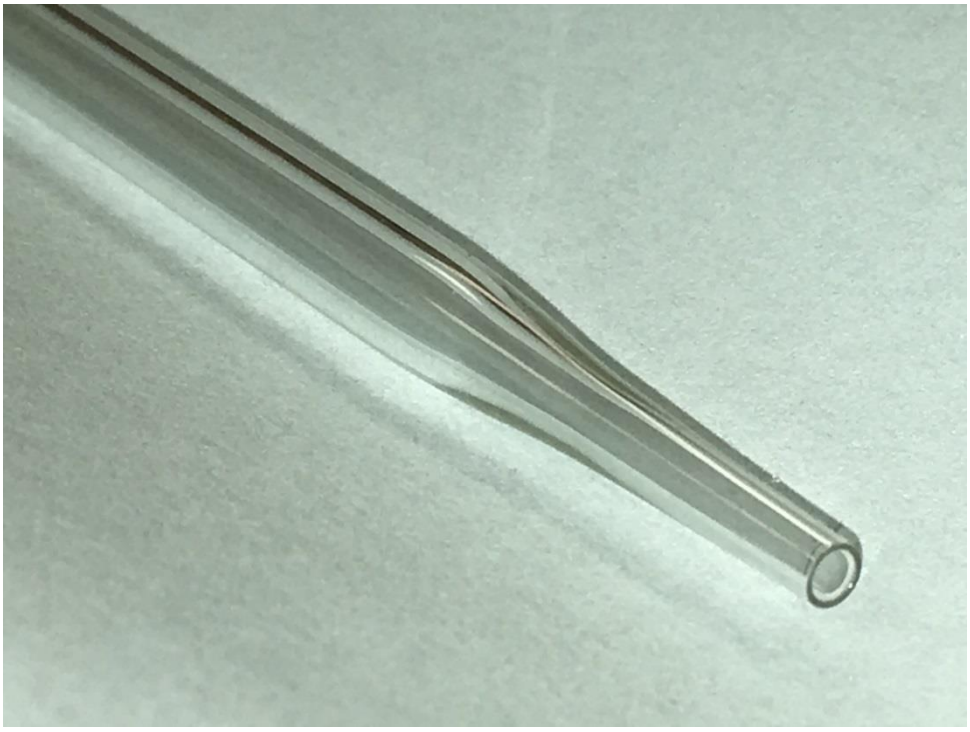

Figure 20: Tapered tube glass insert

All of these inserts were clamped by a nylon tube (bushing) that had a flush fit with the insert. This Nylon tubular bushing was then held in place by a regular compression fitting. The compression fitting pressed onto the nylon tube, making a very tight seal fit between the nylon and the tube without damaging the fragile glass tube. This kind of Nylon support was also used for the Straight Tube Glass, Brass and Tapered glass Insert. As mentioned earlier, the 3D Printed Solid insert had a standard outer diameter of 3/8" and hence was held by a standard 3/8" Compression Fitting sealed with Nylon ferrules.

2.4 Flow Measurements

The converging diverging nozzle test section was characterized by measurements of the temperatures, pressures and flowrate. Hence, these measurements were taken by the appropriate instruments at discrete locations within the system.

The volumetric flowrate entering the nozzle test section was measured by a rotameter as a percentage of its maximum flow rate which was 0.81 gpm (51 mL/s). The rotameter was located upstream of the nozzle inlet as depicted in Figure 9. In order measure more accurate and time-resolved behavior of the nozzle flowrate, a Coriolis flowmeter was also added in series with the rotameter.

Temperature measurements were made at selected points within the system. K-Type Thermocouples were installed at the nozzle inlet, nozzle outlet and the upstream/inlet reservoir as shown in Figure 9. These thermocouples are represented by T1, T2 and T3 respectively in the figure.

The absolute pressure was measured at selected locations in the system based on the type of setup. The pressure in the downstream low pressure (vacuum) chamber was measured by a dial gauge, which was calibrated against one of the absolute pressure transducers. This pressure is referred to as the back pressure or P_b as indicated in Figure 9. When the setup had no additional "annular" flow line, the pressures were measured at two locations: nozzle inlet and nozzle outlet. These pressures were measured by two Viatran 245 absolute pressure transducers designated by P1 and P2 in Figure 9. When an additional bypass flow line was added to accommodate the inserts, the absolute pressures were measured in both the core flow and the annular flow lines. The pressure in the core flow line was measured by a Viatran 245 absolute pressure transducer illustrated by P2

in Figure 15 and in the annular flow line by an Omegadyne PX429 absolute pressure transducer illustrated by P3 in Figure 15.

All instruments, the Coriolis mass flow meter, thermocouples and pressure transducers were connected to a HP34970A Data Acquisition Unit which was connected to a computer running "Agilent BenchLink Data Logger 3" software that allowed one to take timely measurements of various flow parameters at different time intervals.

Chapter 3 - Experimental Procedure

This chapter summarizes the procedure carried out to run the system as well as the procedure to calculate the important flow parameters in the nozzle, including the velocities, static pressures, pressure drops, and flow regime characteristics etc. Water was used in all the cases as the working fluid, and it flowed from the upstream elevated (high pressure, open to the atmosphere) reservoir to the downstream reservoir or the vacuum tank. All the lines leading from the upstream reservoir to the nozzle inlet were thermally insulated with a flexible polyethylene foam thermal insulated to minimize the heat loss to the surrounding. The temperature was controlled with the help of two immersion heaters installed in the upstream reservoir. One of them was accompanied by a stirrer to cause effectively uniform heating in the bulk of the liquid water.

3.1 Operation of Flow System

The upstream reservoir was filled with water until up to a consistent fixed level. In order to keep the nozzle inlet pressure approximately constant throughout the course of experiments, this upstream liquid reservoir level was allowed to decrease no more than 200 mm. The upstream reservoir was open to the atmosphere and the downstream reservoir was basically a vacuum tank where a negative gauge pressure was created using a vacuum pump. The flow was controlled with the help of the ball valve “BV1” represented in Figure 9. The ball valve “BV2” was used to shut off the supply of water into system in order to prevent leakage if any repair or modification was being made to the system.

Before running the experiment, the water in the inlet reservoir was heated to a required level by both the immersion heaters. Because the inlet reservoir was open to the atmosphere and was not thermally insulated, only the immersion heater with the higher power, and without the stirrer, was shut off. The immersion heater with the stirrer was still kept turned on. This immersion heater

had less power and it added to the water roughly the same amount of heat that was being lost to the surrounding, thus maintaining the temperature of the water at the desired level. The downstream reservoir was partially evacuated by a vacuum pump for each run, so as to create a negative gauge pressure in the downstream reservoir. This was done by closing all the valves connected to the downstream reservoir except the valve between the reservoir and the vacuum pump. The vacuum pump was then turned on and the back pressure in the reservoir reduced until the desired back pressure was reached. The pump was then shut off. The difference in pressure between the upstream and the downstream reservoir caused the flow of water between the reservoirs. To ensure steady state cavitation, air bubbles were evacuated from all the pipes and tubes by running the water across the system at very low flowrates.

After attaining the desired back pressure in the downstream reservoir, the main control valve or BV1 was opened slowly thereby increasing the mass flowrate in the system. The valve was opened slowly to have effective throttling or fine control over the flowrate just prior to the onset of cavitation. The flowrate kept on increasing with the valve opening until the apparent choking condition was reached. Any further reduction in the back pressure (or BV1 opening) had no effect on the mass flow rate of the water through the nozzle. Each experimental run was carried out for a period of few seconds up to as much as a minute or longer, and then the main control valve was then shut off. The downstream reservoir was brought back to atmospheric condition by opening a valve to let ambient air into it, and then the accumulated liquid water was subsequently drained out through a valve on the bottom of the reservoir. Since the downstream reservoir was partially filled with water after every run, it had to be drained out after every few experimental runs so it could be re evacuated to once again establish negative gauge pressure level. Therefore, the downstream reservoir had to be drained out after every few experimental runs.

3.2 Operation of High Speed Camera

The high speed camera was mounted in front of the nozzle on a scissor jack platform within a suitable distance away from the nozzle. The vertical height of the camera was adjusted until a proper field of view was obtained that covered the nozzle region under investigation. The high speed camera was connected to a computer through an Ethernet cable. The software accompanying the digital camera was called Photron Fast Viewcam (PFV). It gave control over various recording parameters including the camera framerate, exposure time, and spatial resolution. It also had the capability to capture and process the recorded images and videos, as well as allow one to perform a time-resolved analysis frame by frame.

Recording at high speeds needs sufficient lighting as mentioned earlier. The light was sent out through a fiber optic cable which was positioned just behind a frosted glass pane that resulted in a high intensity diffuse light illumination. This backlight illumination resulted in clear images of the nozzle without any shadows.

The high speed camera recorded videos at high frame rates and stored them in its on-board memory before transferring them to the computer memory. This gave a limited video recording time at high frame rates. In order to accommodate the limited memory of the camera, either frame rate, resolution or recording time had to be adjusted together. Frame rates above 35,000 gave a small field of view because of the required reduction in the spatial field of view. At 35,000 frames per second (fps), the maximum recording resolution was 192 x 356 pixels which gave a field of view much smaller than what was required to cover enough region of the diverging section. After going through many combinations of the frame rates and resolution, the optimum resolution was 320 x 680 pixels at 30,000 fps. At this optimal condition, the resolution was high enough to cover

a part of the nozzle converging section, throat and enough length of the diverging section. The detailed specifications of the camera can be found in Appendix-A.

After the resolution and the frame rate was set, the camera was calibrated by covering the lens with and the brightness was rebalanced using the PFV software. Once the brightness was calibrated, the focus of the camera was adjusted. This allowed the focal plane to be adjusted at different locations in the nozzle test section, such as the nearest wall or the mid-plane of the nozzle test section. After the camera position and focus were fine adjusted, the camera was triggered via the PFV software. Raw video was captured until the camera ran out of memory. This video was then saved to the desktop to perform the analysis later.

Chapter 4 - Experimental Results

This section includes the results of various experiments performed on the nozzle test section at different conditions. This section will provide a summary of the findings of the tests performed at different water temperatures and will include the data showing the variation of the flowrates and cavitation length with varying nozzle back pressure at each temperature. High speed visualization results of the initiation of cavitation are also discussed. The calculated negative pressures involved during steady state cavitation as well as just prior to cavitation in the metastable state are shown. A Coriolis mass flow meter was installed in the flow system to get time resolved measurements of the flowrate near the onset of cavitation. The effect of fluid temperature on the onset of cavitation is presented and certain hypotheses are made regarding the boundary layer separation effects to explain the results. These hypothesis are tested by using various inserts previously mentioned in Chapter 2 - and the test results involving these inserts are presented.

4.1 Variation of Flowrate

The effect of water temperature and inlet conditions on the nozzle flow rate variation is presented in this section. The steady state and transient behavior of the flowrate are also presented.

As mentioned earlier in Chapter 3, the water in the upstream reservoir was heated to the desired temperature level by an immersion heater. Three nominal inlet reservoir temperature levels of 25°C, 50°C and 70°C were chosen. Since all the lines leading to the nozzle from the upstream reservoir were thermally insulated, there was only about 2-3°C temperature drop noted between the upstream reservoir and the nozzle inlet. As the back pressure to the nozzle was reduced, by slowly opening the main control valve, the flow through the nozzle kept on increasing until it reached a threshold beyond which the flowrate did not increase further regardless of the any further reductions in the back pressure. This condition is indicative of a so-called choking condition [12].

At the choking condition, the flow through the nozzle remains constant and independent of back pressure. The volumetric flowrate was measured by the rotameter which measured the flowrate as a percentage of its maximum flowrate, i.e. 0.81 gallons per minute with an accuracy of ±2% full scale. The flowrate was measured for each temperature, first by setting the lowest back pressure in the downstream reservoir and then incrementing the back pressure gradually until it was close to atmospheric conditions. Thus, the measurements were taken at the lowest back pressures followed by incremental increases in the back pressures. The variation of flowrate with the back pressure for the three different temperatures is shown in Figure 21. For this data, the inlet pressure was kept constant.

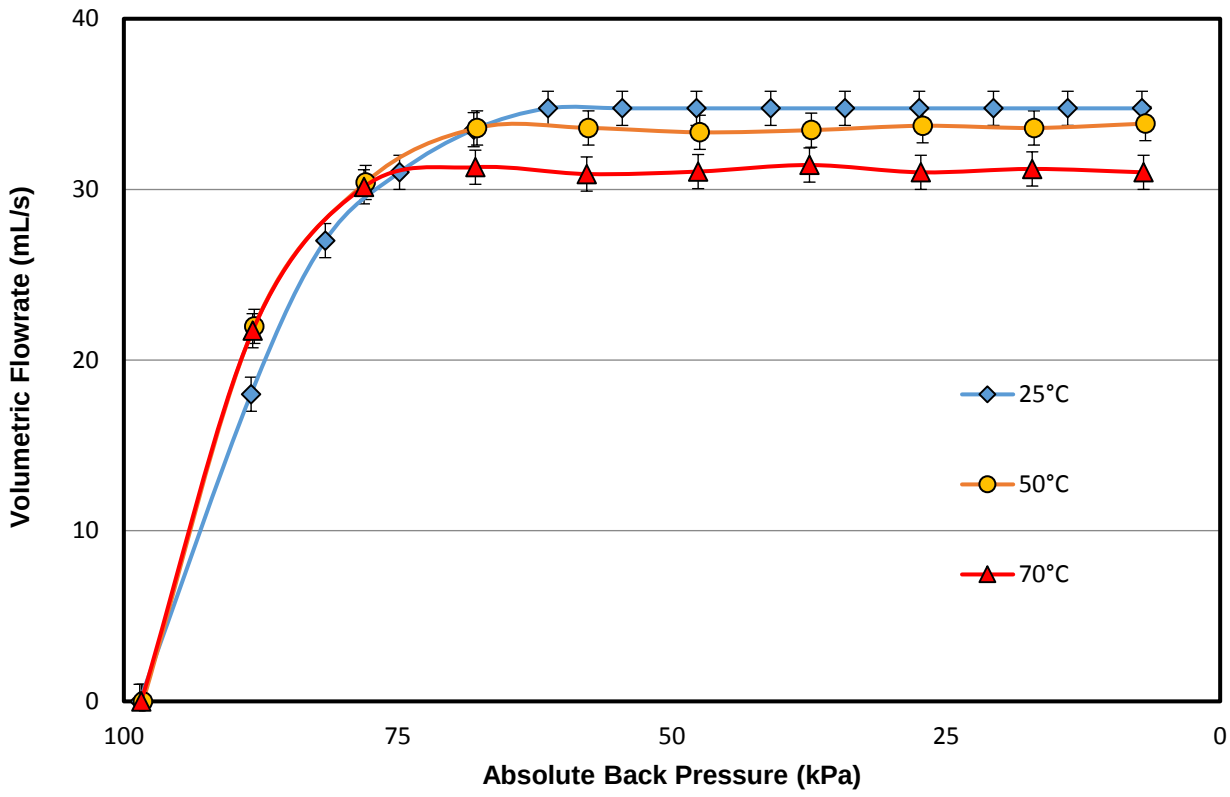

Figure 21: Temperature effects on flowrate through the nozzle at constant inlet pressure

It was observed that as the temperature was increased, the steady state choking flowrate level also decreased. Under steady state conditions, the choking flowrate of water for room temperature (25°C) was measured to be about 35mL/s. However, for the highest elevated temperature (70°C), the choking flowrate was reduced to about 31 mL/s as shown in Figure 21.

This choking condition suggests that sonic conditions are attained at some point in the nozzle. Since information travels at the speed of sound in a medium, when the flow achieves sonic conditions, any information regarding any further reduction in back pressure in the downstream region cannot travel upstream within the nozzle. Hence, the nozzle inlet region does not know about the reduction in the driving force in the downstream region, and the flowrate through the nozzle remains at a steady constant value. The average velocities obtained in the throat of the nozzle are easily calculated by dividing the measured volumetric flowrate with the known throat area. The resulting calculated velocities in the throat were around 10m/s to 15m/s.

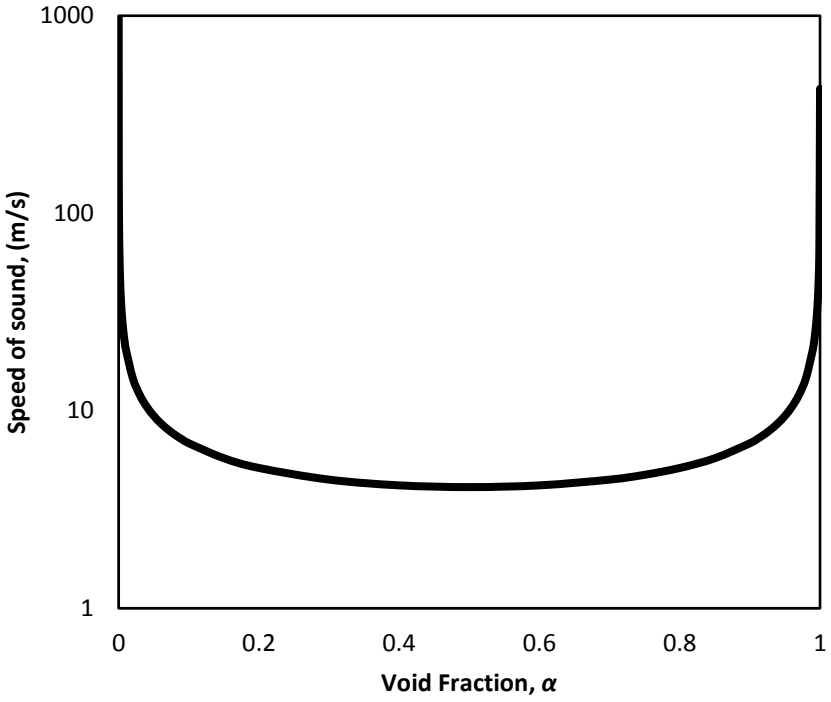

Figure 22: Variation of speed of sound with Void fraction of the liquid-vapor mixture

While the speed of sound in liquid water is very high, around 1,500 m/s, the speed of sound in the liquid-vapor mixture is quite low. The speed of sound was calculated by using Equation (2), from Wallis [15],which assumes that the two-phase flow is in thermodynamic and mechanical equilibrium.

$$c^2 = \left[(\alpha\rho_v + (1-\alpha)\rho_l)\left(\frac{\alpha}{\rho_v {c_v}^2} + \frac{1-\alpha}{\rho_l {c_l}^2}\right)\right]^{-1} \quad (2)$$

The speed of sound is dependent on the void fraction of the two-phase mixture. The speed of sound for the single phase liquid and single phase vapor is much higher compared to that of the mixture. An example would be the speed of sound for R-134a at 20°C, where the liquid sonic velocity is about 530 m/s and vapor sonic velocity is about 145 m/s. But using Equation (2), the speed of sound for the R134a mixture can be as low as 43 m/s.

Figure 22 is a plot of the speed of sound, calculated for different void fractions for water at 25°C using the above mentioned Equation 4. As depicted in the figure, the sonic velocities of the mixture are quite low and go as low as 4.3 m/s for a void fraction of 0.5. The velocities attained in the nozzle throat are very similar to these sonic velocities of the two phase mixture. Thus the sonic conditions are reached in the nozzle only when the flow has cavitated (flashed) and is present as a two phase mixture in the downstream region. Hence, we can conclude that the flow is sonic when the flow is cavitating and is a two phase mixture in the downstream region.

This conclusion does not, however, mean that the cavitation inception is associated with sonic flow. It was also observed that the flow cavitation initiated when the back pressure was such that the value of the flowrate was lower than the choking or the maximum flowrate. The flow started cavitation when the flowrate was about 90-95% of the maximum flowrate that could be achieved in the nozzle at the given conditions. This is presented in Figure 23, which shows the point of

cavitation initiation slightly less than the choked flow condition for the case of room temperature (25°C).

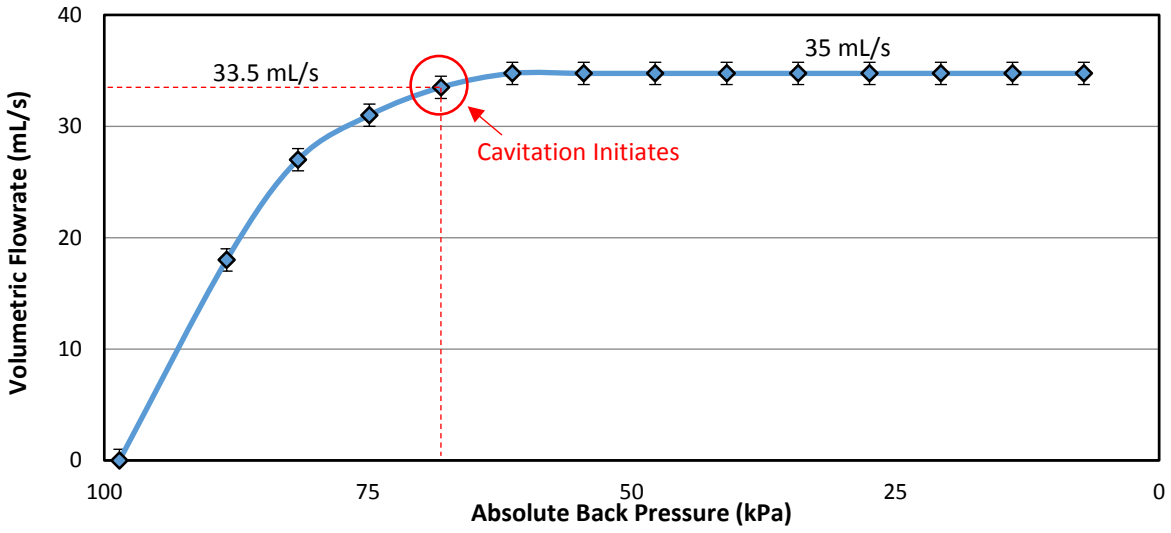

Figure 23: Measured Volumetric Flowrate for room temperature (25°C)

The observation made in Figure 23 is similar to the one pointed out by Brinkhorst [3] where cavitation inception or cavitation initiation did not correlate with the maximum choking flowrate. This points out to the possibility that the flow is not sonic when the cavitation initiates. At this subsonic condition, the information regarding the reduction in Back Pressure in the downstream region is transmitted across the nozzle into the inlet region and therefore, the system reacts by increasing its flowrate. The flowrate is increased until sonic conditions are reached in the nozzle and any further reduction in Back Pressure is not reflected back by increasing the flowrate of the system. Since the flow is subsonic at the cavitation inception or cavitation initiation point, the mixture velocity in the downstream section of the nozzle reduces as the area of the flow is increased. This is what we would expect for any subsonic flow. But, when the flow is sonic, the velocity of the two-phase mixture keeps on increasing in the diverging section as the area of flow is increased.

This points out to the speculation that the two phase flow gradually condense back to a single phase liquid in the subsonic condition (prior to the choking condition) with a small cavitation length without going through any condensation shock. And when the flow is sonic, the two phase mixture condenses back to single phase liquid through a condensation shock in the diverging section. The primitive analysis through which this conclusion was obtained is explained in the Appendix-C.

The discussion above corresponds when the steady state conditions have been reached. Transient measurements of the flowrate show that the flowrates goes beyond the choking flowrate momentarily before cavitation. To measure the transient behavior of the flowrate, a Coriolis flowmeter was added to the flow system that would measure the time resolved behavior of the mass flowrate with much higher accuracy. The flowmeter was connected to a HP 34970A Data Acquisition system that was connected to a computer via a RS232 cable; hence, it was possible to record time resolved measurements of the mass flowrate during the cavitation initiation process.

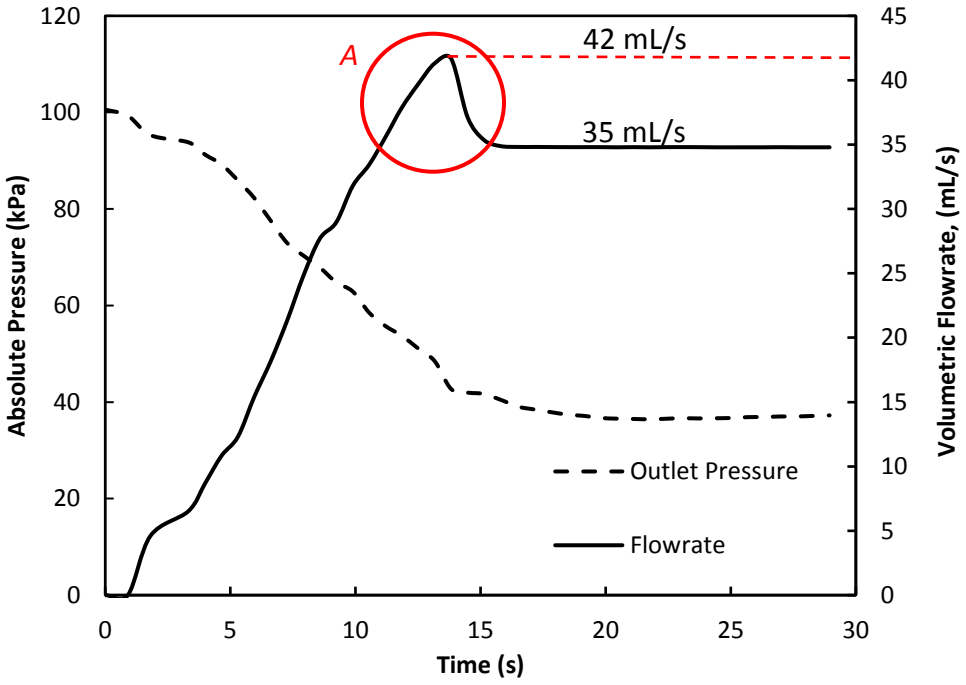

Figure 24: Timely behavior of flowrate at room temperature (25°C)

Figure 24 above shows the time resolved behavior of the flowrate measured by the Coriolis flowmeter for water temperature of 25°C. The variation of the nozzle outlet pressure measured by the pressure transducer *P2*, (refer to Figure 9), is also compared. As the main control valve is slowly opened, the outlet pressure is gradually reduced. With the reduction in outlet pressure, the flowrate kept on increasing, to a level well beyond expected choking flowrate, (35 mL/s for the room temperature), while still being in a single phase liquid state. The flow stayed beyond the choking flowrate momentarily, reaching a peak flowrate up to 42 mL/s, before it snapped back to the steady state choking flowrate of 35 mL/s as soon as cavitation initiated. This region of overshot flowrate is represented by region *A* in Figure 24. Therefore, the region *A*, where the fluid stayed beyond the choking condition, is an indication of the fluid existing in a metastable state. The fluid came out of the metastable state by cavitating and hence the flowrate adjusted to the more stable choking flowrate. When the fluid cavitated from the metastable condition, the resulting cavitation was quite explosive and violent due to the sudden vaporization of a large volume of the liquid water.

The effect of the inlet pressure level on the nozzle flowrate characteristics was also measured, while keeping the temperature constant. In order to control the nozzle inlet pressure, the elevation of the inlet reservoir was changed. Measurements were taken for two different inlet pressures (elevations). At the higher elevation, the nozzle inlet pressure was measured to be 97 kPa. The second level of elevation was when the reservoir was kept on the floor, which resulted in a much lower nozzle inlet pressure of 82 kPa.

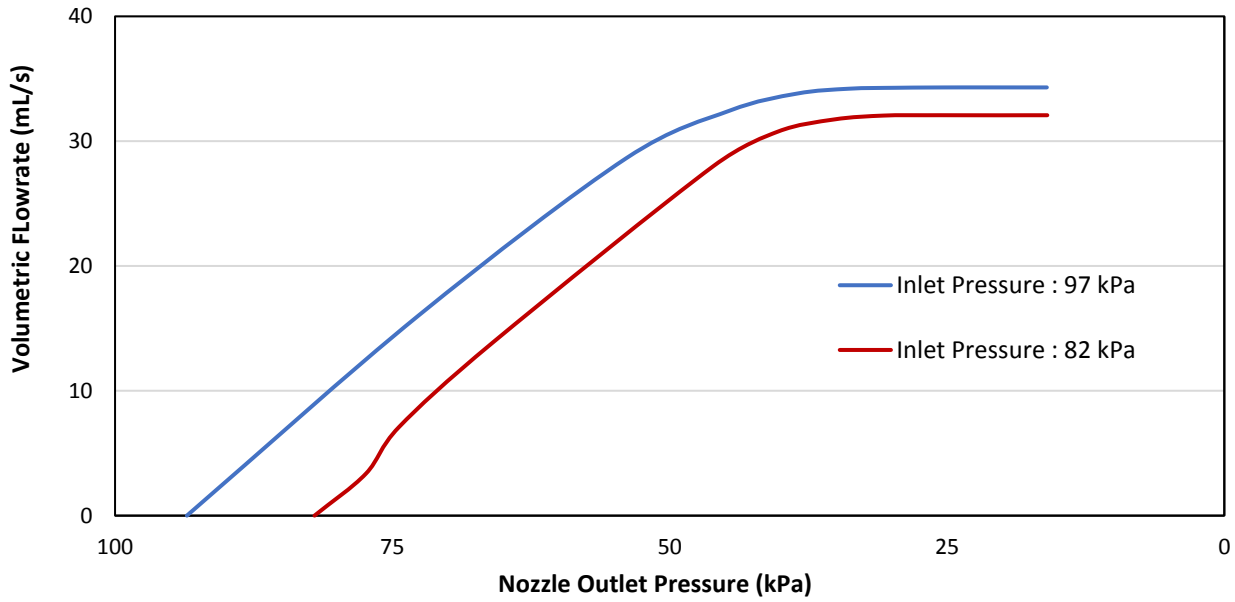

Figure 25: Variation of flowrate with inlet pressure at water temperature of 22°C

The flowrate of water at 22°C was measured by the Coriolis flowmeter and it is represented as a function of the absolute nozzle outlet pressure in Figure 25. Comparison of the flowrate can be made against either the nozzle outlet pressure or the nozzle back pressure. This is because the outlet pressure is always only around 2 kPa higher than the back pressure due to the frictional pressure drop between the nozzle outlet and the downstream vacuum chamber or the downstream reservoir.

As depicted in Figure 25, the flowrate increases as the nozzle outlet pressure is decreased until it reaches a maximum value or the choking condition beyond which the flowrate is unaffected by any further reduction in the nozzle outlet pressure. The flow chokes at different flowrates depending on the nozzle inlet pressure. For lower nozzle inlet pressure, the choking flowrate was about 32 mL/s; where as for higher nozzle inlet pressure, it was measured to be 35 mL/s.

Thus, from Figure 21 and Figure 25, it is verified that the choking flowrate depends on the inlet pressure and the saturation pressure of the fluid at the given temperature. This is what would

be expected from the analysis presented by Brinkhorst [3], where the mass flow rate is dependent on the saturation pressure and the inlet pressure, as shown in equation (1)

$$\dot{m} = \rho_l V_{th,\infty} A_{th} C_{cav} \tag{3}$$

Here, ρ_l is the liquid density, A_{th} is the area of the throat, which is 2.30 mm^2 for the nozzle currently under investigation. $V_{th,\infty}$ is the throat velocity which is calculated from:

$$V_{th,\infty} = \sqrt{\frac{2(P_{01} - p_v)}{\rho_l}} \tag{4}$$

The assumption here is that the cavitation (and hence, the sonic condition) occurs at the throat and the pressure at the throat is equal to the saturation pressure. C_{cav} is a correction factor that is obtained arbitrarily from one of the measured value of choked mass flowrate.

Equation (3) was used to calculate the mass flowrate for the nozzle currently under investigation at various conditions. The value of correction factor was calculated from one of the measurement of the choked mass flowrate of water at 25°C. The correction was calculated to be C_{cav} = 1.086. This correction factor was used to predict the choking mass flowrate at different inlet conditions and different water temperatures (hence different corresponding saturation pressures). Table 1 summarizes the calculated predicted and the experimentally measured choking flowrates for different flow conditions. The throat velocity in column 5 is calculated by using Equation (4).

Table 1: Calculations of the predicted mass flowrate

Temperature (°C)	Saturation Pressure (kPa)	Inlet Pressure (kPa)	Liquid Density (kg/m^3)	Calculated Throat Velocity (m/s)	Predicted Mass Flowrate (g/s)	Measured Mass Flowrate (g/s)
25	3.2	97	997	13.7	34.6	34.8
50	12.4	102	988	13.5	33.7	33.2
70	31.2	102	977	12.0	29.8	30.4

The predicted and measured mass flowrate were also compared in Figure 26 below against a 1-1 line.

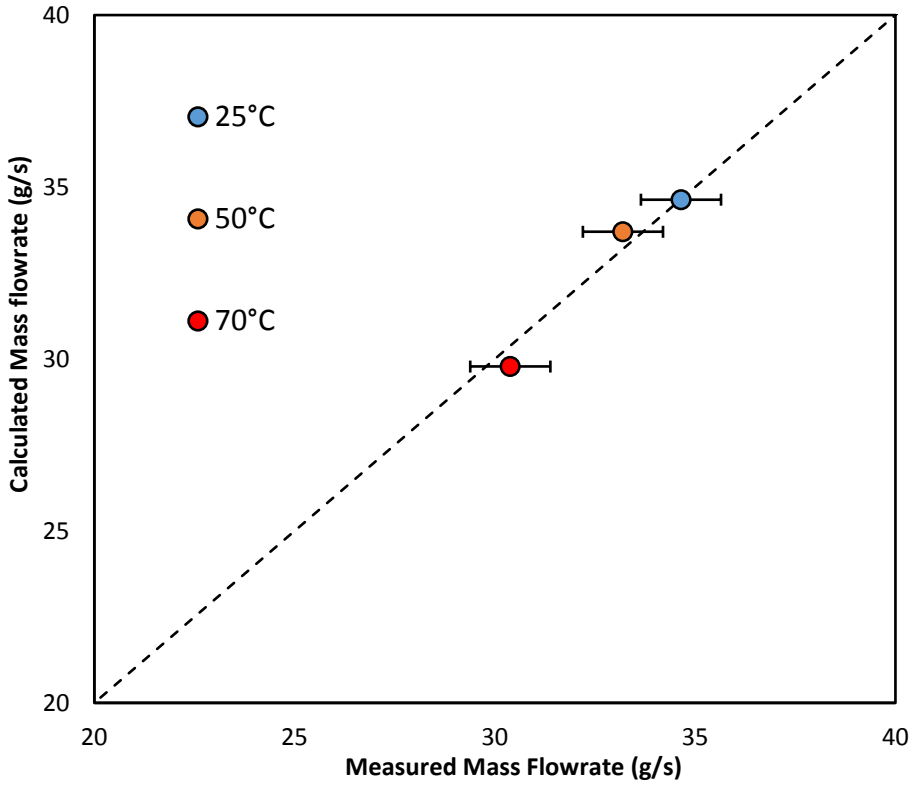

Figure 26: Comparison of predicted and measured mass flowrates at different flow conditions

4.2 Pressure Distribution in the Nozzle

The nozzle inlet and outlet pressures were registered by the pressure transducers *P1* and *P2*. Since the inlet pressure and the mass flowrate were known through experimental measurements, and the cross sectional area at any given location in the nozzle was calculated from the nozzle profile equations developed in Section 2.1, a 1D pressure profile inside the nozzle was estimated based on Bernoulli's principle. This 1D pressure profile was calculated by assuming a constant single-phase liquid density. Following this basic procedure, and also incorporating a simple model

(based on pipe flow) for frictional drop in a single phase liquid flow, the 1D pressure at any location in the nozzle is given by:

$$P(z) = P_i + \frac{1}{2}\rho\left[\frac{Q^2}{\left(\pi {R_i}^2\right)^2} - \frac{Q^2}{\left(\pi {R_z}^2\right)^2}\right] - \rho g h_z - \Delta P_{fz} \quad (5)$$

Equation (5) represents an approximate mechanical energy balance applied between the inlet conditions, denoted by the symbol *i*, and any arbitrary position in the nozzle, *z*. *Q* is the measured volumetric flowrate and *R* is the radius at the cross section under consideration. The third term on the right hand side of the equation takes into account the hydrostatic pressure difference due to gravity. The last term is the pressure drop due to friction in the nozzle. For simplicity, the pressure drop is estimated by integrating the frictional pressure gradient obtained from Equation (6), which is based on simple frictional pipe flow.

$$\frac{dP_f}{dz} = \frac{1}{2}\frac{\rho {v_z}^2 f}{D_z} \quad (6)$$

Here, v_z is the local average velocity at *z* calculated by dividing the volumetric flowrate with the cross sectional area at *z*. *f* is the friction factor for fully developed turbulent flow in a smooth pipe, and is given by:

$$f = \frac{0.316}{Re^{0.25}} \quad (7)$$

Using Equation (5), the pressure in the throat of the nozzle was calculated for different temperatures. These calculations are summarized in Table 2. The calculations presented in the table are obtained from the experimentally measured value of the choking flowrate (3rd column), rather than the calculated choked flowrate. The last row in the table shows the calculations for the case when the inlet pressure was lowered to 82 kPa as explained earlier. As mentioned earlier,

these pressures are calculated from the experimentally measured flowrates and inlet pressures. The results shown in Table 2 indicate that negative pressures are obtained in the throat of the nozzle. These negative pressures suggest that the liquid was under tension in the throat of the nozzle. Also, the difference between the Saturation Pressure at that temperature and the throat pressure remains roughly constant, around 27 kPa.

Table 2: Steady state pressure calculation results

Temperature	Saturation Pressure (kPa)	Choked Flowrate (mL/s)	Calculated Throat Pressure (kPa)	P_{sat}-P_{throat} (kPa)
25°C	3.2	34.8	-23.2	26.4
50°C	12.3	33.7	-14.4	26.7
70°C	31.2	30.5	4.7	26.5
22°C (Lower P_i)	2.6	32.0	-24.8	27.4

However, the difference in the saturation pressure and throat pressure shown in Table 2 is for the flow when frictional effects are taken into consideration. When the energy lost due to friction is ignored, the difference between the saturation pressure and the throat pressure is still approximately constant, but reduces to a value around 20 kPa.

Going back to Section 4.1, where the overshot flowrate was discussed in the region *A* in Figure 24, the flowrate went as high as 42 mL/s momentarily before snapping into steady state cavitation. When the flowrate was at its peak, the calculated pressure at the throat of the nozzle (from Equation 1) at that flowrate went as low as -70 kPa. This suggests that the liquid was under high tension prior to cavitation. Under this metastable state, the high tension is released by the fluid "snapping" or cavitating rapidly into a two phase mixture.

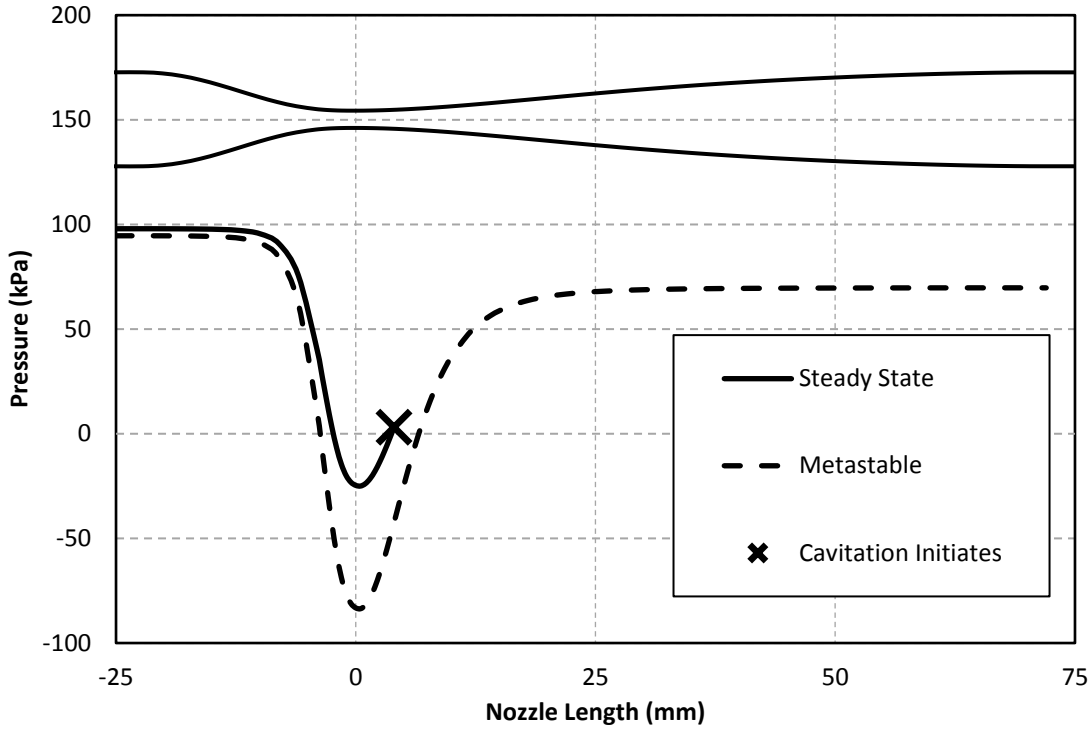

Figure 27: Calculated pressure distribution prior to cavitation (Metastable) and after cavitation (Steady State)

The calculated pressure distribution in the nozzle just prior to cavitation, while being in the metastable state, and after the cavitation onset into steady-state, is depicted in Figure 27. However, this pressure distribution model is only valid for single phase liquid flow. The pressure distribution cannot be calculated assuming steady state liquid flow beyond the point of cavitation initiation, which occurs approximately 2 mm downstream of the throat, because downstream of the cavitation initiation there exists a two-phase-liquid-vapor mixture flow, including a more complex two phase pressure drop model.

4.3 Cavitation Onset

This section presents flow visualization results and discussions of the cavitation onset and the position of cavitation initiation front in the nozzle. The visualization results of cavitation initiating from the metastable state are also shown for different water temperatures.

To capture the cavitation initiation process visually required the use of a high speed camera. Because of the high frame rates required, it was crucial to trigger the high speed camera recording at the right moment, since the recordings only took place for about 600 milliseconds at the typical frame rates of 30,000 frames/sec. Within this short time frame, the cavitation initiation process was captured for different water temperatures. Figure 28 shows selected frames from the video recording of cavitation initiation of water at 25°C when the back pressure in the downstream reservoir was set to 17 kPa. The main control valve, BV1, was slowly opened, and midway through the process of opening the valve, the high speed camera recording was triggered. The video recording was done at 37,500 frames per second. Frame (a) inFigure 28 shows the moment when a bubble is formed in the throat of the nozzle. This bubble expands as it propagates into the diverging section of the nozzle. The bubble explodes into a vapor cloud in frame (c), and goes into steady state behavior from frame (e) onwards. Frame (a) shows the bubble formation right at the center of the throat of the nozzle. However, the bubble formation does not occur at the center of the throat all the time. The vapor bubble in frame (a) might have formed near the wall closer to the camera, or the wall away from the camera. The bubble was formed at the side walls of the nozzle throat in other trials of the same visualization experiment. It was also observed that the steady state cavitation front, or the distance downstream of the throat at which steady state cavitation occurs remains at a fixed value of approximately 2 mm. This will be discussed further later on in this section.

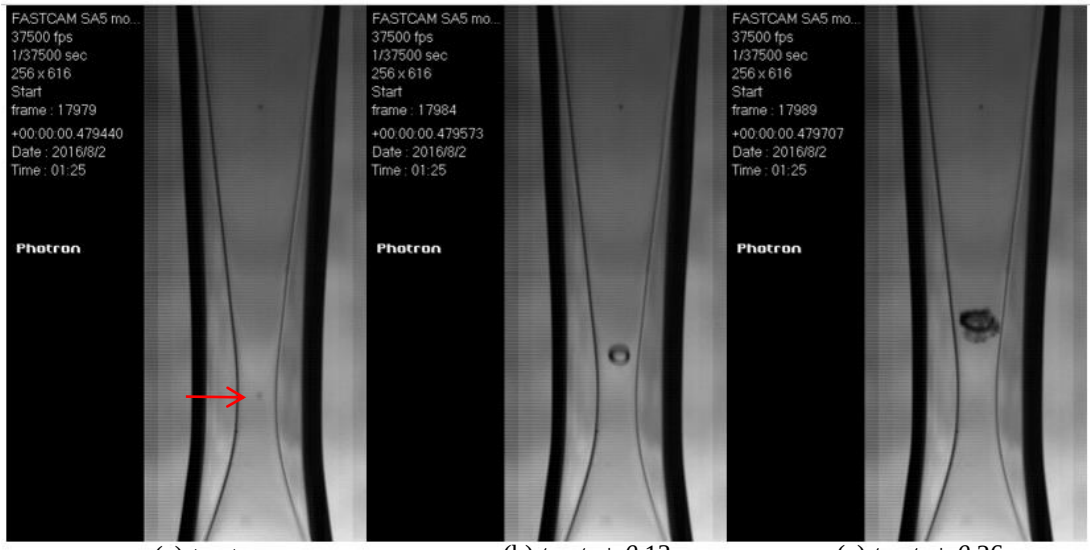

(a) $t = t_0$ (b) $t = t_0 + 0.13$ (c) $t = t_0 + 0.26$

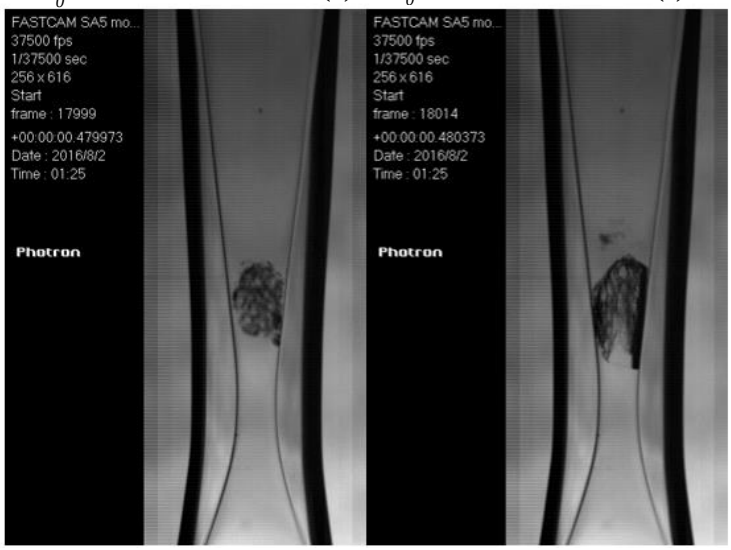

(d) $t = t_0 + 0.53$ (e) $t = t_0 + 0.93$

Figure 28: Cavitation initiation for water at 25°C, P_b = 17 kPa

Figure 29 shows selected frames of the high speed recording of cavitation initiation at a water temperature of 70°C. The high speed video was shot at 30,000 frames per second. After going through the vapor bubble expansion, the cavitation front stayed at a semi-stable state much further into the downstream region for an extended amount of time as seen in Frames (a)-(c) in Figure 29. The cavitation front then fell back to a stable location and stayed in a steady state condition for the

rest of the video recording as shown in frame (d). The horizontal lines drawn in Figure 29 indicate the location of the cavitation front.

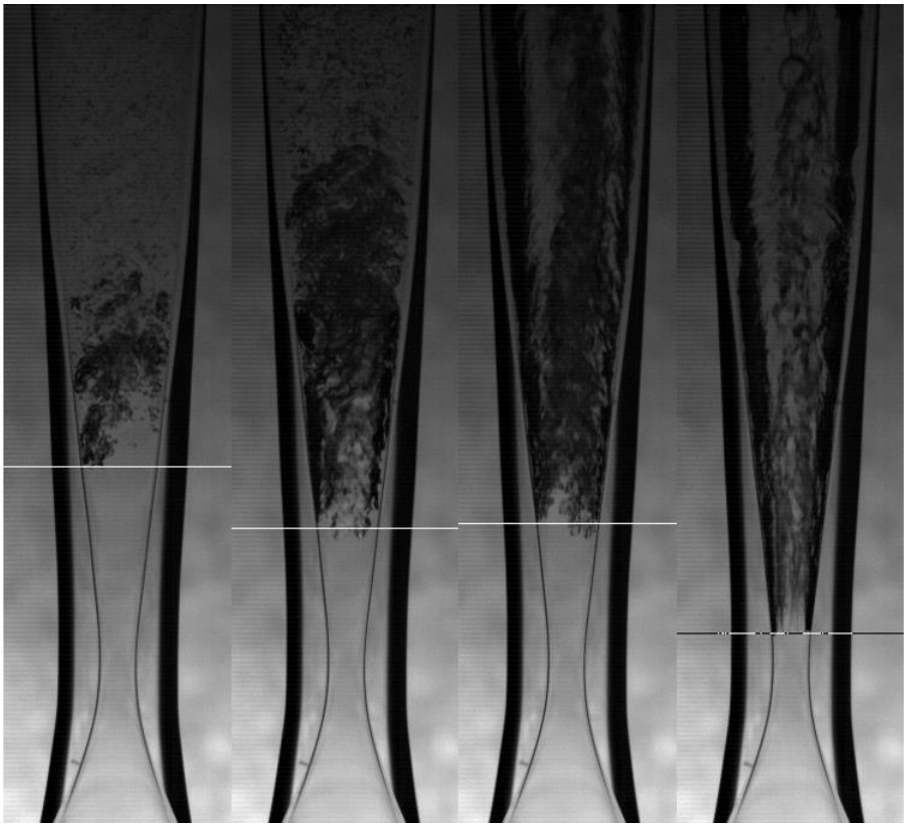

(a) $t = t_0$ (b) $t = t_0 + 33$ ms (c) $t = t_0 + 266$ ms (d) $t = t_0 + 333$ ms

Figure 29: Intermediate cavitation front at a semi-stable state observed for water temperature of 70°C

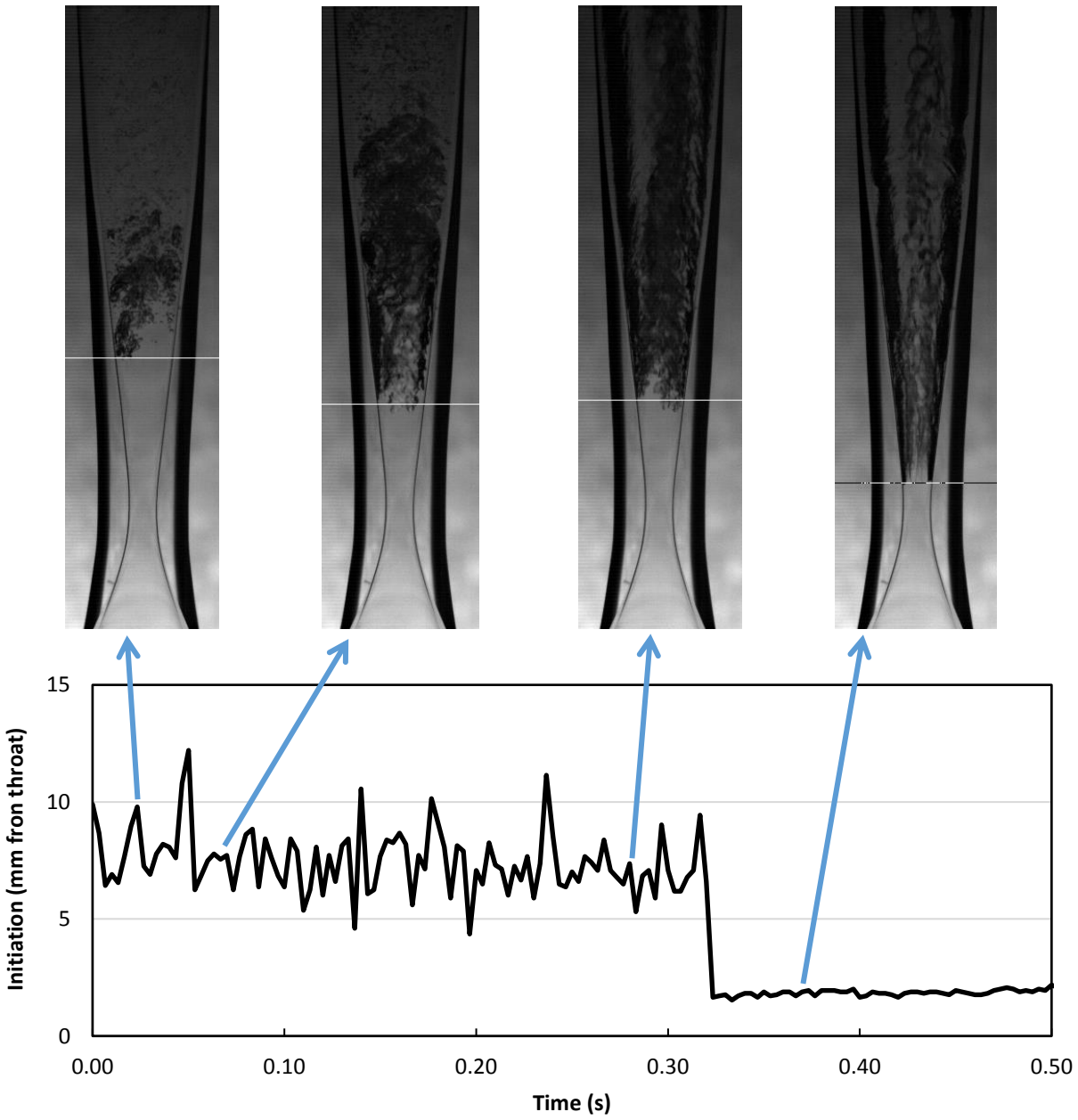

Figure 30: Time resolved distance of the cavitation front from throat of nozzle at a water temperature of 70°C

Time resolved measurement of the distance of the cavitation front from the nozzle throat were taken for the visualization results shown in Figure 29. The PFV software measured the vertical distance between the throat and the cavitation front and then converted it to millimeters through an appropriate scaling. These transient measurements are summarized in Figure 30 along with the

flow visualization results. The cavitation front stayed at the semi-stable location at about 5 mm to 10 mm away from the throat for about 300 ms and then moved rather abruptly to the more stable location which was about 2 mm downstream of the throat.

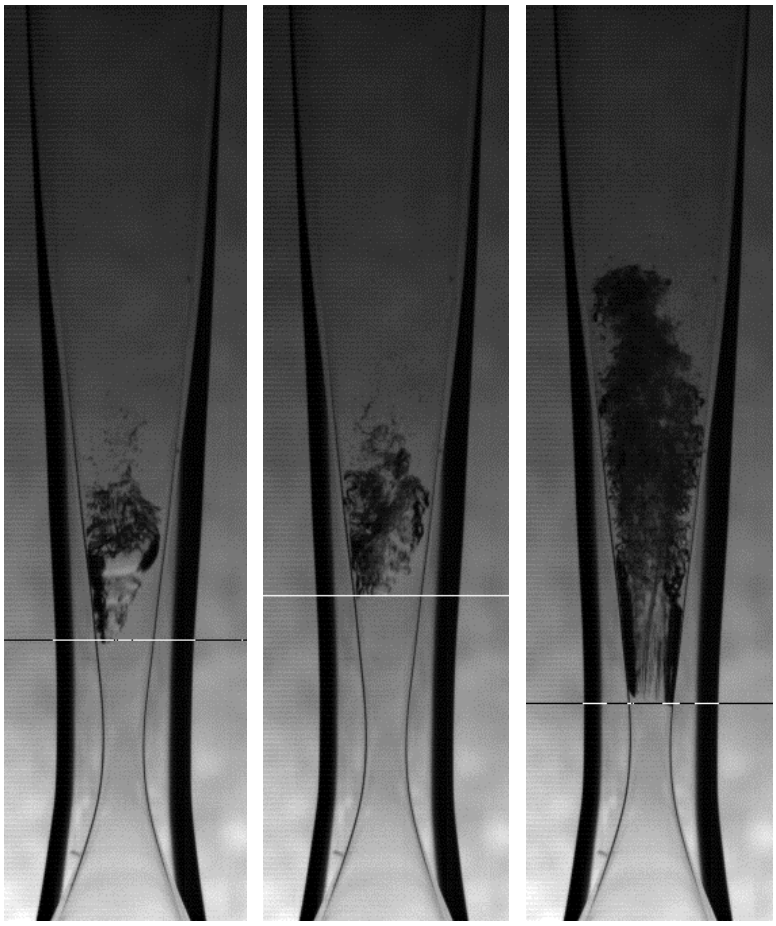

(a) $t = t_0$ (b) $t = t_0$+3 ms (c) $t = t_0$+7 ms

Figure 31: Intermediate cavitation front at a semi-stable state observed for water temperature of 50°C

Figure 31 shows selected frames of the high speed recording of cavitation initiation at a water temperature of 50°C. The high speed video was shot at 30,000 frames per second. After going through the vapor bubble expansion, the cavitation front stayed at a semi-stable state much further into the downstream region for an extended amount of time as seen in Frames (a) and (b) in Figure 31Figure 29. The cavitation front then fell back to a stable location and stayed in a steady state

condition for the rest of the video recording as shown in frame (c). The horizontal lines drawn in Figure 31 indicate the location of the cavitation front.

Time resolved measurement of the distance of the cavitation front from the nozzle throat were taken for the visualization results shown in Figure 31. These transient measurements are summarized in Figure 32 along with the flow visualization results. The cavitation front stayed at the semi-stable location at about 5 mm to 7 mm away from the throat for about 5 ms and then moved rather abruptly to the more stable location which was about 2 mm downstream of the throat

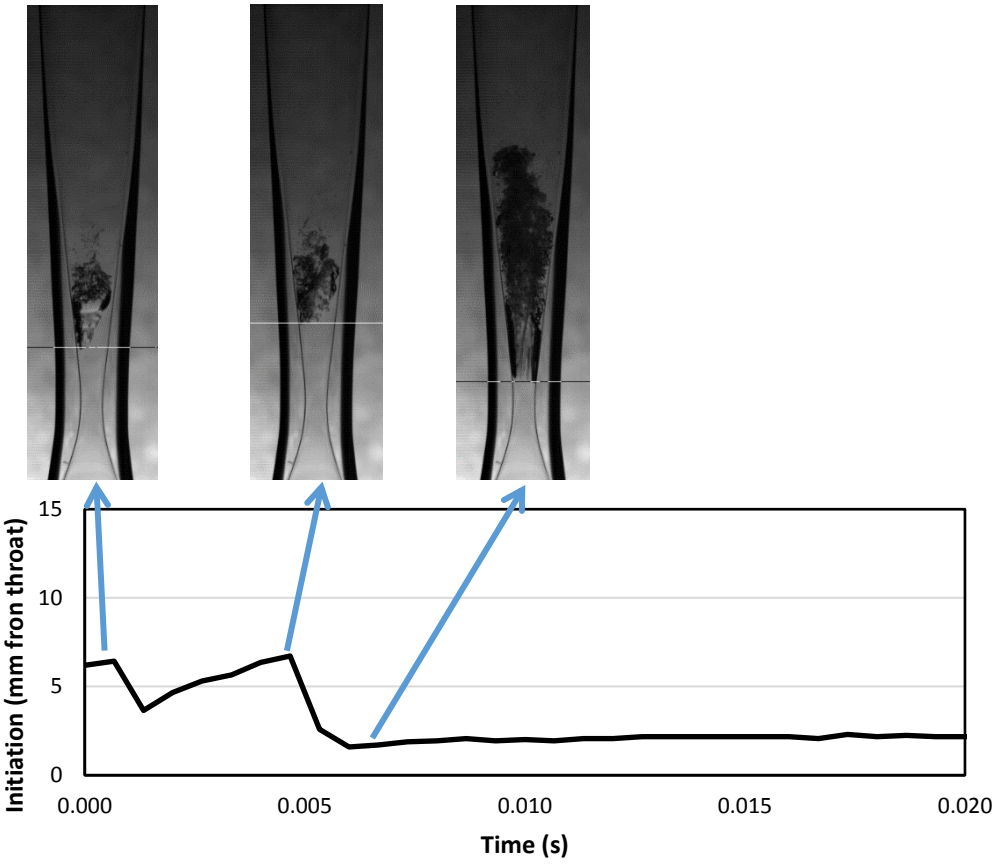

Figure 32: Time resolved distance of the cavitation front from the throat of nozzle

The implications of the occurrence of this transient cavitation front are not fully known, and this phenomena is still under investigation.

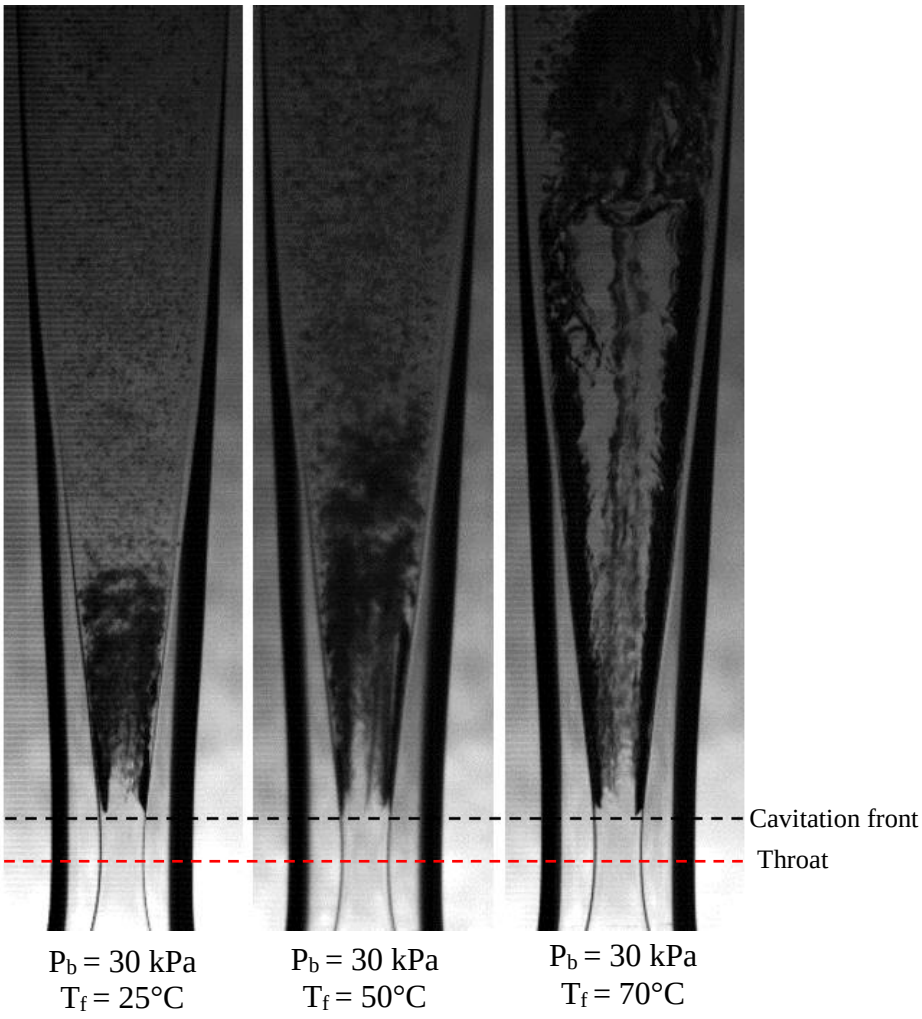

Figure 33: Cavitation at different temperatures and constant back pressure

The lowest static pressure in the nozzle is at the location where the flow area is the lowest, i.e. at the throat of the nozzle. Therefore one would expect the cavitation front to be at this position of lowest pressure. The flow visualization results however, reveal that under steady-state conditions, the cavitation front location stays, not at the throat, but a few millimeters downstream, resulting in a two-phase region which persists well downstream of the throat. This could be attributed to the presence of the "Vena Contracta" effect in the diffusing section of the nozzle, causing the smallest flow area, and hence the lowest pressure downstream of the throat [16]. The point of initiation of cavitation was captured for different water temperatures and is shown in Figure 33 above. The

figure shows that cavitation initiation occurs at the same distance downstream of the throat regardless of the water temperature.

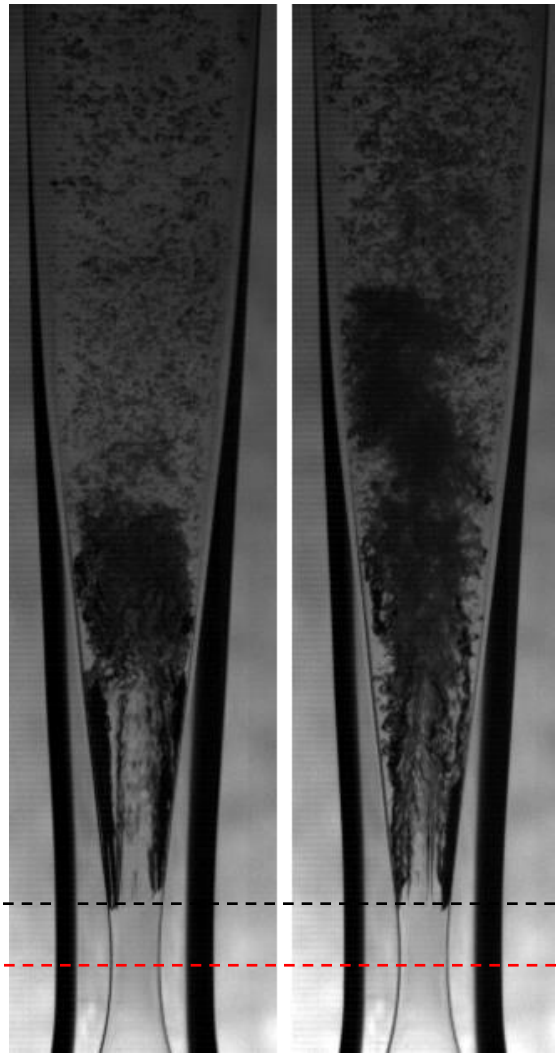

$P_b = 10 \pm 2$ kPa
$P_i = 82$ kPa

$P_b = 10 \pm 2$ kPa
$P_i = 97$ kPa

Figure 34: Cavitation at different inlet pressures and constant back pressure

Figure 34 above shows cavitation front in the nozzle at a constant back pressure but at different inlet pressures at a water temperature of 22°C. Once again, the position of the cavitation front remains at the same location, approximately 2 mm downstream of the throat.

When the back pressure to the nozzle is such that the cavitation just starts to initiate, the flowrate is lower than the choking flowrate, as described earlier in section 4.1. Keeping that in

mind, if the flow is in the choking condition, and if the effective back pressure to the nozzle is increased gradually, the flowrate reduces from the choking to the non-choking flowrate while the flow is still cavitating. The flow cavitates until the back pressure becomes high enough and the flow does not cavitate anymore. The position of cavitation initiation was captured for this case, i.e. when the flow goes from the cavitating choking condition to the cavitating non-choking condition and then goes the single phase all liquid flow.

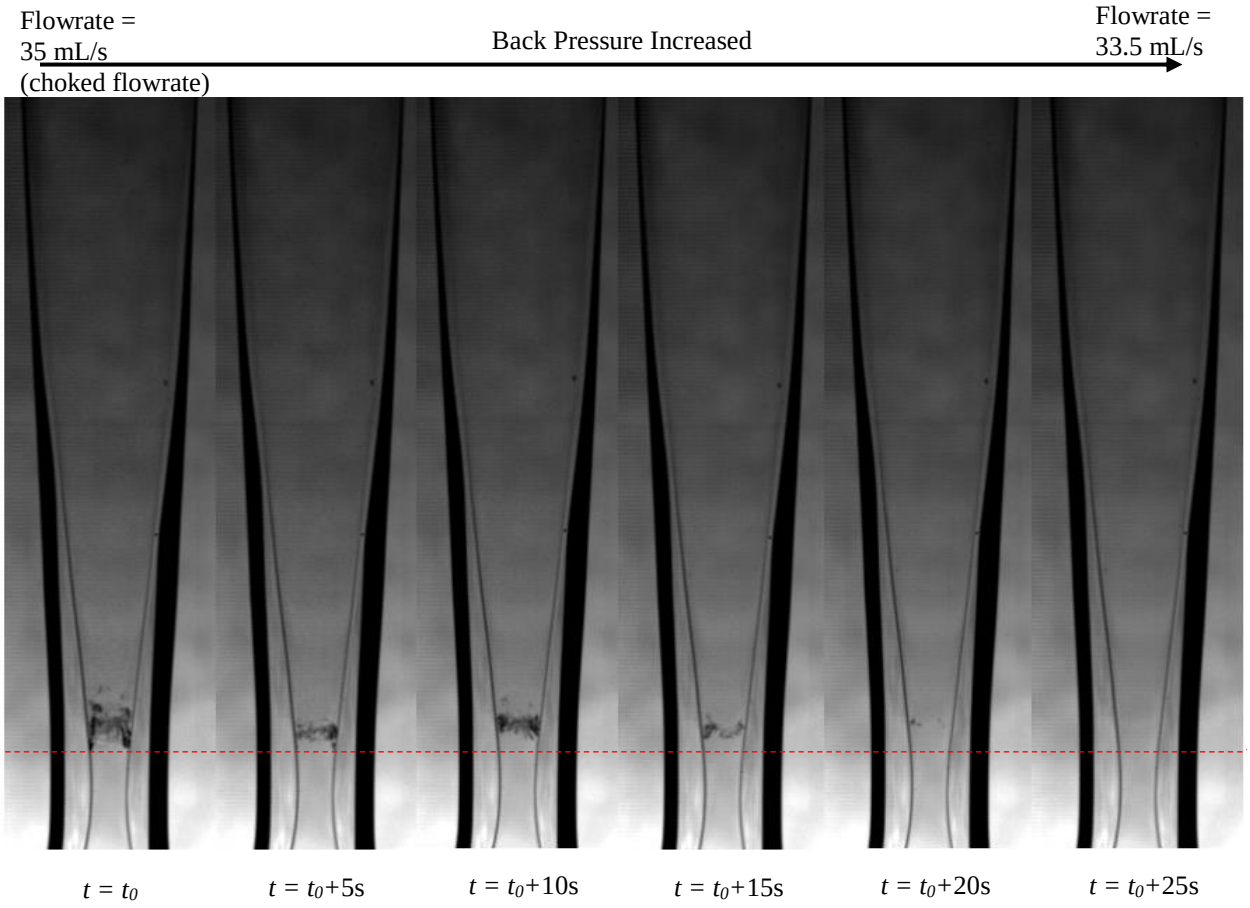

Figure 35: Movement of cavitation initiation position at high back pressures for water temperature of 25°C

Figure 35 shows the position of cavitation initiation front as the back pressure in the downstream reservoir was increased. The back pressure in the downstream reservoir increased with time due to the fact that the water kept on filling the downstream reservoir as the fluid flowed

through the nozzle. The figure above shows selected frames from the video recording at 60 frames per second. The first frame shows the steady state choked condition where the position of cavitation initiation front was approximately 2 mm downstream of the throat (red line). As the back pressure was increased, and hence a corresponding decrease in flowrate, the upstream cavitation front appeared to move downstream in the diverging section; whereas the condensation region, or the position beyond which the flow was single phase liquid flow, appeared to stay at the same location. The right most frame shows when the flow didn't cavitate anymore and was single phase liquid flow all the way to the downstream reservoir.

4.4 Cavitation Length

The flow visualization results in Figure 33 and Figure 34 show that after a certain length within the diverging section, the flow condenses back to single-phase liquid flow before exiting the nozzle. Although for water, the temperature variation throughout the nozzles was observed to be small, this two-phase zone corresponds to the region of low temperature and pressure which could conceivably be utilized for heat absorption with other refrigerant fluids. The length of this two-phase region, thus becomes important since, the longer the length of the low temperature region, the greater is the surface area the heat transfer from the surroundings (potential cooling effect).

The length of this two phase region was measured for various back pressures at different water inlet temperatures. The basic technique used to calculate the length of the two-phase region is shown in Figure 36. As shown in the figure, the cavitation initiates at Position 1. The two phase region persists for some distance along the diffuser/diverging section and then starts to dissipate at Position 2 and completely collapses at Position 3. The average, or the midpoint of Position 2 and Position 3 is labelled as Position 4. The length of the two-phase region is calculated as the distance between Position 1 and Position 4. The distance between Position 2 & Position 4, and between Position 4 & Position 3 is considered as an estimate of the nominal uncertainty in the length measurement.

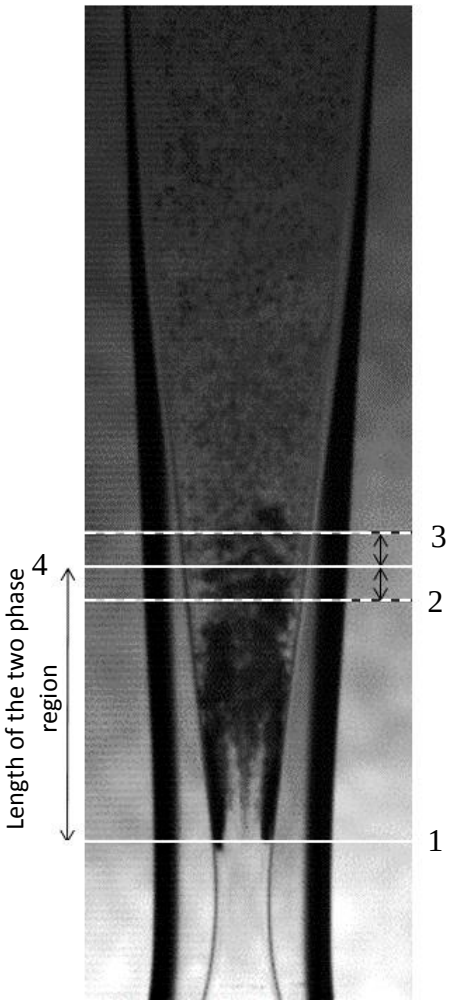

Figure 36: Measurement of the length of the two-phase region

This length of the two phase region varied for different back pressures and different water temperatures. The length was measured for the three different water temperatures of 25°C, 50°C and 70°C. High speed video was recorded at 30,000 frames per second for selected values of back pressure for about 0.5 second when the cavitation was in a steady state. Selected frames from the high speed video recording were then analyzed manually. The length and the position uncertainty estimate were calculated for each of these frames by using the procedure explained above. This measurement of length and the uncertainty estimate was then time-averaged for the analyzed frames to give the length measurement at the given value of back pressure. The length was

measured in pixels using the PFV software and then was converted to millimeters from appropriate image scaling information.

The sequence of images shown in Figure 37 show the cavitation phenomena at a water temperature of 25°C for three different values of back pressure in the downstream reservoir. As mentioned earlier, the cavitation initiation or the cavitation onset is at the same location within the nozzle irrespective of the back pressure.

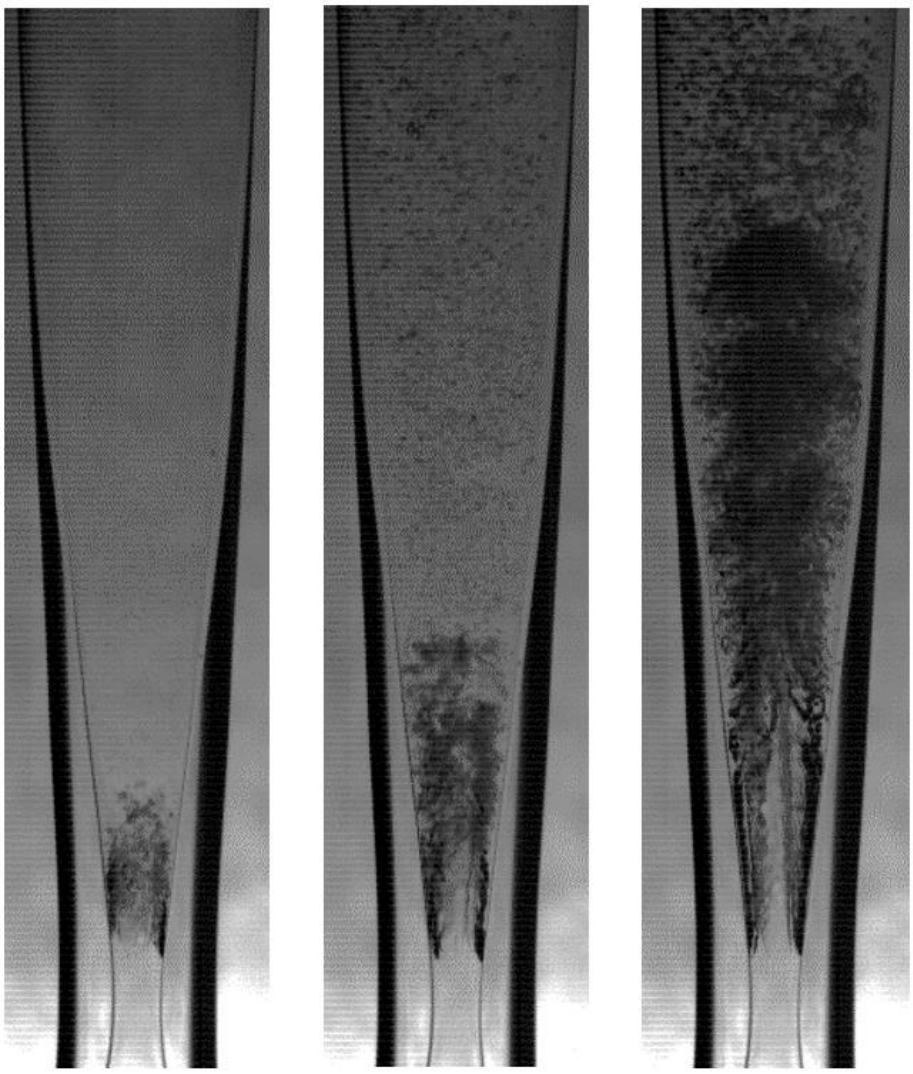

P_b = 50 kPa
T_f = 25°C

P_b = 30 kPa
T_f = 25°C

P_b = 10 kPa
T_f = 25°C

Figure 37: Cavitation at different back pressures for T_f = 25°C

However, the location where the majority of the flow condenses back to single phase liquid at some distance downstream of the throat varies significantly with the back pressure. This distance, referred to as the cavitation length, or the length of the two-phase region, increases as the back pressure is reduced. Three nominal values of absolute back pressures, 50 kPa, 30 kPa and 10 kPa are illustrated in Figure 37.

The measured length of the two phase region at a water temperature of 25°C is represented in Figure 38. As the back pressure is reduced, the length of the cavitating region kept on increasing, reaching peak values of 17 mm at a back pressure value of 13 kPa absolute.

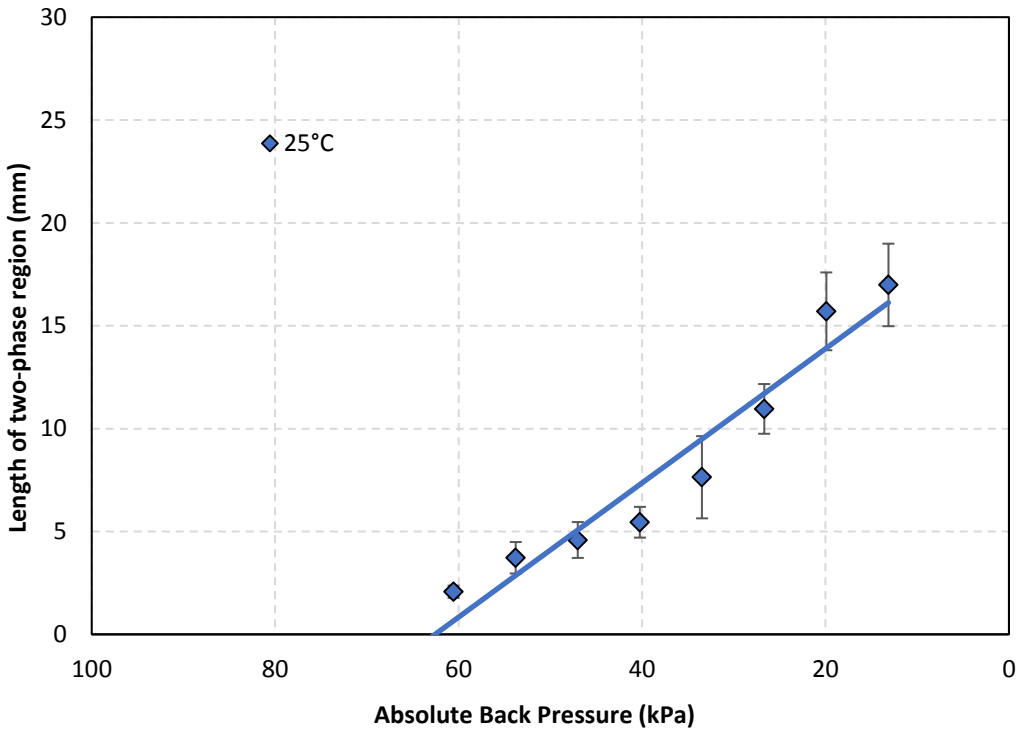

Figure 38: Variation of cavitation length with back pressure for T_f = 25°C

The sequence of images shown in Figure 39 show the cavitation phenomena at a water temperature of 50°C for three different values of back pressure in the downstream reservoir. As mentioned earlier, the cavitation initiation or the cavitation onset was at the same location within

the nozzle irrespective of the back pressure. Cavitation for three different nominal back pressures of. 50 kPa, 30 kPa and 10 kPa are represented in the Figure.

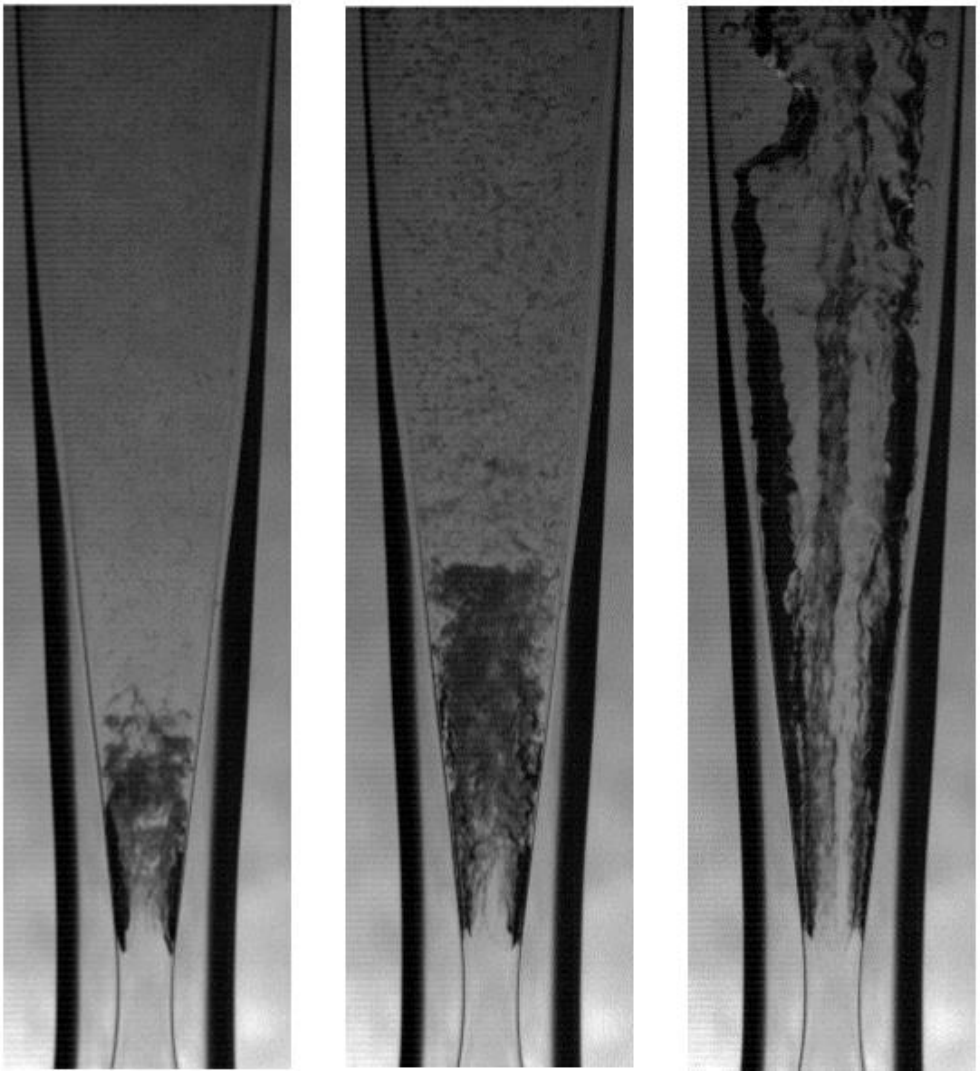

P_b = 50 kPa
T_f = 50°C

P_b = 30 kPa
T_f = 50°C

P_b = 10 kPa
T_f = 50°C

Figure 39: Cavitation at different back pressures for T_f = 50°C

The length of the two phase region increased as the back pressure was reduced. For back pressure values of 50 kPa and 30 kPa, the two phase flow condensed back to single phase within the diverging section. However, for a back pressure value of 10 kPa absolute, the flow did not condense back to single phase liquid within the diverging section. The flow remained in a liquid-

vapor mixture state throughout the flow passage leading to the downstream reservoir or the vacuum chamber,

The measured length of the cavitation region as explained by the procedure earlier in this section is represented in Figure 40. The cavitation length increased as the back pressure reduced, and for much lower values of back pressure, the flow never condensed back to single phase liquid within the diverging section.

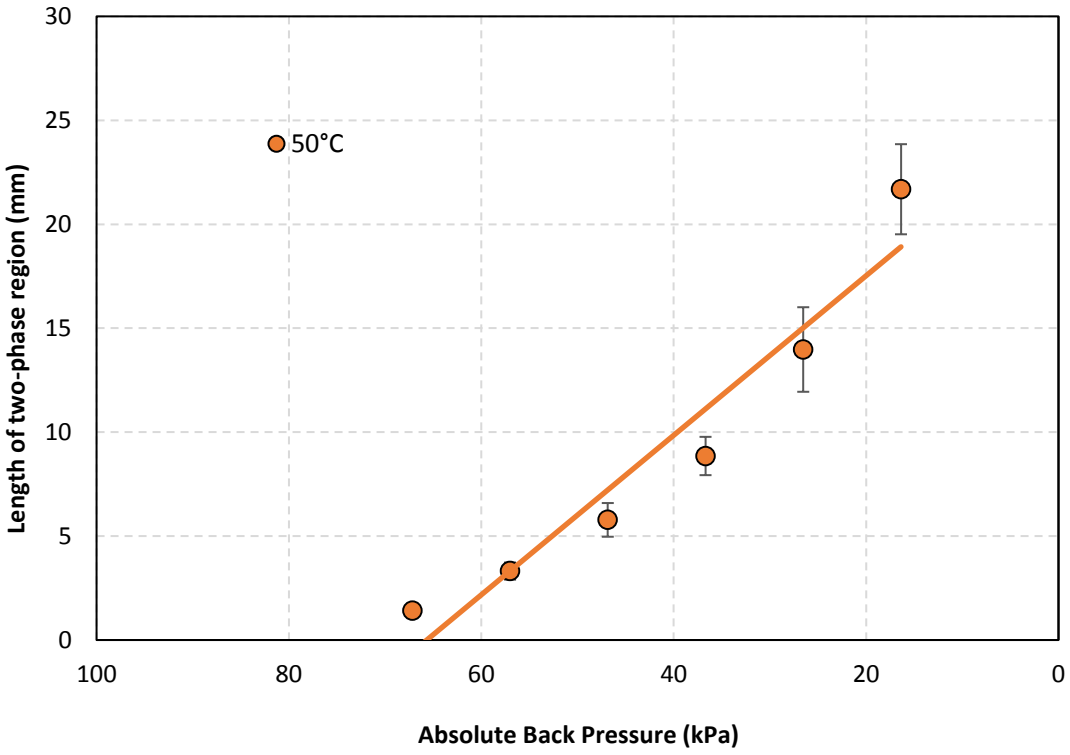

Figure 40: Variation of cavitation length with back pressure for T_f = 50°C

The sequence of images shown in Figure 40 show the cavitation phenomena at a water temperature of 70°C for three different nominal values of back pressure in the downstream reservoir. Once again, the position where the cavitation initiated in the nozzle remained at the same distance downstream of the throat regardless of the back pressure. Cavitation for four different nominal back pressure values of 70 kPa, 50 kPa, 30 kPa and 10 kPa is represented in Figure 41.

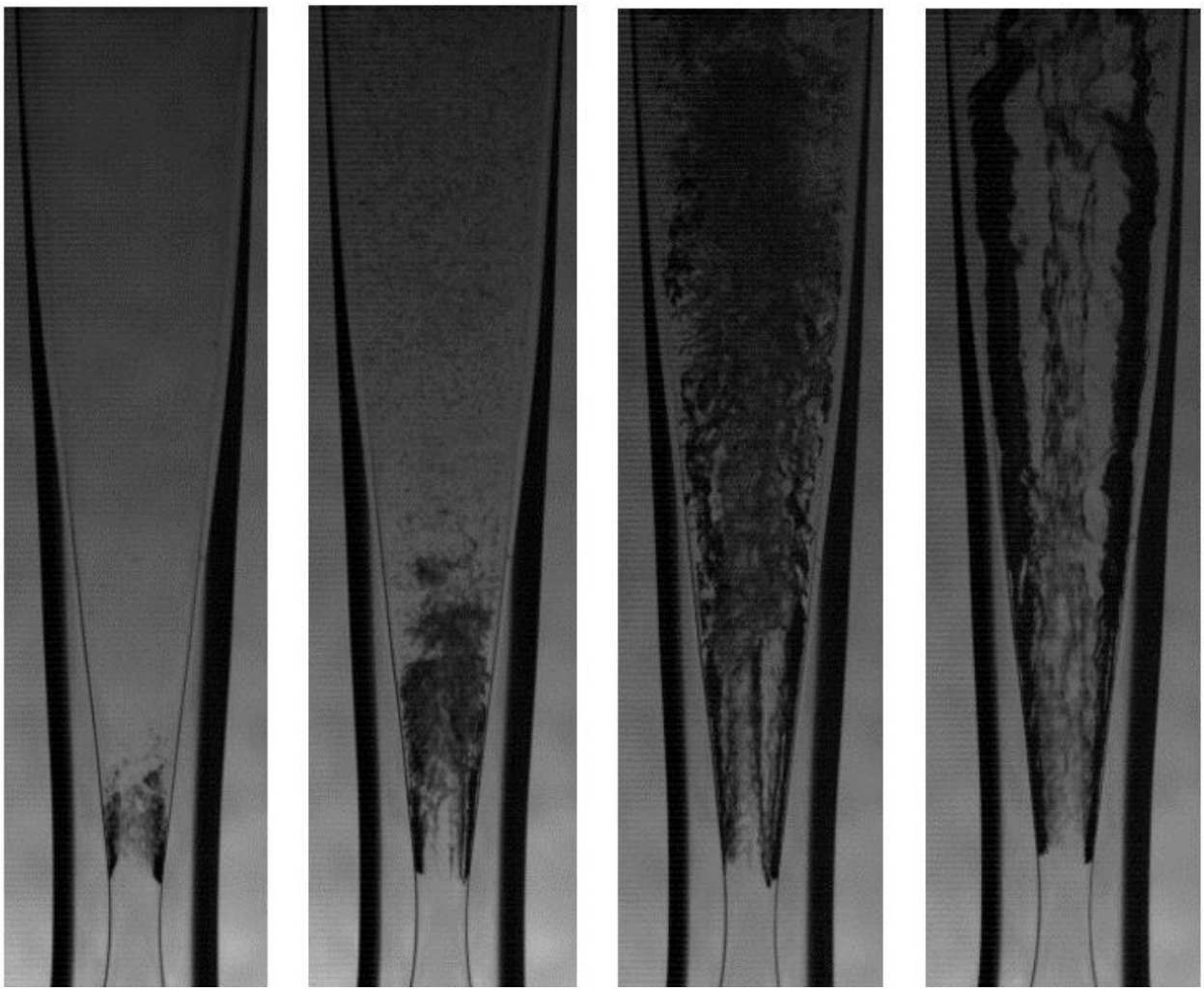

P_b = 70 kPa
T_f = 70°C

P_b = 50 kPa
T_f = 70°C

P_b = 30 kPa
T_f = 70°C

P_b = 10 kPa
T_f = 70°C

Figure 41: Cavitation at different back pressures for T_f = 70°C

As seen in the flow visualization results in Figure 22, the cavitation length kept on increasing as the back pressure in the downstream reservoir was reduced. The first two still in Figure 22 show the cavitation length for absolute back pressure values of 70 kPa and 50 kPa. The flow condensed back to single phase within the diffuser or the diverging section. For much lower back pressures, the flow didn't condense back to single phase liquid within the nozzle and proceeded as a two-phase mixture flow through the rest of the flow lines leading to the downstream reservoir. This

suggests that the static absolute pressure in the downstream region never went below the saturation pressure of water at 70°C, i.e. 31 kPa.

The measurements of the cavitation lengths for the three different temperature values of 25°C, 50°C and 70°C are summarized in Figure 42. A linear trend line is shown through each of the different data points. The point where the linear trend line intersects the x-axis is an indication of the absolute value of back pressure at which cavitation would initiate.

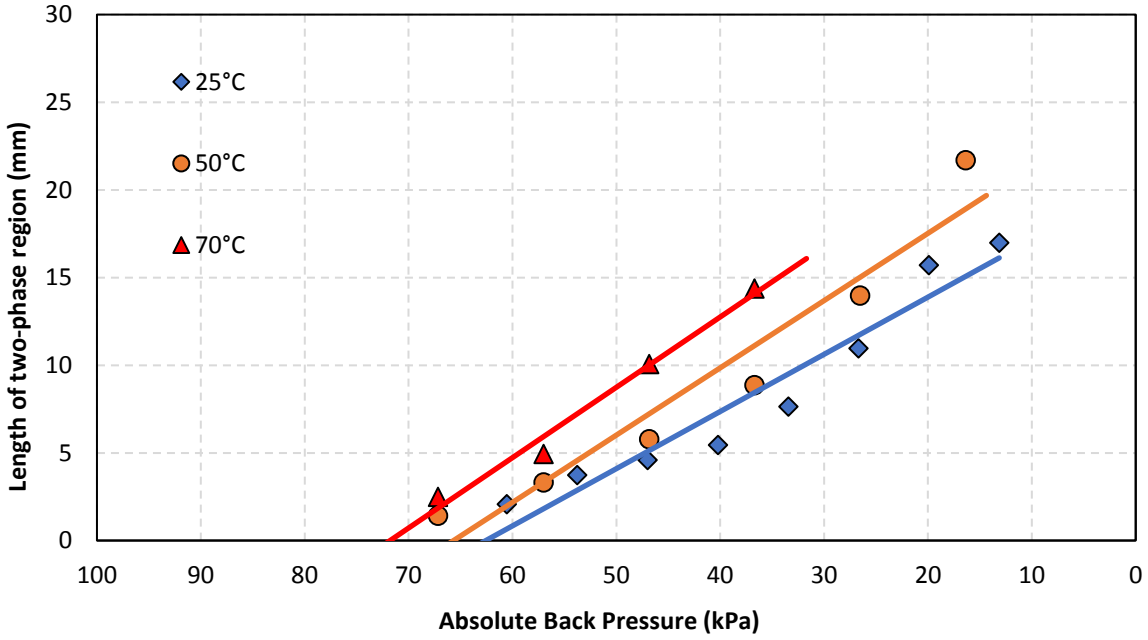

Figure 42: Variation of cavitation length with temperature and back pressure (Linear curve fit)

However, if a second degree polynomial trend line is used to represent the data points, a closer fit is obtained as seen in Figure 43. However, this kind of fit doesn't intersect the x-axis and seems to be asymptotic to the horizontal axis, thereby not giving information about the pressure at which cavitation would initiate. A linear fit gives more insight into the cavitation initiation pressures as compared to a 2nd degree polynomial fit. Hence, a linear fit may be more suitable for the current case, until a theoretical analysis is available to compare with these experimental results.

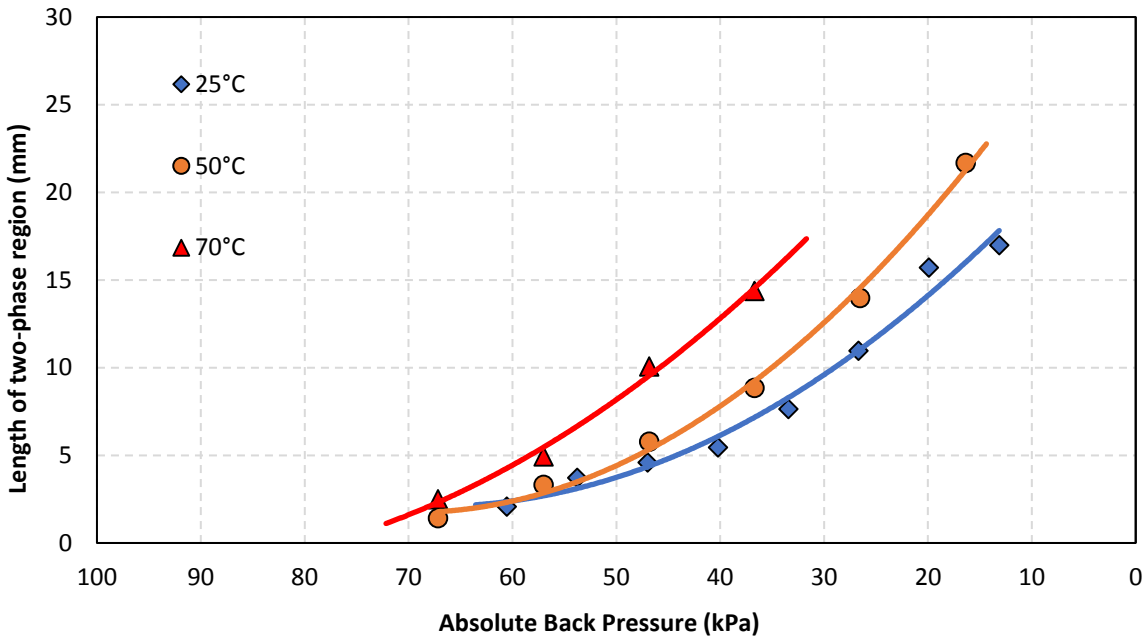

Figure 43: Variation of cavitation length with temperature and back pressure (2^{nd} degree polynomial fit)

The largest source of error in these length measurements explained above is because of the scatter in the location of the condensation region of the two-phase flow. The location of the condensation was based on the visual judgement of where most of the two-phase mixture seemed to condense into the single phase liquid. Another approach by which the "effective" length of the two-phase region could be measured is by utilizing a long camera exposure time. This method was used by Brinkhorst [3] in their experimental study of cavitation in Herschel Venturi tubes where an exposure time of 3 seconds was used to get measurements of the cavitation length. This "blurs" the image and results in a more continuous and well-defined average location of the two-phase boundary.

4.5 Inserts Test Results

This section includes a discussion of results involving the testing of the different types of inserts listed and described in 2.3 Inserts. As explained earlier, the inserts were used to test the hypothesis that delaying the flow separation would delay the point of flashing of the flow in the nozzle. It is well known that suction delays separation in both internal and externa flow. Since, it is not easy to apply suction through the outside of the nozzle diffuser section, as it is made of glass, an insert was introduced. The insert would essentially create two flow paths: core flow and annular flow, where the annular flow path would suck off the fluid near the walls and delay the flow separation in the diverging section of the nozzle and the main core flow would pass through the center of the insert.

4.5.1 3D Printed Solid Insert

As a first step towards creating two flow paths to achieve the purpose mentioned above, a solid insert was used that created an annular diffuser. This solid insert provided some of the basic annular flow characteristics that would exist if suction removed the boundary layer region just downstream of the throat; however, it still involved only a single flow stream.. This insert was 3D printed from a transparent polymer material called *Veroclear* by *Stratasys.* The post processing was performed on the part as explained in 2.3.1 3D Printed Solid Insert.

Experiments were performed using this solid insert where the insert tip was positioned at several nominal distances from the throat of the nozzle. These distances were chosen as 7 mm, 7.5 mm 10.5 mm and 40 mm. For the last distance, the insert was positioned as far back as possible and yielding the distance between the throat and the insert tip as 40 mm. Captured images of the insert positioned in the nozzle for the first three distances are shown in Figure 44. The last position

yielded the insert tip being out of the field of view of the camera, hence it is not represented in Figure 44.

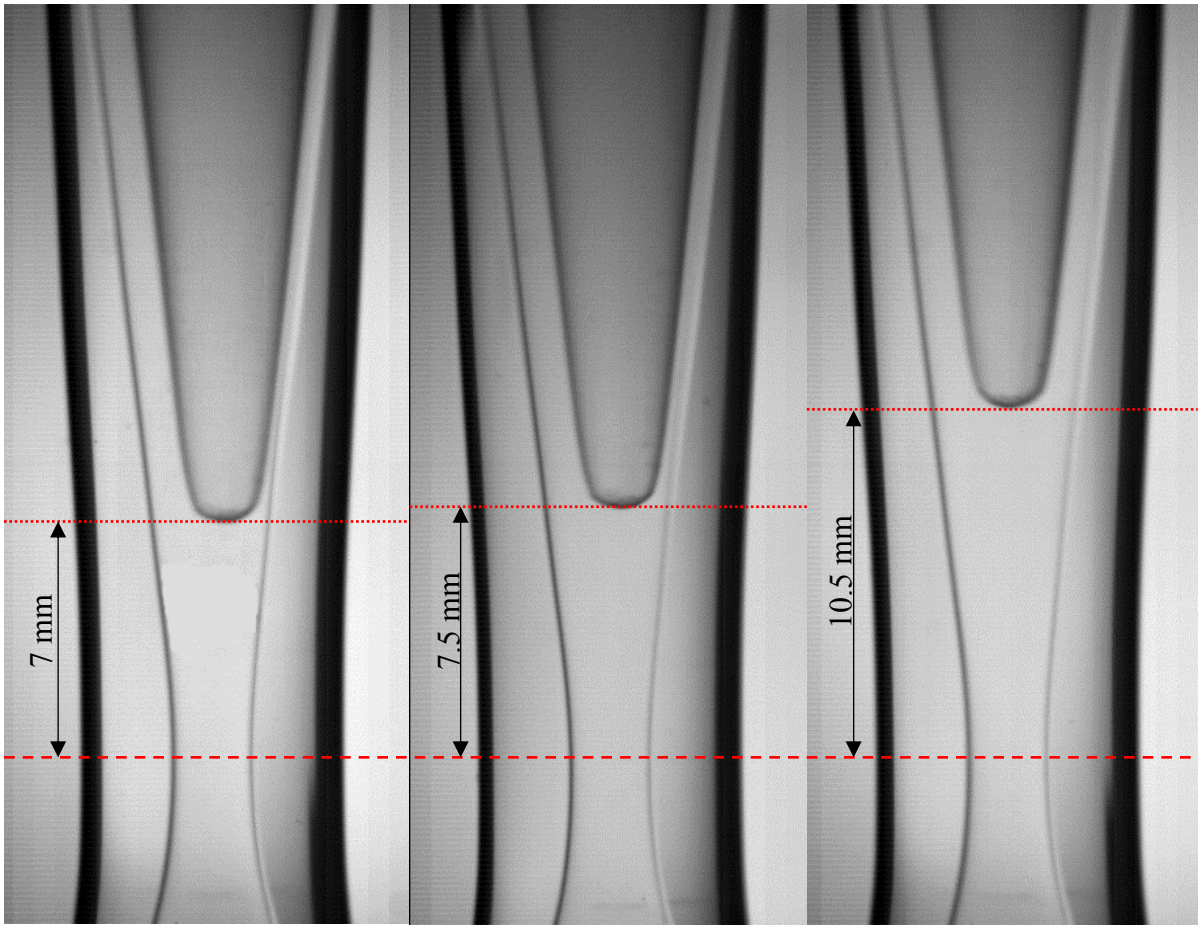

Figure 44: Various positions of the solid insert in the nozzle

It was observed that the cavitation initiated at a much lower value of back pressure compared to the case without any insert. Figure 45 shows the the variation of flowrate with back pressure, and indicates that the choked conditions were achieved at a much lower back pressure than without the insert. As the distance between the throat and the insert tip was reduced, the back pressure to reach choked conditions decreased. In the figure, '*h*' is the distance between the throat and the tip of the insert. The flowrate behavior when the insert was positioned as far back as possible was very similar to the case with no insert.

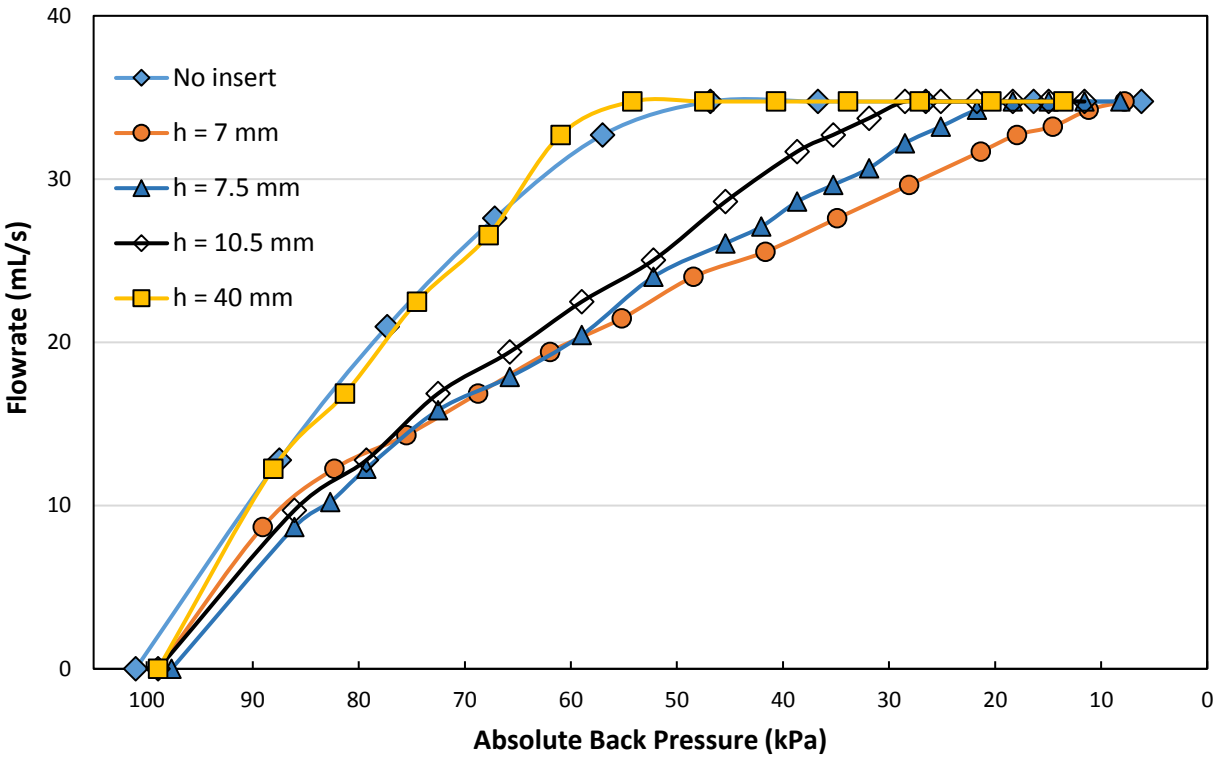

Figure 45: Comparison of flowrate for various insert positions in the nozzle

The reason for requiring such lower back pressures to reach higher flowrates could be attributed to the higher friction in the diffuser region of the nozzle. As the insert tip was brought closer to the nozzle throat, the area of flow across around the insert, especially near the tip of the insert was reduced tremendously and this added resistance to the flow due to friction. The pressure loss in the nozzle was estimated by calculating the difference in the inlet and outlet pressure for each insert position. The results are plotted in Figure 46. As shown in the figure, the pressure drop across the nozzle increased as the flowrate increased in the nozzle. The results shown in the Figure 46 do not include the choked condition and only show the pressure losses for the conditions leading up to the choked condition.

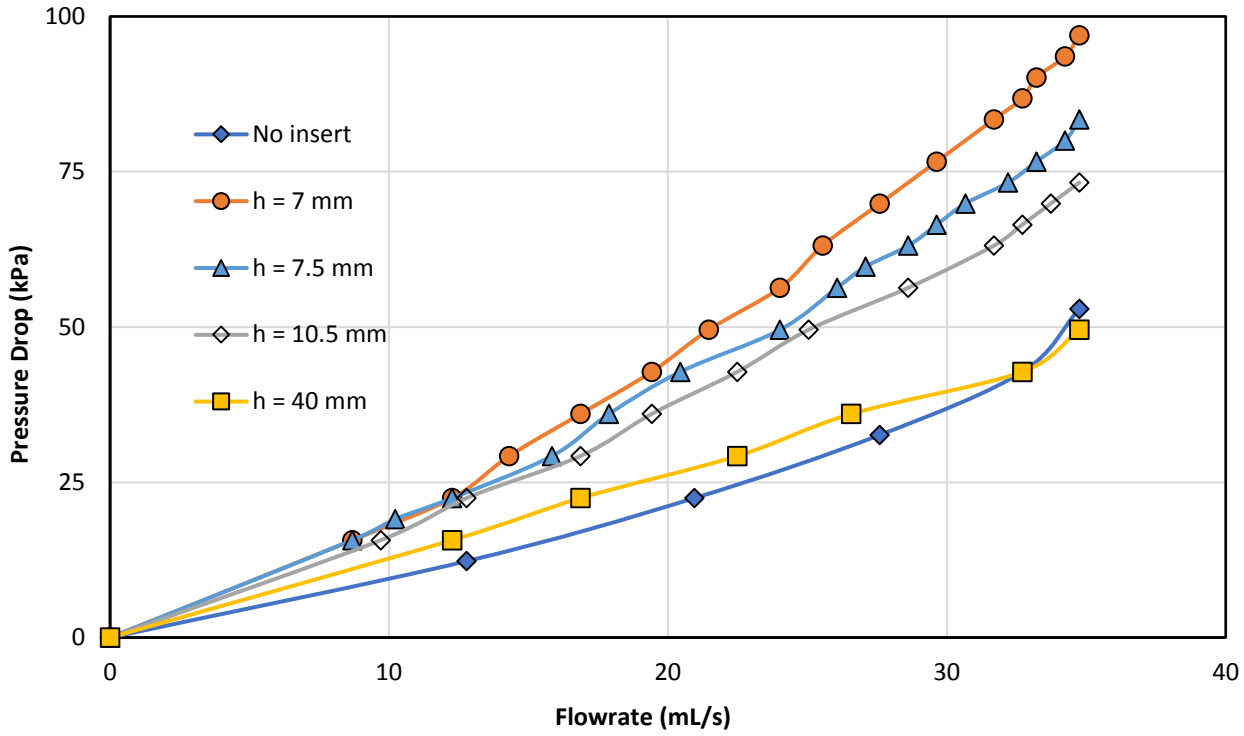

Figure 46: Comparison of pressure drop in the nozzle for different insert positions prior to reaching the choked condition

The point of cavitation initiation in the nozzle was analyzed for different insert positions when the flow was at a steady state choked cavitating condition. Figure 47 compares the position of cavitation initiation for no insert and for different positions of the insert when the back pressure in the downstream was at very low values. It can be seen that cavitation occurred at the same position regardless of the insert position. However, the length of the cavitating region got shorter as the insert was brought closer to the throat, which could again be attributed to the increased frictional losses in the system. This suggests that the solid insert did not create enough suction near the throat to delay the point of flow separation. Had the tip of the insert been smaller in size, the insert could have gone even closer to the throat and possibly more significantly altered the flow separation point in the diverging section.

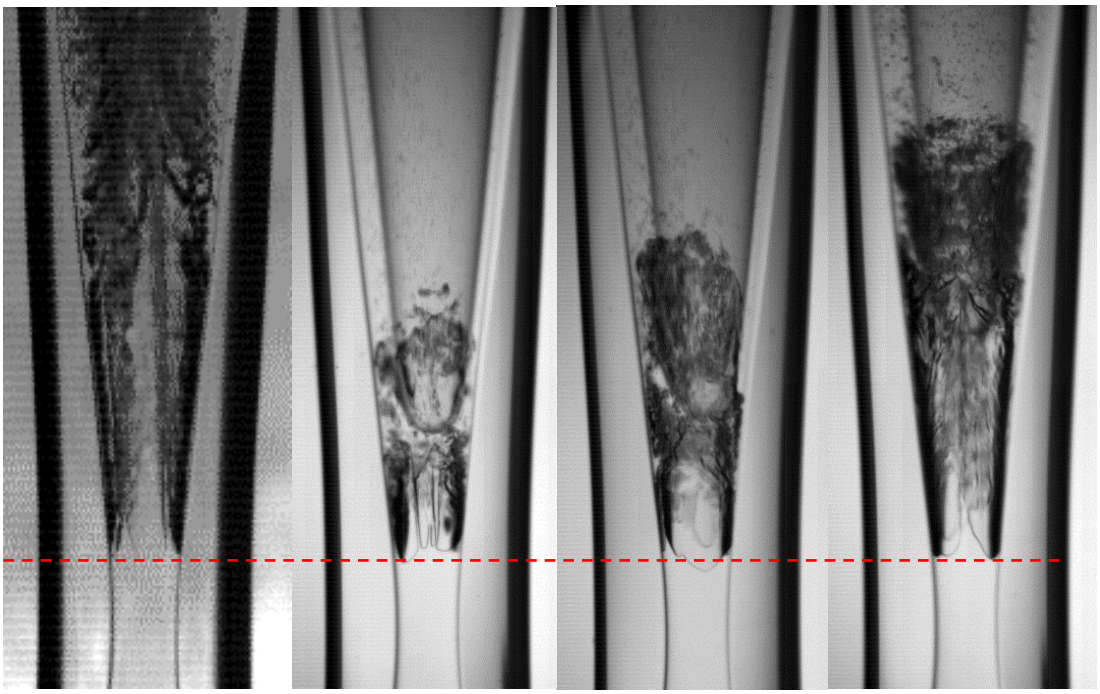

Figure 47: Comparison of cavitation initiation position for no insert and different insert

The length of the cavitating region was also measured using the technique explained in 4.4 Cavitation Length. The comparison of the cavitation length for different insert positons is represented in Figure 48. Again, it was found that the cavitation length increased as the back pressure to the nozzle was reduced. However, cavitation initiated at different values of back pressures. This information was obtained by extending the linear fit curve to intersect the horizontal axis. The intercept would indicate the approximate value of back pressure at which cavitation would initiate.

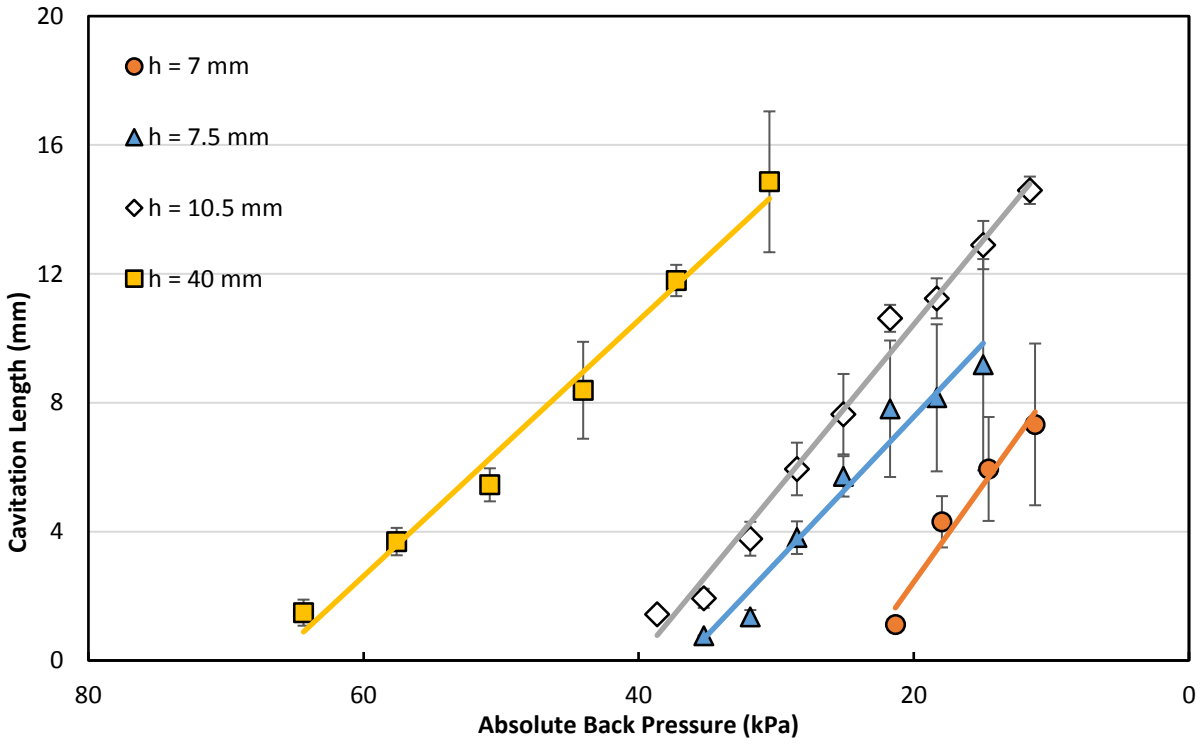

Figure 48: Cavitation length comparison for different positions of the insert

The cavitation initiation pressure (calculated from Figure 48) is plotted in Figure 49 for different insert positions. As mentioned earlier, it took much lower back pressures to reach choking condition as the insert was moved closer to the throat of the nozzle. As seen in Figure 49, cavitation would not occur if the insert were positioned closer than a minimum distance of about 6-7 mm between the insert tip and the throat of the nozzle. As the insert was brought closer and closer, much lower back pressure was needed to initiate cavitation. If the insert was positioned any closer than 6-7 mm from the throat, the frictional effects became so dominant, that the flowrate never reached high enough values to cause effective lowering of static pressure near the throat of the nozzle. Hence, cavitation did not occur if the insert was positioned any closer than 6-7 mm from the throat of the nozzle.

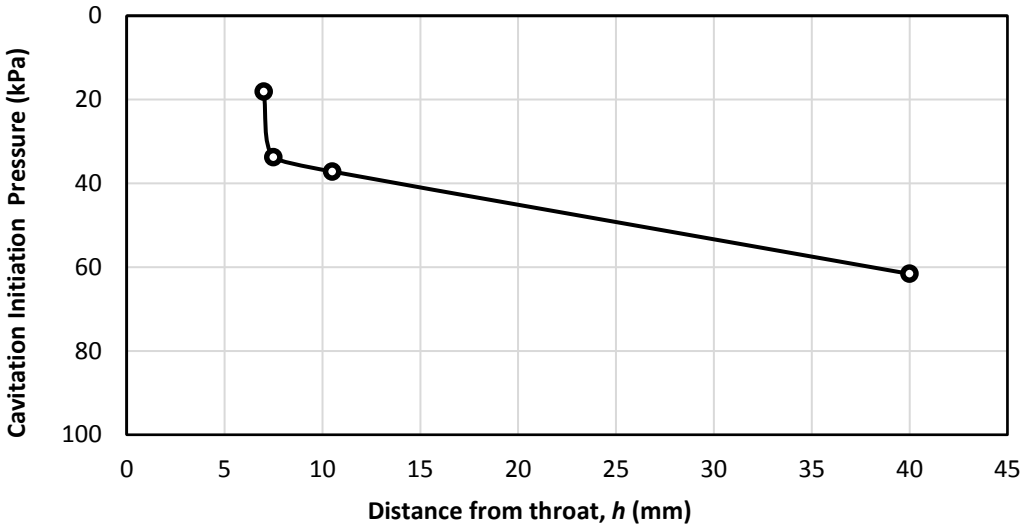

Figure 49: Cavitation initiation pressure for different insert positions

4.5.2 Straight Glass Tube Insert

As a next step towards an attempt to delay the flow separation by sucking off the boundary layer near the walls of the nozzle, tubular inserts were used. Unlike the solid insert, with only the annular flow region, the tubular inserts had provisions for both the core and annular flow regions. Since the straight glass tube insert had a tip outer diameter of 5 mm, there was a limited distance into which the insert could go inside the diverging section of the nozzle. The schematic of the insert positioned in the nozzle is shown in Figure 50 .

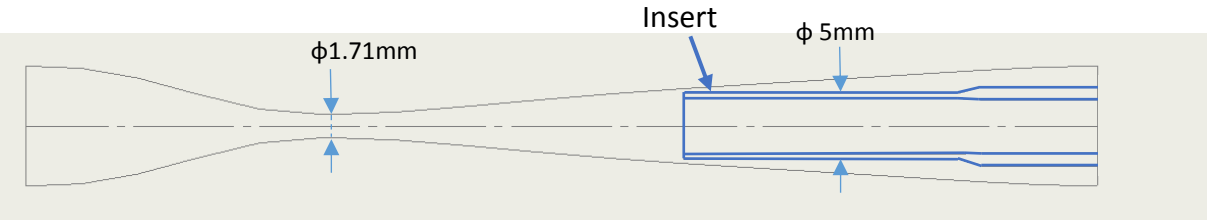

Figure 50: Schematic of insert positioned in the nozzle

Flowrate measurements were taken for this insert at different values of back pressure. These results are summarized in Figure 51.

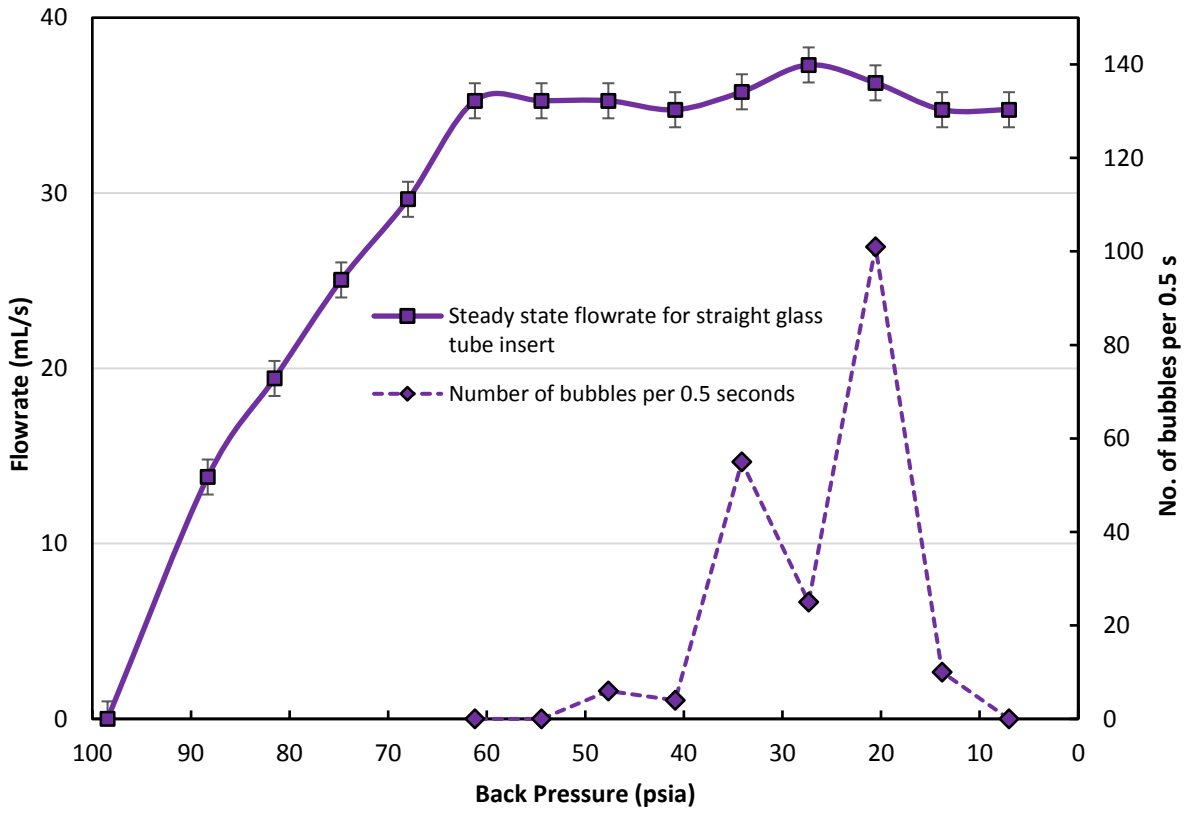

Figure 51: Comparison of steady state flowrate with the number of bubbles formed at the throat for straight glass tube insert

As seen in the Figure 51, the flow choked at the expected flowrate of about 35 mL/s when it was cavitating under steady state conditions. However, for a back pressure range of 10 kPa – 30 kPa absolute, the steady state choked flowrate was higher than expected. Visualization results show that at this back pressure range, distinct bubbles were formed at the throat of the nozzle, a little upstream of the stable flashing front (cavitation initiation location). A sequence of selected frames from the high speed video recording at 30,000 frames per seconds, shows the bubble formation and propagation in Figure 52. Once steady state conditions were reached, and a stable cavitation front was established, secondary bubbles were formed continuously at the throat of the nozzle. These secondary bubbles propagated in the diverging section and mixed up with the bulk

of the two phase mixture. This phenomena was observed only for the range of back pressures where the steady state choked flowrate was higher than expected.

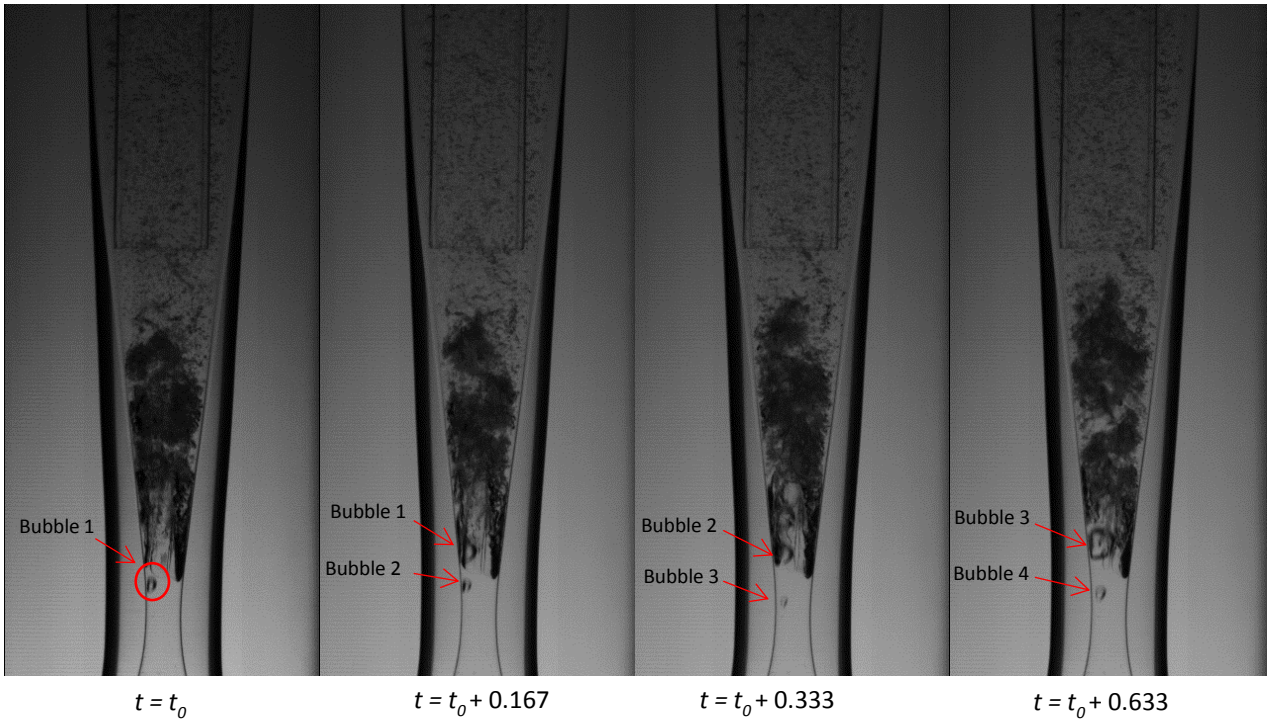

Figure 52: Secondary bubble formation at the throat of the nozzle

The number of bubbles being formed at the throat of the nozzle were counted over 1500 frames, corresponding to 0.5 seconds. They were then plotted alongside the steady state flowrate as shown in Figure 51. These bubbles seemed to contribute to the higher steady state choked flowrate. Further analysis needs to be done to assess if this behavior was due to the boundary layer regions being sucked into the annular region. The secondary bubbles could also be formed due to some kind of an impurity present at the throat that acted as a nucleation site, and promoted formation of bubbles at that point.

4.5.3 Straight Tube Brass Insert

Because the straight glass tube insert had its tip made of out a thin NMR tube, the tip of the insert shattered frequently as the collapse of the cavitation bubbles caused lateral vibration of the tube, which led to possible contact with the inside walls of the nozzle and subsequently led to fracture after every few experimental runs. To deal with this issue, thin walled brass tube inserts were used. Two different brass tubes were used with outer diameters of 1/8th inch (3.18 mm) and 3/16th inch (4.77 mm). These inserts were positioned as close as possible to the throat. The 1/8th inch insert was positioned closer to the throat than the 3/16th inch tube because of the smaller outer diameter. Their positioning in the nozzle is represented in Figure 53Figure 53

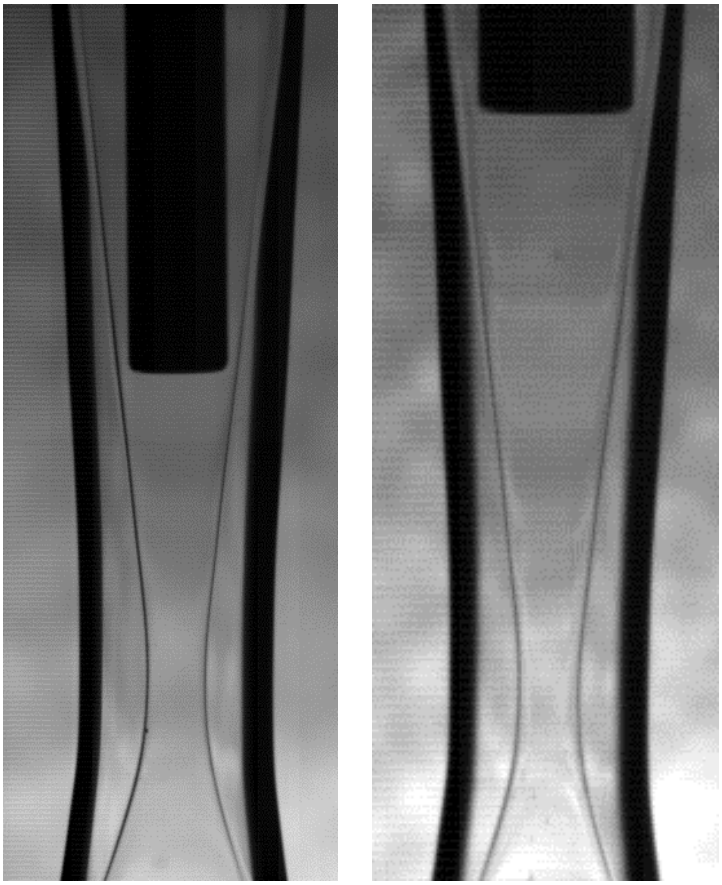

1/8th inch OD brass insert

3/16th inch OD brass insert

Figure 53: Position of brass inserts within the nozzle

Flowrate measurements were made for the two inserts for different values of back pressures. The number of bubbles being formed at the throat, like those explained in 4.5.2 Straight Glass Tube Insert.2, were also counted over 1,500 frames for a duration of 0.5 seconds. These were plotted together and are compared in Figure 54.

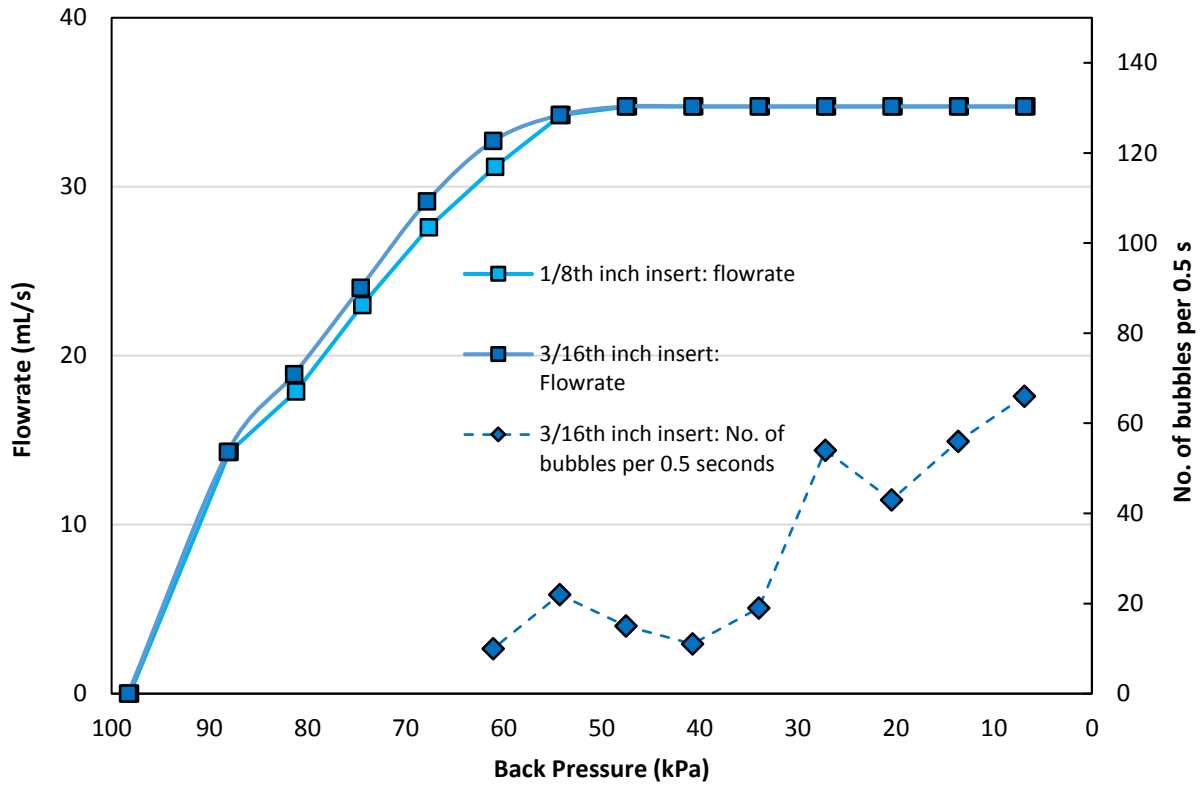

Figure 54: Comparison of steady state flowrate with the number of bubbles formed at the throat for 1/8" and 3/16" straight brass tube insert

As expected, the flowrate through the nozzle keeps on increasing until it chokes at the expected flowrate value of around 35 mL/s However, secondary bubble formation at the throat, like that described in 4.5.2 Straight Glass Tube Insert, was observed only for the 3/16th inch OD insert. No secondary bubbles were formed at the throat for the 1/8th inch insert. Unlike the process shown in Figure 51, the flowrate did not seem to change because of these bubble formations. The flow remained at a constant value of about 35 mL/s for both the inserts.

4.5.4 Tapered Tube Glass Insert

Because of the conical characteristic of the diverging section, the straight tubes could not be made parallel to the inner wall downstream of the nozzle throat. The tapered insert had a conical characteristic to it and also had a small tip outer diameter that made it possible to get much closer to the throat of the nozzle and be more parallel to the inner walls of the diverging section.

The insert was positioned inside the nozzle as shown in Figure 55. Because the insert was made of glass, capturing cavitation visually inside the core flow region was also now possible. The insert was positioned as close to the throat of the nozzle as possible, while leaving a small flow area for the annular flow region.

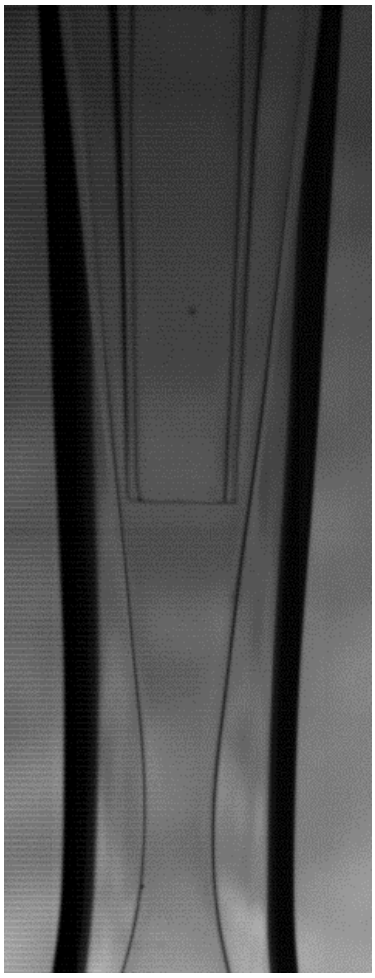

Figure 55: Positioning of the tapered insert in the nozzle

Few combinations of the flow line valve openings were tested and high speed videos were recorded for each combination. The different combinations of the valve openings were:

1. Case 1: Core flow & Annular flow → BV3 and BV4 open
2. Case 2: Core flow only → BV3 open, BV4 close
3. Case 3: Annular flow only → BV3 close, BV4 open

These combinations will be referred to by their case numbers in this section. The flow control in this preliminary setup was limited and the setup did not include direct measurement of the valve settings. The cavitation phenomena for these three flow combinations for a low back pressure value of 30 kPa are illustrated in Figure 56.

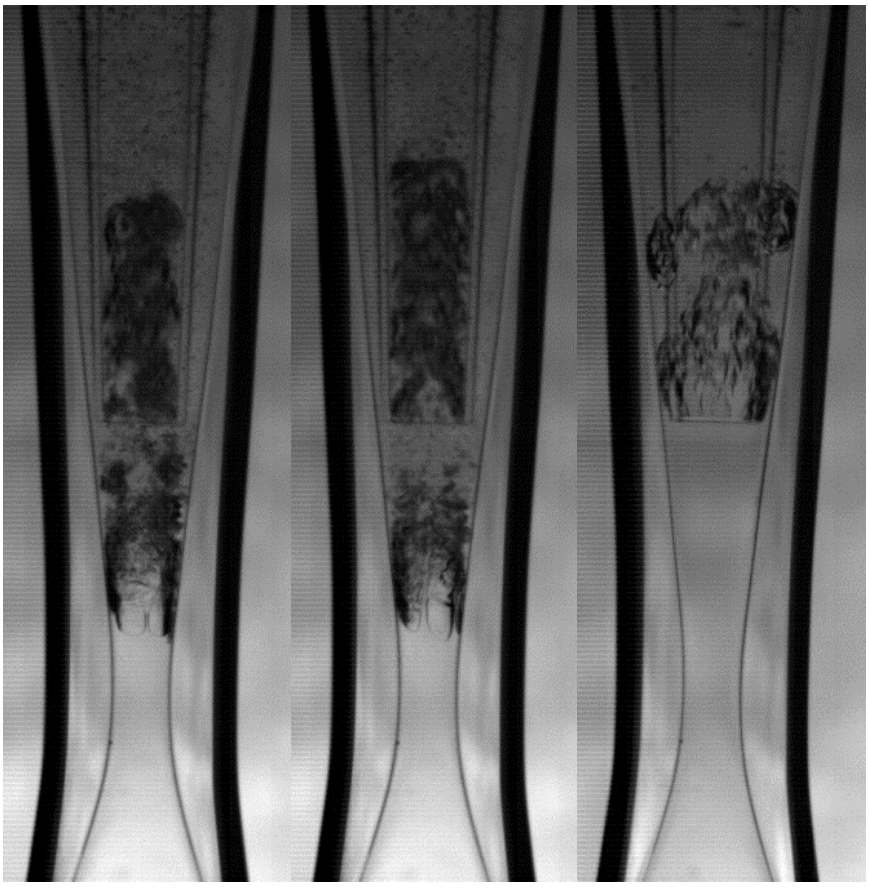

Case 1
P_b = 30 kPa

Case 2
P_b = 30 kPa

Case 3
P_b = 30 kPa

Figure 56: Cavitation for different combinations of flow

Case 1 and case 2 had very similar kind of cavitation at low back pressures as seen in Figure 56. Two kinds of cavitation were observed: cavitation at the throat and cavitation at the entrance of the core flow region. The flow appeared to cavitate at the throat and condensed back to single phase liquid before entering the core flow region. At the inlet of the core flow region, the flow cavitated once again and stayed in a liquid-vapor mixture phase for some length before finally condensing back to single phase liquid.

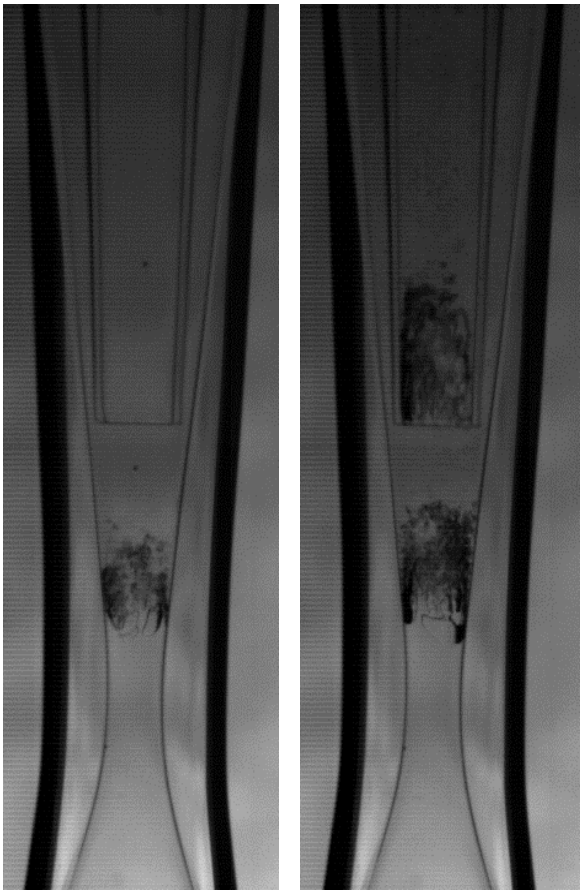

Case 1: $P_b > 45$ kPa Case 1: $P_b < 45$ kPa

Figure 57: Case 1 cavitation at different values of back pressure

In case 1 and case 2, at low back pressures, steady state cavitation occurred at two places in the nozzle: at the throat and at the entrance of the core flow region. This kind of cavitation was observed only for back pressures below 45 kPa absolute. For back pressure values above 45 kPa

absolute, cavitation occurred only at the throat of the nozzle and did not occur at the entrance of the core flow region. This is illustrated in Figure 57.

In case 3, the fluid did not enter into the insert through the core region, but went around the insert in the annular region. As shown in Figure 56, it was observed that steady state cavitation occurred only around the tip of the insert, or at the place where the flow area seemed to be the lowest. Unlike case 1 and case 2, cavitation did not seem to occur near the throat of the nozzle.

The process of formation of a stable steady state cavitation was also captured by the high speed camera for case 3. Low values of back pressure were set in the downstream reservoir and the main control valve BV1 was open. While the valve was being opened, the high speed camera was triggered to record the cavitation initiation phenomena. The sequence of the cavitation initiation process is shown by selected frames from the high speed video in Figure 58.

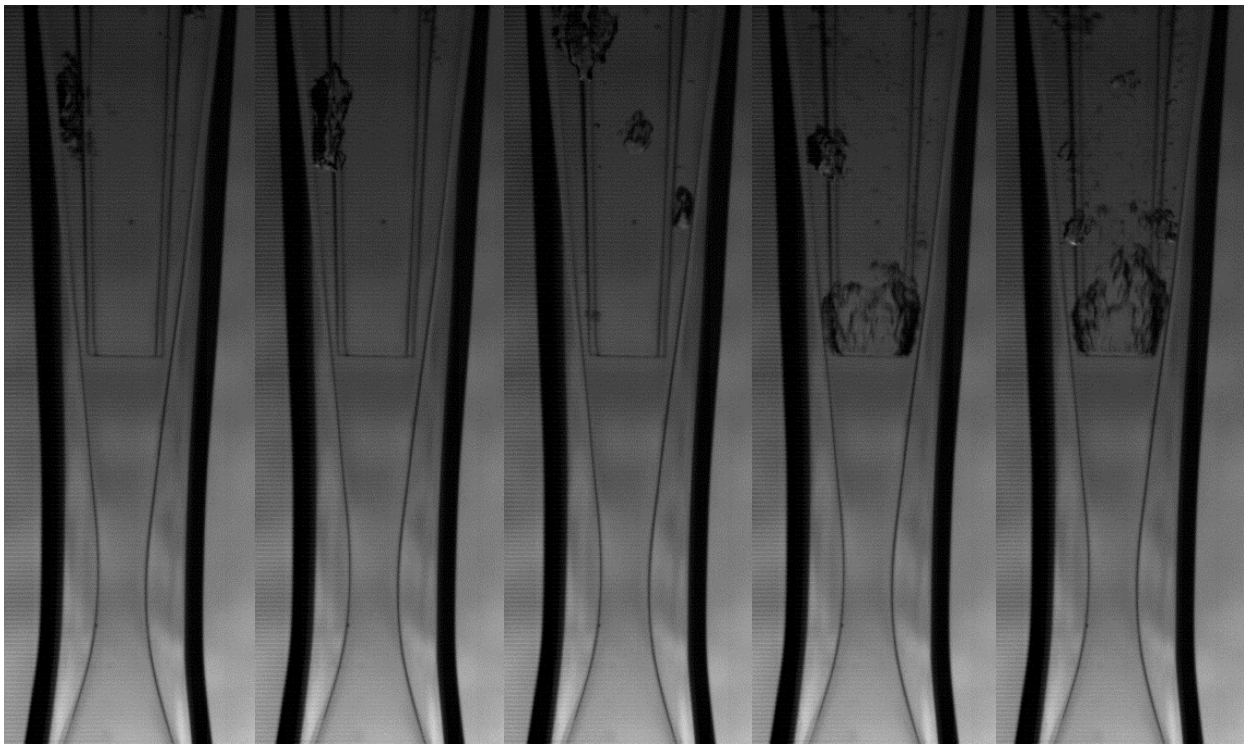

$t=t_0$ $t = t_0 + 100$ ms $t = t_0 + 266$ ms $t = t_0 + 366$ ms $t = t_0 + 400$ ms

Figure 58: Cavitation initiation process for case 3, captured at 30,000 frames/sec

As seen in Figure 58, small individual bubbles were formed around the insert, even at places where the area did not seem to be the lowest. Bubbles formed and collapsed at random locations around the insert for some time and then steady state conditions were reached after the cavitation front was established around the tip of the insert in the annular region. The flow cavitated around the insert tip from this point later on.

Thus, from the results of the experiments performed on the inserts, it appeared that the flow separation point was not affected by the inserts, possibly because the inserts were not close enough to the throat of the nozzle to cause effective delay in flow separation point.

Chapter 5 - Summary, Conclusions and Recommendations

5.1 Summary and Conclusions

This thesis presented the results of an experimental investigation aimed to characterize the cavitating flow of water in a converging-diverging nozzle. Experiments were performed at different fluid temperatures. High speed digital camera flow visualization was utilized to observe the onset of cavitation, and to provide measurements of the length of the two phase region downstream of the diffuser section of the nozzle. Transient (time-resolved) onset of cavitation was also investigated.

The quantitative measurements of the flowrate showed that a choking condition is apparently reached in the nozzle when the flow is in a cavitating state. Regardless of any further reduction in the back pressure, the flowrate would never go beyond the choking flowrate. The choked flow rate reduced as the temperature of the fluid was increased. The choked flowrate also depended on the pressure at the inlet of the nozzle. The measured mass flowrate and the calculated mass flowrate were compared and the predictions fell roughly within 3% of the measurements. Transient measurements of the flowrate were also taken and the flow appeared to go into metastable state momentarily before undergoing cavitation in a stable steady state. The flow stayed in a single phase liquid state for some time, even when the flowrate was beyond the choked condition. The flow then snapped back to the choked flowrate as soon as cavitation initiated. Calculated pressures, at the throat of the nozzle during metastable state, were as low as -70 kPa. A constant difference of about 27 kPa (friction effects included) was observed, between the calculated pressure at the throat and the saturation pressure at that fluid temperature. The reasons for this constant pressure difference are to be investigated in the future.

It was also found that the cavitation inception did not necessarily coincide with the choked flow conditions. Cavitation initiated in the nozzle when the flowrate was lower than the choked flowrate. As the flowrate increased, and the cavitation developed further, choked conditions were achieved.

The cavitation inception location was studied for different fluid temperatures and different nozzle inlet pressures. Under choked flow conditions, it was found that the inception location stayed at the same location, about 2 mm downstream of the throat in the downstream region, regardless of the flow conditions. The inception location however seemed to vary when the flow was cavitating in the non-choked cavitating conditions, i.e. when the flowrate was lower than the choked flowrate. The establishment of the stable cavitation front downstream of the throat, and not at the throat, could be attributed to a "Vena-contracta" effect in the diffuser region of the nozzle.

A high speed camera was used to visualize and record the process of cavitation initiation leading to stable steady state cavitation. Cavitation was observed to initiate from small bubbles that originated near the throat of the nozzle, which propagated downstream before "exploding" into a vapor cloud and establishing a steady state stable cavitation front. At higher temperatures, a semi-stable cavitation front was established several millimeters further downstream in the diffuser section of the nozzle. The front stayed at this semi-stable state for some time before going back to the stable cavitation front.

The length of the cavitating region was also measured using the high speed camera. It was found that the length of the two-phase region downstream of the throat increased as the back pressure to the nozzle was reduced. Once cavitation initiated at a given back pressure, further reduction in the back pressure caused the two-phase region to extend further into the diverging

section of the nozzle. It was also found that as the temperature of the fluid was increased, the cavitation length increased at a given back pressure.

Different kinds of inserts were used in an attempt to delay the flow separation in the diffuser region of the converging diverging nozzle. As a first step towards testing the inserts, a solid insert with which provided only an annular path downstream of the throat. The location of cavitation inception was analyzed and it appeared to remain at the same location regardless the flow conditions or the position of the insert in the nozzle relative to the throat. When tubular inserts were used, due to the two flow paths created by the insert, different kinds of cavitation regimes were observed in the two flow paths. The cavitation inception location still stayed at the same location regardless of the flow condition. Fluctuations in the choked flowrate were observed and it appeared to be because of a secondary bubble formation near the throat of the nozzle. The transient cavitation initiation process for tapered glass insert for the case when only the annular flow was open, was also captured through the high speed camera and it was observed that cavitation bubbles initiated in the annular region, around the insert at random locations first, before establishing a stable cavitation front around the tip of the insert in the annular region.

5.2 Recommendations for future work

The use of the inserts in the diverging section did not appear to have an influence on the flow separation position in the nozzle, as the cavitation inception location did not appear to move or change location downstream of the nozzle throat. The inserts could be modified to enable their tip to go further into the diverging section of the nozzle near the stable cavitation inception position. The PIV technique should be utilized to get insights into the complex flow structures accompanying the inserts, at least prior to cavitation. Thin walled transparent inserts should be made by an appropriate rapid prototyping technique to have more dimensional control on the

profile of the insert and also to facilitate optical measurements of the phenomena. The flow separation point also depends on the rate of expansion of the diverging section, and lowering the expansion angle of the diffuser region can affect the flow separation point in the diverging section. Different diverging angles should be tested to investigate their influence on the delay of the flow separation point and the effect of this on the cavitation inception location.

The lack of pressure data inside the nozzle, especially near the throat of the nozzle limits the ability to observe the conditions just before the cavitation inception location. Taking pressure measurements in the nozzle, especially during the metastable state, would provide a direct measurement of the negative pressures obtained in the throat of the nozzle.

Since the water was not treated prior to testing, the impurities present in the water act as nucleation sites and prevent the liquid from achieving much lower pressures in the metastable state. Having purified water would number of potential nucleation sites and thus enable the liquid to achieve much higher values of negative pressure at the throat. The fluid could then be in the metastable state for longer periods of time.

The experimental results obtained should be compared, to the extent possible, with reliable and accurate CFD models to get significant insights into the flow conditions leading up to cavitation.

References

[1] Franc, J. P., & Michel, J. M. (2006). Fundamentals of cavitation (Vol. 76). Springer Science & Business Media.

[2] Ulas, A. (2006). Passive flow control in liquid-propellant rocket engines with cavitating venturi. Flow Measurement and Instrumentation, 17(2), 93-97.

[3] Brinkhorst, S., von Lavante, E., & Wendt, G. (2017). Experimental and numerical investigation of the cavitation-induced choked flow in a herschel venturi-tube. Flow Measurement and Instrumentation, 54, 56-67.

[4] Alkotami, A. (2016). An investigation of cavitation cooling effect in converging-diverging nozzles (Doctoral dissertation, Kansas State University).

[5] Asher, W. (2014). Fluid dynamics of cavitating sonic two-phase flow in a converging-diverging nozzle (Doctoral dissertation, Kansas State University)

[6] Brennen, C. E. (2013). Cavitation and bubble dynamics. Cambridge University Press.

[7] Franc, J. P. (2006). Physics and control of cavitation. GRENOBLE UNIV (FRANCE).

[8] Wilms, J. (2016). Flow visualization of cavitation (Doctoral dissertation, Kansas State University)..

[9] Caupin, F., & Herbert, E. (2006). Cavitation in water: a review. *Comptes Rendus Physique*, *7*(9-10), 1000-1017.

[10] Appel, D. W. (1960). Cavitation along surfaces of separation (No. 60-WA-265). KANSAS UNIV LAWRENCE.

[11] Arakeri, V. H. (1975). Viscous effects on the position of cavitation separation from smooth bodies. Journal of Fluid Mechanics, 68(04), 779-799.

[12] Davis, M. P. (2008). Experimental investigation of the cavitation of aviation fuel in a converging-diverging nozzle. ProQuest.

[13] Sou, A., Hosokawa, S., & Tomiyama, A. (2007). Effects of cavitation in a nozzle on liquid jet atomization. International journal of heat and mass transfer, 50(17), 3575-3582.

[14] Schmidt, A. J. (2016). Quantitative measurement and flow visualization of water cavitation in a converging-diverging nozzle (Doctoral dissertation, Kansas State University).

[15] Wallis, G. B. (1969). One-dimensional two-phase flow.

[16] Alam, M. M. A., Setoguchi, T., Matsuo, S., & Kim, H. D. (2016). Nozzle geometry variations on the discharge coefficient. Propulsion and Power Research, 5(1), 22-33.

Appendix A - High Speed Camera Specifications

The Photron FASTCAM SA5 high speed camera used to capture high-speed videos had an internal memory of 8GB. This allowed the camera to capture at 7000 frames per second at its maximum resolution of 1,024 x 1,024 pixels. At lower resolutions, recording at much higher frame rates can be achieved. Table 3 describes the detailed specifications of the high speed camera.

Image Sensor	CMOS image sensor	
Sensor Resolution	1,024 x 1,024 pixels	
Frame Rate	When full frame: 7,000fps max. When a frame segment: 775,000 fps max.	
Lens Mount	F mount, C mount, Lens Mount with Filter Changer (optional)	
Recording Color Depth	Monochrome	12bit
	Color	RGB, each 12-bit (Bayer color filter method)
Shutter Method	Electronic shutter	
Recording Method	IC memory	
Recording Memory Capacity	8 GB (model 1), 16 GB (model 2), 32 GB (model 3)	
Trigger Method	START, CENTER, END, MANUAL, RANDOM, RANDOM RESET, RANDOM CENTER, RANDOM MANUAL, TWO STAGE	
Gain Control	Hardware LUT on camera Controllable via LCD Remote Controller or software	
Image Output Customization	Customizable LUT, brightness is changeable	
External Synchronization Input Signal	5 Vp-p, negative polarity/positive polarity (switchable)	
External Synchronization Output Signal	5 Vp-p, negative polarity/positive polarity (switchable)	
Trigger Input Signal	TTL, contact	
Other Output Signals	Other timing signal outputs, event marker input	
External Control	LCD Remote Controller, RS-422 external control I/F, Gigabit Ethernet I/F (PC)	
Video Output Signal	NTSC/PAL, SDI (Serial Digital Interface) Includes digital zoom, scroll, fit functions	
Digital Interface	Gigabit Ether (1000BASE-T)	

Table 3: High speed camera specifications

The maximum recording times and the maximum frame rates for different recording resolutions are listed out in Table 4 below.

Resolution	Frame Rate	8GB	
(h x v pixels)	Max fps	Frames	Time (sec)**
1024 x 1024	7,000	5,457	0.78
1024 x 1000	7,500	5,588	0.75
1024 x 800	9,300	6,985	0.75
1024 x 744	10,000	7,511	0.75
960 x 528	15,000	11,289	0.75
832 x 448	20,000	15,352	0.77
768 x 320	30,000	23,284	0.78
512 x 272	50,000	41,090	0.82
320 x 264	75,000	67,737	0.90
320 x 192	100,000	93,138	0.93
256 x 144	150,000	155,230	1.03
256 x 64	300,000	349,269	1.16
128 x 64	420,000	698,538	1.66
128 x 48	525,000	931,384	1.77
128 x 24	775,000	1,862,769	2.40
128 x 16	930,000	2,794,154	3.00
64 x 16	1,000,000	5,588,309	5.59

Table 4: Photron FASTCAM SA5 recording times and frame rates at different resolutions

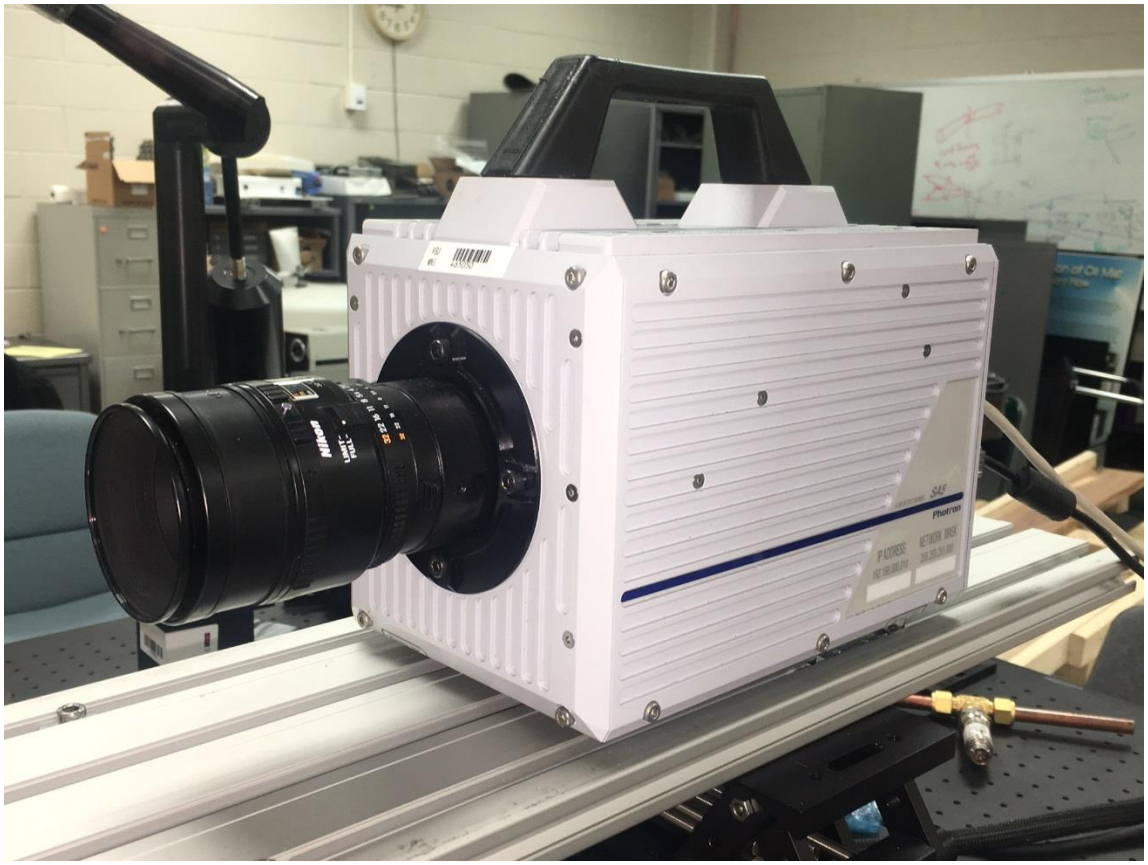

Figure 59: High speed camera with a 60 mm lens

Appendix B - Measurement Instruments Specifications

The auxiliary instruments used to measure flow parameters in the flow system illustrated in Figure 9 and Figure 15 are mentioned below. The specifications of the instruments were provided by the manufacturer.

Pressure Measurements

The pressure at the inlet of the test section was measured by a Viatran 245 pressure transducer and is represented by P1 in Figure 9. The pressure at the outlet of the test section, without the insert in place, was measured by another Viatran 245 transducer with the same specifications as that of P1. This pressure transducer is represented by P2 in Figure 9.With the additional flow line with the insert in place, the pressure at the outlet of the test section was measured by two transducers, one at each flow line. A Viatran 245 transducer measured the pressure in the core flow line, represented by P2 in Figure 15. The pressure in the annular flow line was measured by an Omegadyne PX429 pressure transducer, represented by P3 in Figure 15. The pressure in the downstream reservoir, or the back pressure (P_b) was measured by a dial gauge. The pressures measured by the gauge pressure measurement devices were calibrated against a Barometer that measured the atmospheric pressure.

- Downstream Reservoir
    - Ashcroft dry pressure gauge (Figure 60)
    - Range: -30 in Hg to +30 in Hg or -100 kPa to +100 kPa
    - Uncertainty: ±2 % of mid-scale

- Pressure Transducers, P1 and P2 (Figure 61)
    - Viatran 245 absolute pressure transducer
    - Range: 0-30 psia
    - Uncertainty: ±0.1 % Full Scale (FS) accuracy
- Pressure Transducer, P3 (Figure 62)
    - Omegadyne PX429 absolute pressure transducer
    - Range: 0-15 psia
    - Uncertainty: ±0.08 % Best Straight Line (BSL) accuracy
- Barometer (Figure 63)
    - Princo barometer
    - Uncertainty: ±0.01 mm Hg

The Pressure transducers were calibrated by a five point calibration using a dead weight tester. The Barometer was used to calibrate and adjust the gauge pressure measurement to absolute pressure.

Flowrate Measurements

Measurement of the flowrate through the system were taken by two instruments. The volumetric flowrate was measured by a Rotameter and the mass flowrate was measured by a Coriolis mass flowmeter.

- Rotameter to measure volumetric flowrate (Figure 65)
    - Fischer & Porter rotameter
    - Range: 0-0.81 gpm
    - Uncertainty: ±2 % FS accuracy

- Coriolis flowmeter to measure mass flowrate (Figure 64)
    - Micro Motion CMF025 sensor
    - Micro Motion Model 2700 transmitter
    - Range: 5 g/cm^3 to 5000 kg/m^3
    - Uncertainty: ±0.10 % reading accuracy

Temperature Measurements

- Thermocouples T1, T2 and T3
    - Omega Type K Thermocouples
    - Range: -200°C to 1250°C
    - Accuracy: ±0.75 % reading below 0°C and ±2 % reading above 0°C.

Immersion Heaters

- Immersion Heater with stirrer (Thermoregulator) (Figure 66)
    - Techne Tempette TE-8A thermoregulator
    - Heater Power: 1000 W at 110 V
    - Operating Temperature Range: -20°C to +95°C
    - Stirrer pump maximum flow : 10 liters/min
- Immersion Heater
    - Tempco TSP02244 Screw Plug Immersion Heater
    - Heater Power: 4500 W at 220 V

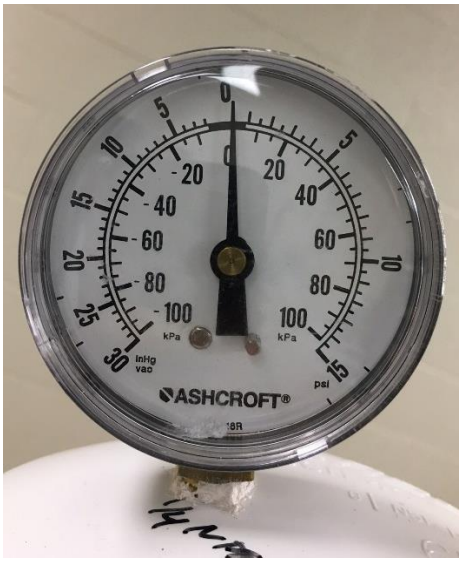

Figure 60: Dry Ashcroft pressure gauge

Figure 61: Viatran 245 Pressure Transducer

Figure 62: Omegadyne PX429 Pressure Transducer

Figure 63: Barometer to measure atmospheric pressure for absolute pressure calibration

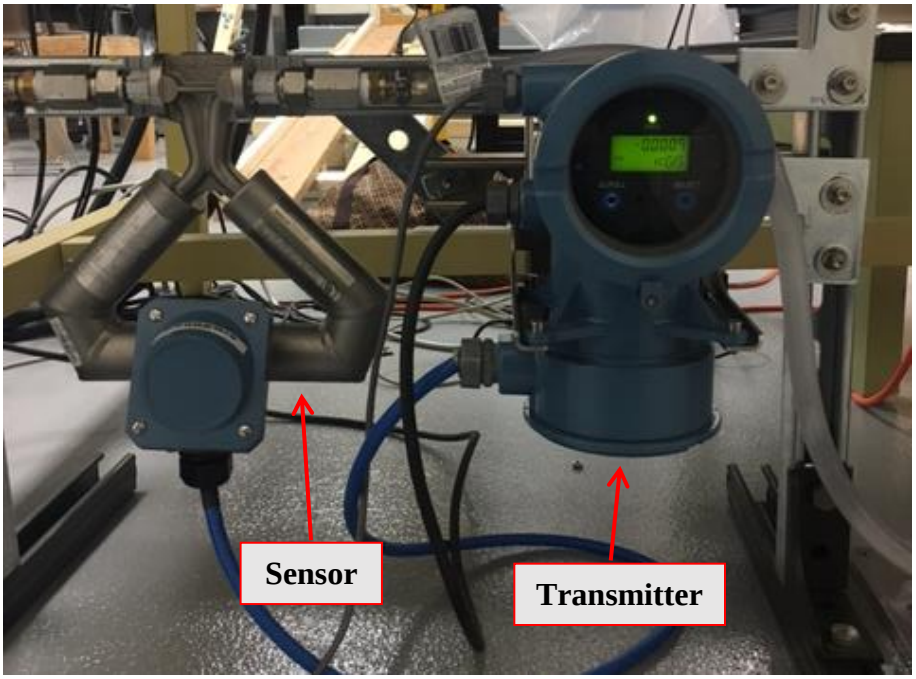

Figure 64: Coriolis flowmeter showing both the sensor and the transmitter

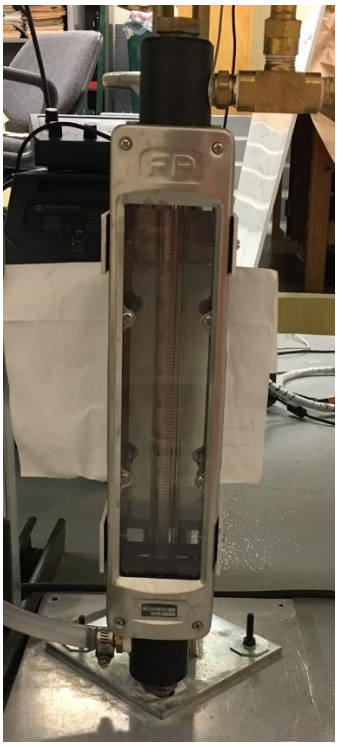

Figure 65: Fischer & Porter rotameter

Figure 66: Techne Tempette TE-8A Thermoregulator

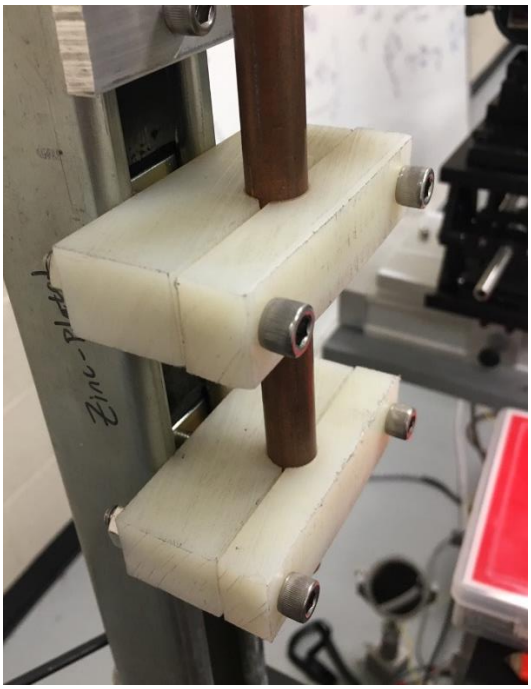

Figure 67: Nylon mounts (shown with Copper tubes)

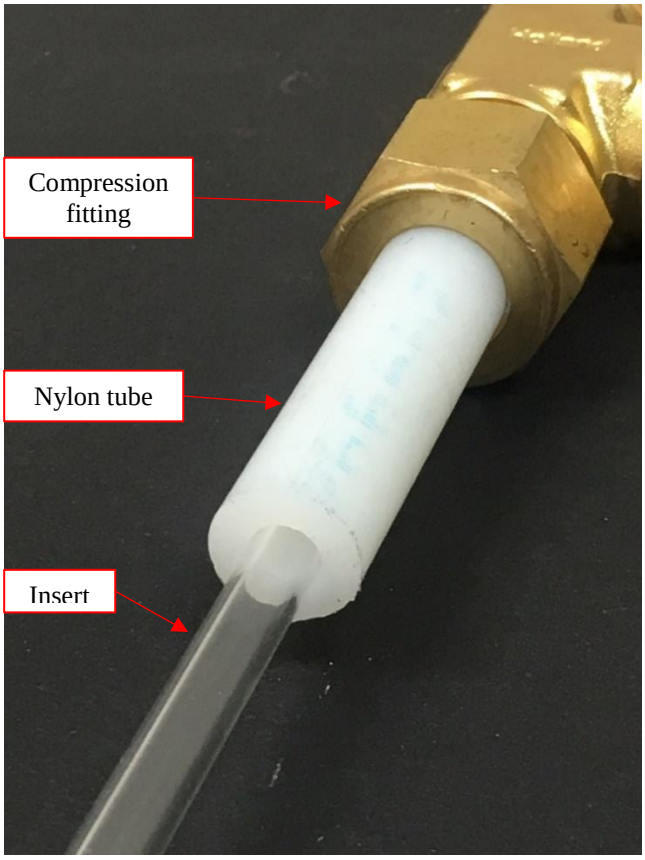

Figure 68: Nylon tube to clamp the glass insert

Appendix C - Analysis of the Two Phase Flow in Diverging Section

A simple one dimensional analysis of the two phase flow in the diverging section was performed. The analysis presented in this chapter is in the primitive stages and further work needs to be done on the analysis to get more detailed insights of the flow characteristics.

The simplified analysis has the following assumptions:

- Cavitation initiates few millimeters downstream of the throat.
- A value of void fraction at the point of cavitation initiation (at the throat) is assumed.
- The velocities and single phase pressures (obtained by simple Bernoulli's approximation) are calculated at nominal values of choked flowrate.

Compressible flow equations were solved to evaluate the pressures, velocity, and void fraction of the two-phase region in the diverging section. Assuming isentropic conditions, a 1D marching process was applied. The variation of pressure, *P* with the distance, *z*, from the throat in the diverging section of the nozzle is given by:

$$\frac{dP}{dz} = \frac{\rho u^2}{A[1 - M^2]} \frac{dA}{dz} \tag{4}$$

Here, *u* is the velocity at the throat, ρ is the mixture density based on the initial void fraction assumed, *M* is the mach number, and *A* is the flow area at the given value of *z*.

The variation of velocity, u_z in the two phase mixture is given by:

$$\frac{du_z}{dz} = -\frac{u}{A[1 - M^2]} \frac{dA}{dz} \tag{5}$$

The variation of the density of the two phase mixture is:

$$\frac{d\rho}{dz} = \frac{M^2}{A[1 - M^2]} \frac{\rho}{A} \frac{dA}{dz} \tag{6}$$

The void fraction was then calculated as a function of the distance from the throat based on the isentropic flow conditions. The pressure in the downstream was calculated and a momentum balance was imposed on the condensation shock in the diverging section. The pressure in the two phase region in the downstream region either increased, or decreased with distance, depending on the initial throat conditions defined. The condensation shock was encountered when the pressure was equal to the pressure obtained through the condensation shock. The momentum balance on the condensation yielded the following equation for the pressure, P_c just upstream of the condensation shock:

$$P_c = P_b + \left[\frac{1}{2}\left(\frac{\rho_3}{\rho_f}\right) - 1\right]\rho_c {V_3}^2 \tag{7}$$

Based on the equations explained above, the pressure variation was obtained as shown in Figure 69. The pressure in the single phase region was obtained from the simple 1D Bernoulli's approximation as explained earlier in 4.2 Pressure Distribution in the Nozzle.

When the flow velocity at the throat was reduced, and the throat conditions were forced to cause the flow to be subsonic at the throat, the void fraction reduced from its initial value to zero, thereby indicating that the flow condensed without going through a condensation shock. When the flow at the throat was sonic, then the condensation shock criteria was met before the void fraction could gradually decrease to 0.

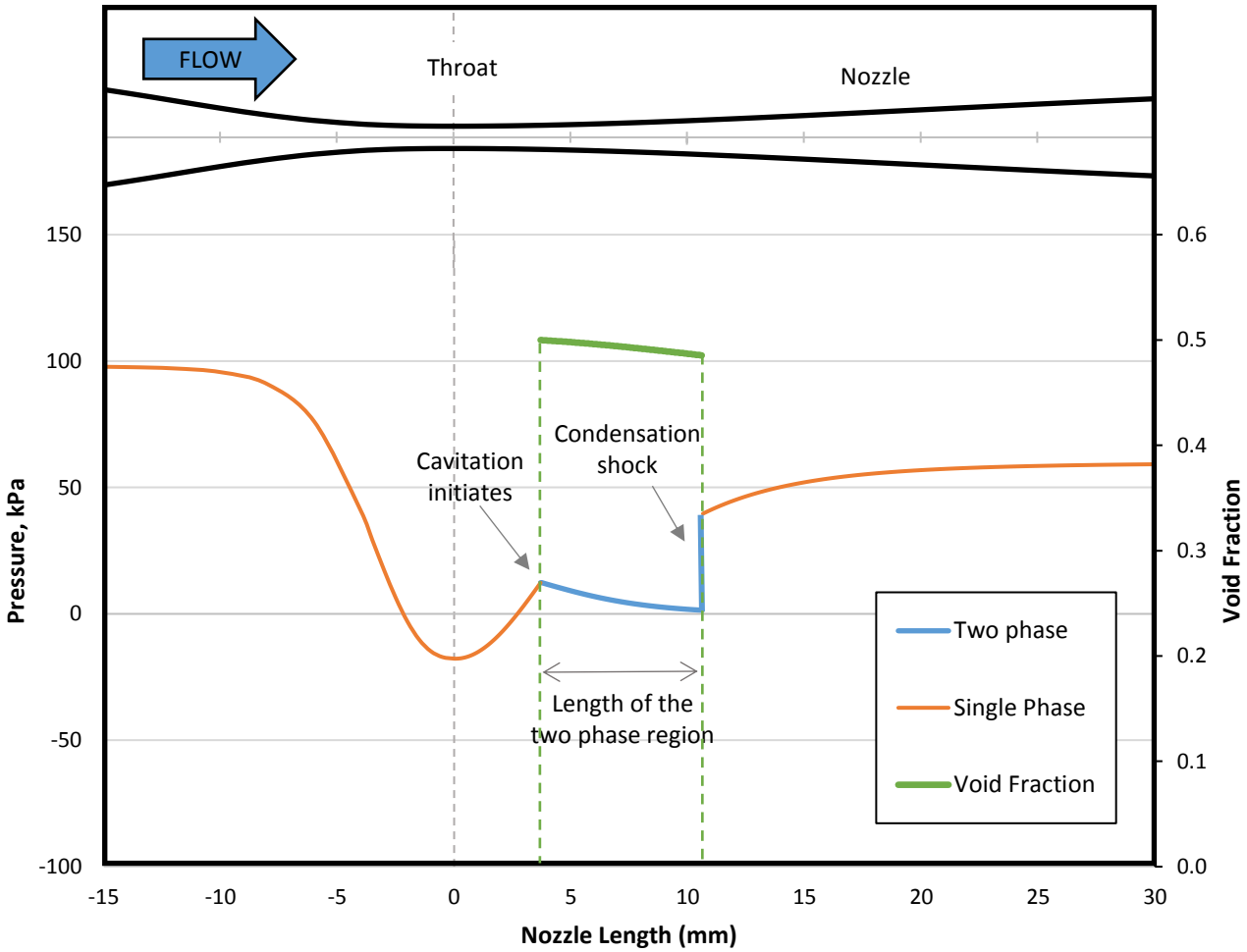

Figure 69: Pressure variation in the nozzle under cavitating conditions, compared with the void fraction

The analysis presented in this chapter was a very primitive analysis performed in an effort to predict the length of the cavitating region. Further work needs to be done to refine the model, by incorporating the proper energy and momentum balance, and by including the flow separation effects in the diverging section.

Appendix D - Copyright and Fair Use

The images shown in Figures 1-8 are from the published books and articles. The copyrights for these images are most likely owned by either the publisher of the article or the writer(s) that produced the images in question. It is believed that the use of the images to illustrate factual information qualifies as fair use under United States copyright law. Any other use of these images may be copyright infringement.